

38th Annual VFS Student Design Competition

2025 Unmanned Vertical Lift for Medical Equipment Distribution

Sponsored by Boeing



Alfred Gessow Rotorcraft Center
Department of Aerospace Engineering
University of Maryland
College Park, MD 20742 U.S.A.



Alfred Gessow Rotorcraft Center
Department of Aerospace Engineering
University of Maryland
College Park, MD 20742 U.S.A.

Dilha

Dilhara Jayasundara
Graduate Student (Team Lead)
dilharaj@umd.edu

Erik W Scott

Erik Scott
Graduate Student
escott28@umd.edu

Andrew Collar

Andrew Collar
Graduate Student
acollar@umd.edu

Spencer Fishman

Spencer Fishman
Graduate Student
fish@umd.edu

Animesh

Animesh Shastry
Graduate Student
animeshs@umd.edu

V.L. Nagaraj

Dr. Vengalattore Nagaraj
Faculty Advisor
vnagaraj@umd.edu

D. Chopra

Dr. Inderjit Chopra
Faculty Advisor
chopra@umd.edu

ACKNOWLEDGEMENTS

The design team wishes to acknowledge the following people for their invaluable discussion, guidance, and support throughout the course of this project.

Industry Professionals

Andreas Bernhard — Director, Aircraft Design at Sikorsky Aircraft

Dr. Peter Lorber — Technical Fellow at Sikorsky Aircraft

Mike Robbins — Sr Engineering Manager at Sikorsky Aircraft

Dan Schuster — Sikorsky Aircraft

Mark Alber — LM Fellow, Advanced System Design at Sikorsky Aircraft

Dan Newman — Senior Technical Fellow / Chief Engineer Advanced VTOL at the Boeing Company

Elia Gianopoulos — The Boeing Company

Pieter Einthoven — Associate Tech Fellow at the Boeing Company

Thomas Zientek — The Boeing Company

University of Maryland Faculty

Dr. Inderjit Chopra — Distinguished University Professor and Alfred Gessow Professor, Director of Alfred Gessow Rotorcraft Center (AGRC), Department of Aerospace Engineering, University of Maryland, College Park

Dr. Vengalattore T. Nagaraj — Research Scientist, Department of Aerospace Engineering, University of Maryland, College Park

Dr. James D. Baeder — Professor, Department of Aerospace Engineering, University of Maryland, College Park

Dr. Anubhav Datta — Associate Professor, Department of Aerospace Engineering, University of Maryland, College Park

Alfred Gessow Rotocraft Research Center Graduate Students

Cheng Chi

Fredrick Tsai

Shashank Maurya

Abhishek Shastry

Yong Su Jung

James Sutherland

Seyhan Gul



Alfred Gessow Rotorcraft Center
Department of Aerospace Engineering
University of Maryland
College Park, MD 20742 U.S.A.

To the Vertical Flight Society:

The members of the University of Maryland Graduate Student Design Team hereby grant VFS full permission to distribute the enclosed Executive Summary and Final Proposal for the 38th Annual Design Competition as they see fit.

Thank you,
The UMD Graduate Design Team

Contents

1	Introduction	1
1.1	Existing UAVs	1
1.2	Demand for Medical Equipment Delivery VTOL Aircraft	2
1.3	Safe System Design	3
1.4	Mission Productivity	4
1.5	Payload Handling	4
2	Mission Profile	4
2.1	Local Delivery and Logistics Mission	4
2.2	Concept of Operations	5
3	Configuration Selection	7
3.1	Voice of the Customer	7
3.1.1	Design Drivers	7
3.1.2	Analytical Hierarchy Process (AHP)	9
3.2	Configurations Considered	10
3.3	Selection of Configuration using Pugh Matrix	13
3.4	SMR vs Tandem	13
3.4.1	Implications of Loading and Unloading Mechanism	14
3.4.2	Outer Mold Line (OML) Development	14
3.4.3	Aerodynamic and Performance Analysis	15
3.5	Thrust Compounding Assessment	16
4	Loading and Unloading Mechanism	17
4.1	Mechanism Requirements	17
4.2	Mechanisms Considered	17
4.3	Comparison, Evaluation, and Selection	20
5	Vehicle Sizing	22
6	Airframe Design	22
6.1	Outer Mold Line (OML)	22
6.2	Aerodynamic Optimization	23
6.3	Material Selection	27
6.4	Landing Gear Design	28
6.5	Fuselage Structure	31
6.6	Payload Handling	33
6.7	Internal Layout	36
7	Rotor Design	38
7.1	Blade Aerodynamic Optimization	38
7.2	Blade Structural Design	41
7.2.1	Structural Design	43
7.2.2	Fan Plots	44
7.3	Actuator Design	44
7.4	Hub Design	45
7.5	Swashplate Design	45

8 Propulsion System Design	47
8.1 Candidate Engines	47
8.2 Engine Selection	49
8.3 Engine Installation and Operation	51
8.4 Fuel System	52
9 Transmission Design	52
9.1 Overview	52
9.2 Gearboxes and Synchronizing Shaft	54
9.3 Drivebelt design	58
9.4 Clutch System	59
10 Avionics	60
10.1 Sensing Suite	60
10.2 Processing Suite	62
10.3 Autonomy Architecture	63
10.4 Communications System	65
10.5 Health and Usage Monitoring System	66
10.6 Thermal Management System	66
10.7 Mounting and Vibration Isolation	67
10.8 Weight, Power and Cost Summary	68
10.9 Electrical Power Components	68
11 Weight and Balance	69
12 Vehicle Performance	70
12.1 Performance Model Validation	70
12.2 Hover	71
12.3 Level Flight, Climb, and Autorotation Performance	73
12.4 Productivity	76
13 Trim and Flight Dynamics	78
13.1 Control Scheme	78
13.2 Trim Strategy	79
14 Safety	81
14.1 Preliminary System Safety Analysis	81
14.2 Critical Parts	87
14.3 Autorotation	89
14.4 Safety Features	89
15 Acoustics	89
16 Ground Operations	92
16.1 Ground Control Station	92
16.2 Servicing	93
16.3 Staging and Tear Down	93
17 Certification	94

18 Cost Analysis	95
18.1 Method	95
18.2 Purchase Price	95
18.3 Maintenance Cost	95
18.4 Operational Cost	95
19 Multi-Mission Capability	96
19.1 Commercial Delivery	96
19.2 Agriculture	96
19.3 Emergency Personnel Hoisting	96
19.4 Search and Rescue	97
19.5 Shipboard Supplies	97
19.6 Airborne Data and Communications relay	97
19.7 Geographical survey	97
19.8 Surveillance, Inspections and Monitoring	98
20 Summary	98

List of Figures

1.1	Autonomous UAVs	1
1.2	Autonomous medical delivery UAVs	2
1.3	Alicorn performing a mission	3
2.1	Logistics delivery mission profile.	5
2.2	Local delivery mission profile.	5
2.3	Concept of operations (ConOps) for dropping package at desired location.	6
3.1	Normalized driver weights	9
3.2	Configurations considered	11
3.3	Conceptual drawing of fixed wing aircraft with ducted fans in body	12
3.4	Displacement plots for semi-monocoque structure	14
3.5	Side by side OML comparison of SMR and tandem configurations	14
3.6	Flowpaths for SMR and tandem configurations	15
3.7	Power vs airspeed for SMR and tandem	15
3.8	Power required for propeller thrust compounding vs. conventional tandem rotor configuration	16
4.1	Designed mechanisms for loading and unloading	19
4.2	Unloading sequence of the winch-assisted gravity cart mechanism	21
4.3	Unloading sequence of the linear-actuated cart mechanism	21
6.1	CFD results for the initial fuselage geometry	23
6.2	Vortex generators (VG) and the resulting vorticity and airflow	24
6.3	Long Oval fuselage family	25
6.4	Wake of Long Oval A and D	25
6.5	Pointed nose versions of Long Oval A	26
6.6	Final fuselage shape	26
6.7	Airflow around the final fuselage	27
6.8	Fixed landing gear options considered	29
6.9	Final retractable landing gears	29
6.10	Stress diagrams for landing gears	30
6.11	Preliminary Structure	31
6.12	Mounting frame of the engine	31
6.13	Stress diagram for limiting case	32
6.14	Displacement diagram for limiting case	32
6.15	The winch assisted gravity cart	33
6.16	Electromagnetic Release	33
6.17	Caster steering lock hook	33
6.18	Cargo Bay	34
6.19	Anti-braking hook	34
6.20	Auto-braking Mechanism	35
6.21	Chassis stress analysis	35
6.22	Ramp and Clamshell Doors	35
6.23	Internal layout overview	36
6.24	Engine bay inspection doors	37
7.1	Mach and Re number distributions in hover and cruise	39
7.2	Variation of $(c_l/c_d)_{max}$ with Mach number for different airfoils	40
7.3	Lift and drag characteristics for the selected airfoils	40
7.4	Refined Pareto plot for rotor blade design	41
7.5	Final blade design	42
7.6	Internal blade structure	43

7.7	Fan plot for flap and lag	44
7.8	Two EHAs in series	45
7.9	Rotor hub	46
7.10	Articulation arm assembly	46
7.11	Swashplate assembly	47
8.1	Powerplant selection finalists	48
9.1	Light helicopter belt drive systems, from left to right: Dynali H3 manned helicopter, Dynali H3 UAV versions prior to shipment for agricultural/logistics/surveillance modification, and Robinson R44 Raven	52
9.2	Front-left isometric view of engine and transmission	53
9.3	Transmission schematic	53
9.4	Forward gearbox	56
9.5	Optibelt V-Belts	58
9.6	Engine, clutch, and alternator integration with transmission	59
10.1	Primary situational awareness sensors	60
10.2	Autopilot and its associated components	60
10.3	Garmin GAP-26 Pitot (heated)	60
10.4	Onboard Processors	62
10.5	Central avionics rack: Internals	63
10.6	Autonomy Architecture	64
10.7	Animal, human, and bird detection	65
10.8	Wire Detection Pipeline	65
10.9	Communications System	66
10.10	Central avionics rack: Liquid Cooling System.	67
10.11	Custom designed liquid cooling block	67
10.12	Vibration isolation	67
10.13	Plane Power AL24-70 Alternator	69
10.14	EarthX ETX680-24-TSO 24 V battery	69
12.1	Performance model Vvalidation	71
12.2	Hover performance (out of ground effect)	72
12.3	Level flight performance, Logistics Mission start weight	73
12.4	Level flight performance, varying gross weight	74
12.5	Climb performance	74
12.6	Variation of allowable payload with range	75
12.7	Autorotation Index	75
13.1	Trim attitude in forward flight	79
13.2	Control and flapping angles in forward flight	80
13.3	Flapping clearance	81
15.1	Observer locations for hover and forward flight	90
15.2	OASPL in dB(A) for hover	91
15.3	OASPL in dB(A) for forward flight	91
16.1	Ground Control Station (GCS)	92
16.2	Alicorn transport vehicle	93
16.3	Skid dollies	93
16.4	Possible blade storage	93
19.1	Ferno Traverse Rescue Stretcher	97
19.2	Combined LiDAR and photogrammetry point clouds.	98
19.3	Thermographic inspection of solar panels.	98
20.1	Alicorn in action	99

List of Tables

3.1	Relationship between customer requirements and engineering design parameters	8
3.2	AHP Matrix	10
3.3	Pugh Matrix	13
4.1	Summary of the unloading mechanisms considered	22
5.1	NDARC mass estimate	22
6.1	Comparison of fuselage drag and downforce characteristics of Long Oval fuselage family with original model	25
6.2	Drag area for the variations of Long Oval A model	26
6.3	Fuselage material pros and cons.	27
6.4	Fuselage material safety analysis	28
6.5	Properties for Al 2024-T361 and Celion 3000/E7K8	28
6.6	Equivalent flat plate drag areas for various landing gear designs	29
7.1	Rotor Characteristics	41
7.2	Actuator Requirements	45
7.3	EMC vs EHA	45
7.4	EHA Breakdown	45
8.1	Powerplant performance data for 200 km (108 nmi) Logistics Mission at 1,350 m (4,430 ft), ISA+20 °C (RFP conditions)	50
8.2	Powerplant selection Pugh matrix	51
9.1	Drivetrain component speeds at maximum continuous and maximum rated power settings	54
9.2	Bevel gear material properties	55
9.3	AGMA bending stress for gearbox input pinion teeth	55
9.4	AGMA contact stress for gearbox input pinion teeth	56
9.5	Bevel gear properties	57
9.6	Sync shaft data	57
9.7	Sheave and belt data	58
10.1	Selected LiDARs	61
10.2	Selected Cameras	61
10.3	Alicorn's Processing Suite	63
10.4	Avionics Breakdown	68
10.5	Electrical Power Components	69
11.1	Weight statement for Logistics Mission	70
11.2	Center of gravity and moments of inertia for various configurations	71
12.1	Productivity for Logistics Mission, minimum speed and fuel required	76
12.2	Productivity for Local Delivery Mission, minimum speed and fuel required	77
12.3	Maximum productivity for Logistics Mission	77
12.4	Maximum productivity for Local Delivery Mission	78
13.1	Trim control strategy	79
14.1	Functional Hazard Assessment (FHA)	81
14.2	Severity definitions modified from SAE ARP4761	83
14.3	Preliminary System Safety Assessment of Avionics, Electrical, and Engine	84
14.4	Severity and Probability based on Failure Effect	85
14.5	Mitigations to the hazards mentioned in Table 14.4	86
14.6	Critical Parts and the replacement/overhaul schedule	88
15.1	Maximum OASPL in different phases of the mission	91

RFP Deliverables

RFP Deliverable	Section
General description of vehicle	5
Design trades to substantiate safety philosophy and claims	all sections
Specific design decisions to achieve acceptable safety	all sections
Productivity metric	12
Segment-wise summary of mission performance	12
Performance data at individual component level	6,7,8,9,10
Description of payload sequence	6
Description of the turn-time procedures	16
Validation of the design of aircraft elements	6, 7, 8, 9, 10
Weight statement	11
Means-to-certification	17
Detailed assessment of safety claims	14
Assessment of critical parts operational life	14

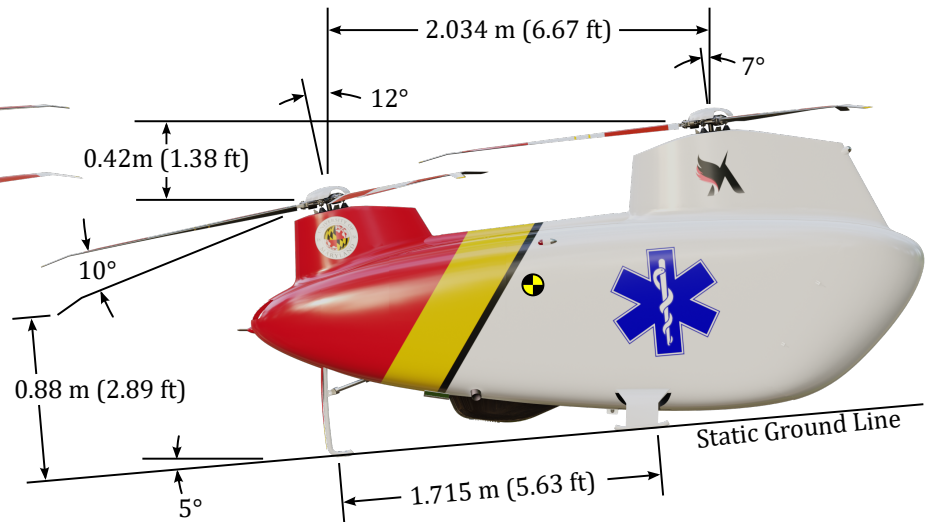
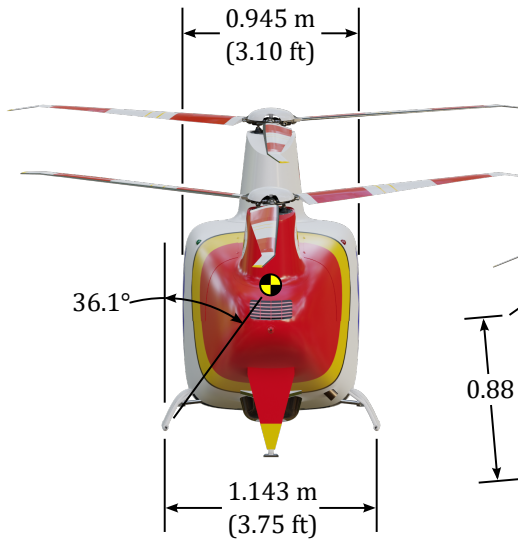
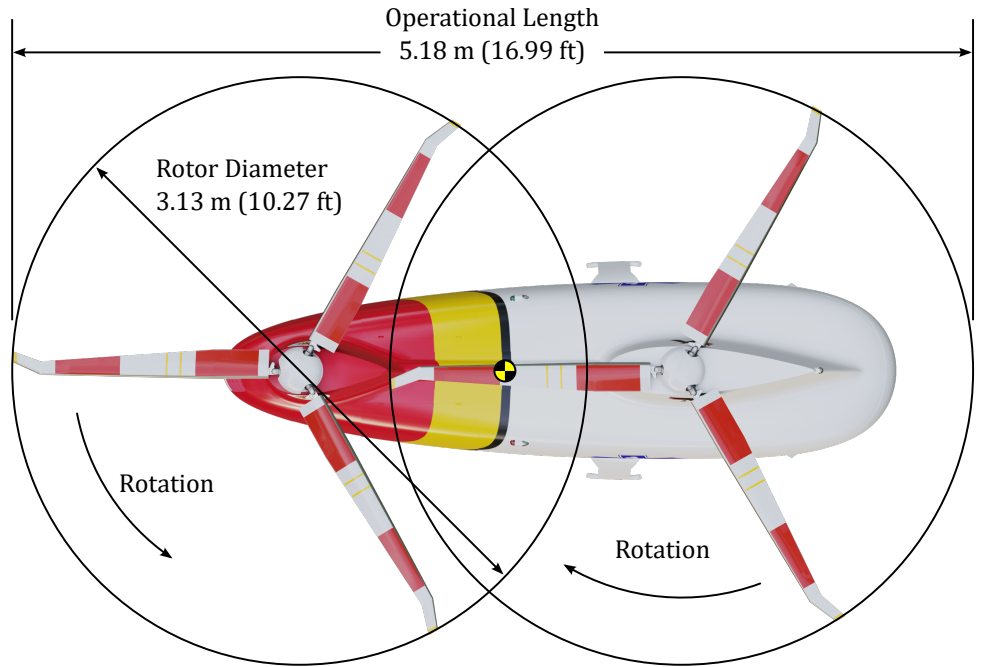
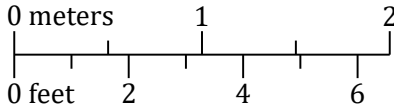
Key Features of Alicorn

Feature	Requirement	Alicorn's Value
Block time (Local Delivery)	28 min	23 min
Block time (Logistics)	75 min	51 min
Productivity (Local Delivery)	-	6.2 m/s (12 kt)
Productivity (Logistics)	-	10.9 m/s (21.2 kt)
GTOW (Local Delivery)	-	288.1 kg (635.2 lb)
GTOW (Logistics)	-	298.3 kg (657.7 lb)
Operational size	6.1 m × 6.1 m	4.6 m × 4.6 m
Maximum speed	-	90 m/s (175 kn)
Empty weight	-	224.7 kg
Maximum payload	-	100 kg
Fuel capacity	-	30 kg (50 l)
Maximum altitude	-	4500 m (15,000 ft)
Installed power	-	104 kW (141 hp)
Rotor radius	-	1.565 m (5.13 ft)
Disk loading	-	192 N/m ² (4 lbft ²)
Drag area	-	0.182
Unloading time	-	24 s
Loading time	-	30 s

Key Specifications

Rotor Radius:	1.565 m (5.13 ft)
Disk Area - Single:	4.92 m ² (52.9 ft ²)
Disk Area - Total:	9.83 m ² (105.8 ft ²)
Root Airfoil:	VR-7
Tip Airfoil:	SSC-A09
Solidity Ratio:	0.0634
Rotor Speed:	1231 RPM
Max Cont. Power:	99 kW (135 hp)
Max Rated Power:	104 kW (141 hp)
Empty Weight:	221 kg (487 lb)
Design Gross Weight:	298 kg (657 lb)

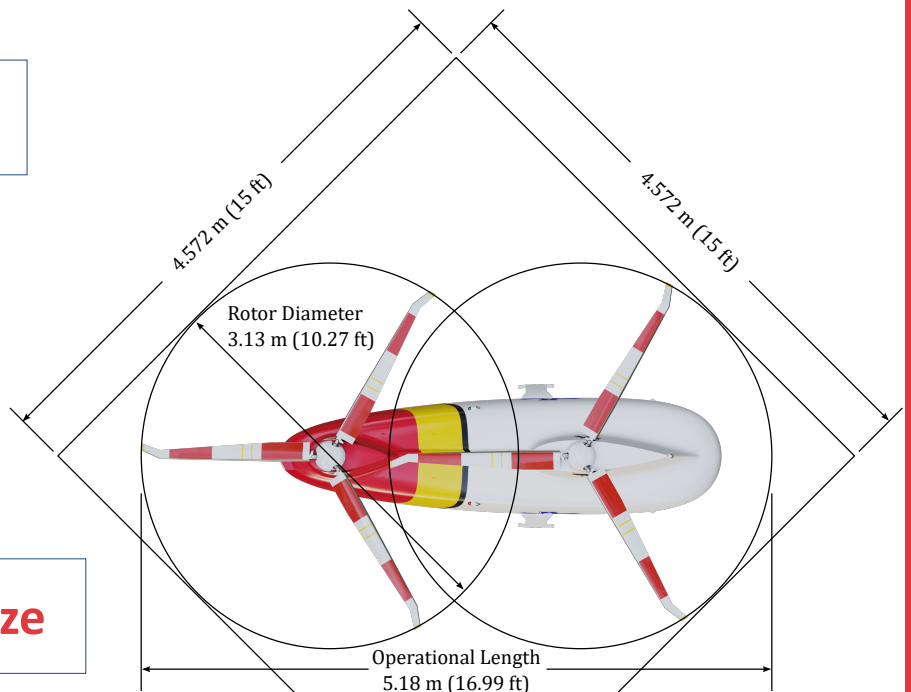
Scale:



Three View Drawing



Operational Size



1 Introduction

The development in unmanned aerial vehicle (UAV) technology has brought about a new era for transportation of supplies and commodities over the past decade. The technology has matured to a level for it to be accepted worldwide as an efficient and reliable form of transportation and to be used extensively for commercial and medical purposes. Automation has taken it one step further to produce autonomous aerial delivery vehicles to be used in various applications such as retail, agriculture, military and healthcare.

1.1 Existing UAVs

Amazon's Prime Air [1] and DHL's Parcelcopter [2] are among the pioneers in experimenting with UAVs for autonomous package delivery. Amazon uses a multicopter and DHL uses a small-scale tilt-rotor aircraft for point-to-point autonomous package delivery but the package sizes and flight distances are quite small. Agras T16 [3] produced by DJI, which is used for pesticide distribution can hover with a heavy payload of 16 kg for 10 to 18 minutes. The Schiebel Camcopter S-100 [4], a small single main rotor helicopter built for intelligence, surveillance and reconnaissance is heavier and can carry a payload of 50 kg up to a range of 180 km at a maximum speed of 220 km/h. A more extreme case of a heavy lifting autonomous UAV would be the DPI DP-14 tandem rotor helicopter [5] which is being developed for potential unmanned medical missions that include supplying of time-critical medical and relief supplies to the battlefields and isolated areas during a natural disaster. It is being designed to have a maximum speed of 195 km/h and a useful load capacity of 195 kg, which currently appears at the top of its class of vehicles.



(a) Amazon Prime Air



(b) DHL Parcelcopter



(c) DJI Agras T16



(d) Schibel Camcopter



(e) DPI DP-14

Figure 1.1: Autonomous UAVs

Autonomous aerial delivery is widely envisaged in the healthcare sector with the primary purpose being the transportation of organs and medical supplies. Among the several UAVs that cater to this market segment, Zipline [6], a San Fransisco based UAV startup, is at the pinnacle. It is a small-scale fixed wing aircraft that currently operates in Rwanda, delivering blood, vaccines and other life saving medical supplies from distribution centers covering the entire country. It has revolutionized the healthcare system in Rwanda

by cutting down the 4 hour ground transportation time to 15 minutes. It has expanded to other African countries such as Ghana and Nigeria as well. Flirtey [7], which was founded in 2013 as the first drone delivery service in the world is another growing player in this segment. The hexacopter that autonomously delivers over-the-counter medicine and other supplies to customers has received FAA approval in March 2019 to conduct drone deliveries beyond the visual line of sight.



(a) Zipline



(b) Flirtey

Figure 1.2: Autonomous medical delivery UAVs

The COVID-19 pandemic has augmented the demand for fast delivery of medical equipment and supplies. As “contactless” delivery has become the new normal in package delivery to prevent the spread of the virus, the world is experiencing a paradigm shift in the transportation of medical supplies and consumer goods. Autonomous UAVs have become the focus of attention in this rapidly expanding air transportation sector as they are well positioned to cater to the demands of the pandemic. Their unique ability to deliver packages quickly and safely to precise locations without the need for human intervention is a key step to face the challenges of the pandemic. The vertical lift technology eliminates the need for sophisticated ground infrastructure allowing UAVs to be able to reach unprepared delivery sites such as hospitals, health camps and community centers. Medical and basic supplies can be quickly distributed within large communities or between different communities, especially in a lockdown situation.

1.2 Demand for Medical Equipment Delivery VTOL Aircraft

The existing fleet of package delivery drones has severe limitations in package size, weight, speed, and range, reducing its effectiveness in a future pandemic or a natural disaster. COVID-19 has highlighted the need to transport not only basic supplies but also specialized medical equipment such as test kits and vaccines in large quantities and long distances at high speeds. It also recognizes the importance of air vehicle system safety, especially because most of these packages could potentially be contagious. Therefore, a niche is identified in the UAV segment that can be fulfilled by an autonomous vertical take-off and landing (VTOL) aircraft, specifically designed to address these needs. Alicorn is a tandem rotor helicopter designed by the University of Maryland Graduate Design Team to efficiently deliver a 50 kg payload to end-user customer sites at a 50 km radius, and to logistic centers 200 km away at a speed of 90 m/s (324 km/h or 175 kn). It is named after the horn of a unicorn, which is said to have powers to protect people from contagious diseases. As required by the Request for Proposal (RFP), the vehicle was sized such that it makes a significant difference within a future pandemic or a natural disaster, as it enables rapid transportation of emergency medical equipment and other supplies to the impacted communities.



Figure 1.3: Alicorn performing a mission

1.3 Safe System Design

Aviation System Safety has been an extremely important design feature for all civil aviation. However, the emergence of urban air mobility (UAM) and small unmanned aircraft systems (UAS) has compelled designers to re-evaluate the design processes in such a way that system safety is given the highest priority. With the removal of the pilot, system safety has shifted focus to a robust software architecture that allows the unmanned system to make logical decisions in emergency situations and to safely land the aircraft. This shift has caused Federal Aviation Administration (FAA) and other certification agencies to redefine certifying new manned and unmanned systems. The new policy focuses on tailored certification to the specific aircraft based on unique safety requirements specific to the mission and aircraft allowing for a streamlined process. The design team recognizes this process and has designed the vehicle accordingly, prioritizing on designing a safe aviation system.

Alicorn is designed to have redundancy in most components to ensure that a single failure does not result in an uncontrolled emergency landing. Critical parts have been identified and will be discussed in detail in Section 14. Alicorn is equipped with state-of-the-art avionics to detect obstacles such as power lines, birds, and other aircraft. The autonomy architecture was designed to continuously re-evaluate its emergency landing plan by identifying safe landing sites using the GPS navigation system and on-board cameras as the vehicle progresses along the mission. It uses a suite of powerful processors specialized in different computation tasks to analyze the large amount of data gathered by the sensors to continuously update the flight path and emergency landing paths in accordance with the flight envelop restrictions and design specifications.

1.4 Mission Productivity

According to the RFP, the aircraft productivity is determined by the productivity index given in (1).

$$\text{productivity index} = \frac{\text{payload} \times \text{block speed}}{\text{gross weight}} \quad (1)$$

The two different payload sizes result in a bulky cargo bay, making the fuselage significantly larger compared to the other aircraft in the same weight class. A larger fuselage leads to higher drag, reducing block speed and hence, the productivity. A higher drag area further reduces productivity by increasing the gross weight due to higher engine power requirement. Therefore, the design team identified fuselage shape as a key design parameter at the early stages of the design. Extensive studies were conducted using computational fluid dynamics (CFD) to develop the optimum outer mold line (OML) of the fuselage that incurs the least amount of drag. This improved Alicorn's productivity significantly, providing it with a competitive advantage over its competitors.

1.5 Payload Handling

The large center of gravity (CG) range of the tandem rotor configuration makes it easy for the ground staff to assemble the package, ensuring its CG is within the acceptable limits. This reduces package preparation time and eliminates the need for specialized personnel at the loading sites, which is extremely useful in a crisis. The added convenience in payload preparation increases Alicorn's competitive edge.

Loading and unloading of the payload is a significant design driver that required thorough investigation. A number of loading and unloading mechanisms were evaluated giving consideration to weight, unloading time, and convenience to the customer. Safety of the package, aircraft, ground personnel were considered to be of paramount importance in deciding the final mechanism.

In addition to its primary purpose of serving in a pandemic or other disaster situations, the vehicle was designed to be used in applications such as commercial delivery, agriculture, search and rescue, geographical survey, and surveillance, so that it will not idle until a disaster strikes. It increases the economic value of Alicorn making it a strong player in the UAV market.

2 Mission Profile

2.1 Local Delivery and Logistics Mission

Alicorn's mission profile maximizes system safety and performance requirements set forth by the RFP. The design team identified the need to have a ubiquitous design that allows Alicorn to perform outstandingly in both the local delivery and logistics missions. The mission profiles for the two missions are given in Figure 2.1 and 2.2. The design maximizes the productivity in both missions, by increasing the block speed and reducing the gross weight of the aircraft.

The design team focused on a robust software package to meet to have a high level of autonomy, while maintaining the highest safety standards. Alicorn makes use of a wide range of high-end active and passive sensing equipment with advanced state of the art filtering techniques for reliable and robust long-range obstacle detection even in non-ideal environmental conditions. High powered, heavy-duty processors ensure high-rate, real time execution of localization, mapping, dynamic motion planning, and decision making software modules. These design choices enable quick reflexes for avoiding birds, wires, trees, animals, other aircraft, and any other obstacles at high speeds. Alicorn's Health and Usage Monitoring System (HUMS) detects any mechanical issues within the aircraft to initiate an "auto abort and return to base" if the



issues detected exceed a predetermined tolerance level. The complete sensing suite has a high degree of built-in redundancy which enables consensus based sensor failure detection. If and when consensus cannot be properly reached, then “Severe Major” condition will be declared and the aircraft will rely on the set of sensors that has a general agreement with each other and low stochasticity. The power and thermal dissipation of all the electrical components are also continuously monitored to ensure healthy runtime of Alicorn’s autonomy stack.

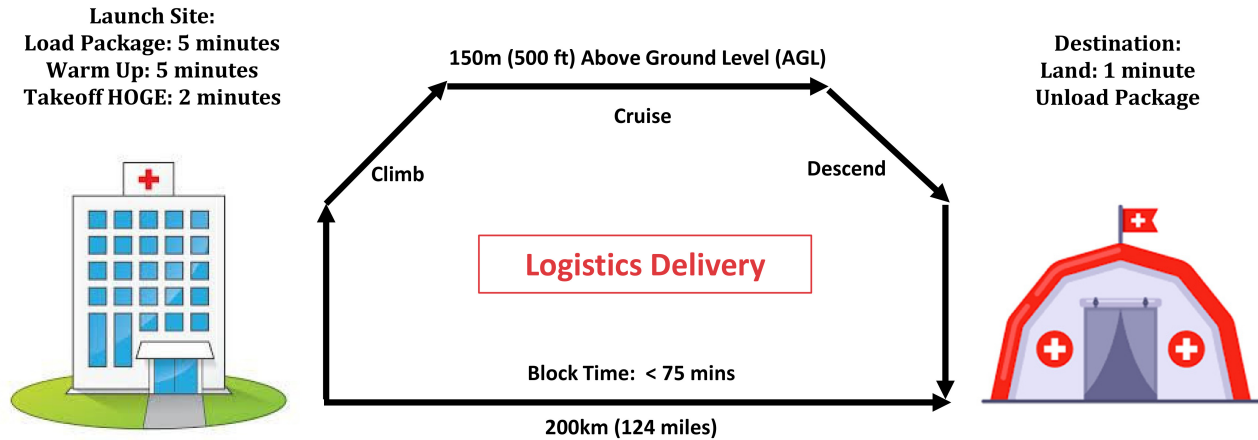


Figure 2.1: Logistics delivery mission profile.

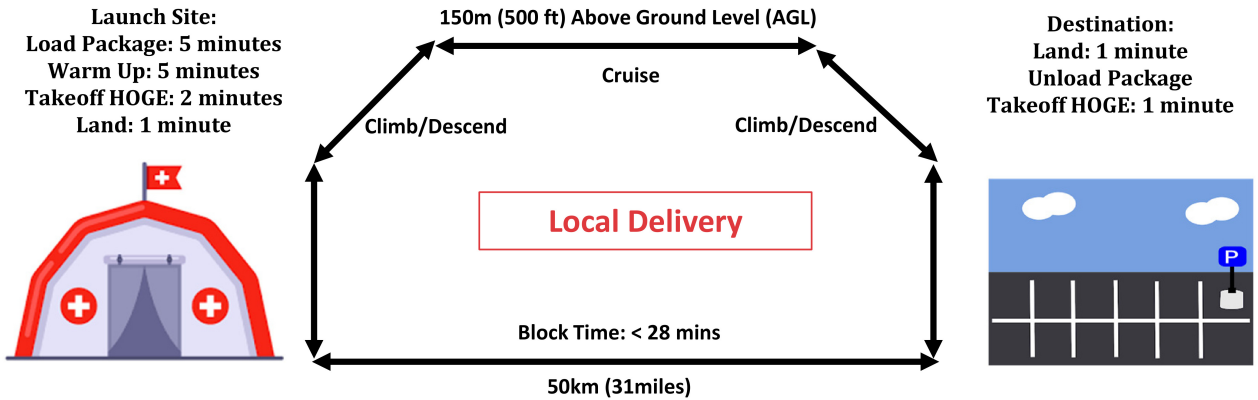


Figure 2.2: Local delivery mission profile.

2.2 Concept of Operations

Alicorn’s concept of operations (ConOps) highlights the importance of system safety as well as completing the mission. ConOps takes the block time described in the RFP and decomposes certain processes required for the aircraft to complete the mission demonstrated in Figure 2.2. Figures 2.3 details a portion of the proposed Alicorn ConOps. Each activity presented describes a stage of the flight operations and signifies the importance of system safety throughout the block time. Using “UAV Engages Rotors”, Alicorn will be designed such that any sensors or systems that detect a Foreign Object Debris/Damage (FOD) will not engage the rotors and impose a safety hazard to the aircraft itself or to the surrounding environment. By deriving this activity, the design team clearly defines what equipment is required (LIDARS, cameras, etc.) and how the software will determine that the surrounding area is clear for it to engage the rotors, emphasizing the importance of system safety in all phases of operation.

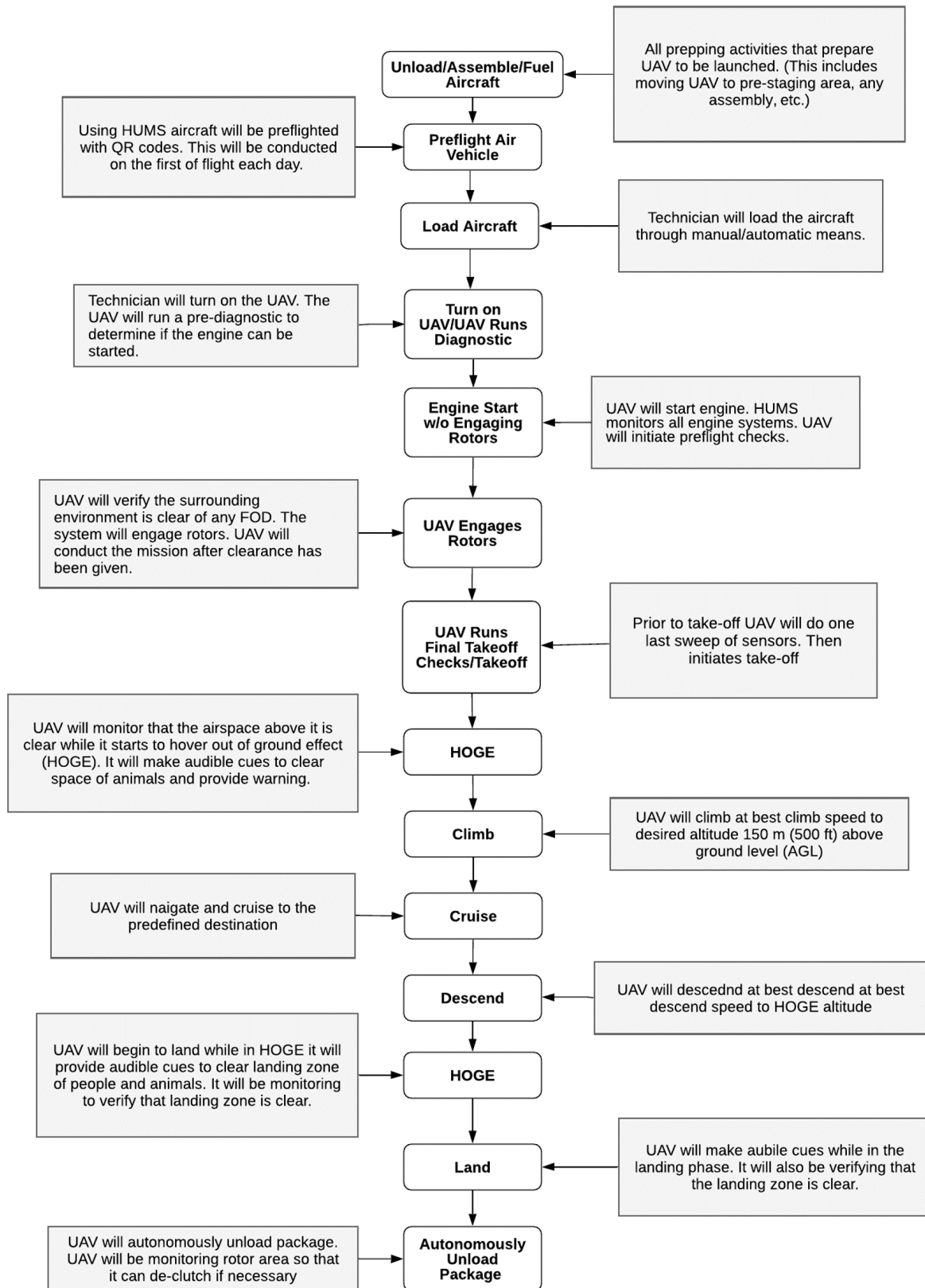


Figure 2.3: Concept of operations (ConOps) for dropping package at desired location.



Alicorn’s ConOps defines the software architecture required for the system to complete the mission with minimum operator intervention. By defining phases of flight, the team identified the key activities that will be implemented within the software of Alicorn, allowing it to remain autonomous throughout the entire mission. Another key importance in defining the ConOps is the design team’s ability to determine what Alicorn shall do in case of an emergency or Severe Major hazard. If a severe major hazard were to occur in cruise, the proposed solution would be to have Alicorn plot a direct course to the desired landing site specified in the RFP Objective:

- Local Delivery Mission: Return to launch site or launch site from destination with full payload,
- Logistics Mission: Return to launch site or destination from destination with full payload,

while monitoring all systems to verify that a catastrophic failure is not imminent. Thus defining the ConOps, allows the design team to make sound safety decisions that will allow Alicorn to beat the competition.

3 Configuration Selection

The configuration selection was considered as a critical part of the design as the decisions taken at this phase have a direct impact on the rest of the design and the lifetime of the vehicle. Therefore, analyzing the mission requirements and understanding the voice of the customer was paramount.

3.1 Voice of the Customer

A thorough assessment of the mission and customer requirements was carried out in order to understand the voice of the customer. The team noted that the term “safe” was mentioned 38 times in the RFP and therefore, system safety was given a special attention right from the beginning. Since the vehicle was to be designed in order to support an initial entry into service in 2025, ease of certification was also identified as a prominent driver. Moreover, the RFP placed a considerable weight on the certification of the vehicle, especially, requesting a means-to-certification.

As both missions were in forward flight for the most part, drag reduction was also identified as an important aspect of the design. The payload was considered to be heavy and bulky for this class of vehicles and therefore, vehicle weight was also given due consideration. These two factors together drive the productivity index for each mission.

The vehicle was primarily designed to assist in a pandemic or natural disaster, and therefore, the payload was identified to be comprised of motion-sensitive medical equipment. In the case of vaccines, the package needs to be held steady during transportation, without changing its orientation [8]. Hence, payload handling was considered to be more critical than for a regular payload. Secure handling of the payload was considered in all three phases: loading, delivery, and unloading.

To further identify how the customer requirements influence the engineering design parameters, a relationship matrix was generated and is shown in Table 3.1. It identified fuselage geometry as a key design parameter that drives the entire design. Therefore, the greatest emphasis was placed on getting the optimum fuselage profile. Engine selection, empty weight fraction, blade design, and material selection were next in importance.

3.1.1 Design Drivers

After a close examination of the RFP eight design drivers were identified to be important enough to drive the selection process of the configuration. The following is a brief description of the design drivers.



Table 3.1: Relationship between customer requirements and engineering design parameters

Legend : Strong Impact = 5 Mid-level Impact = 3 Minimal Impact = 1		weights (0-5)	Aerodynamic performance													Fuselage		Safety, Reliability					Environmental impact					
			Empty Weight	Cruise speed	Tip speed	Discloading	Power loading	Engine selection	Engine SFC	Hinge offset	Blade design	Autorotative index	Flat plate area	Auxiliary power	Wing Morphing	Landing gear morphing	Fuselage geometry	cabin modularity	aviotics	Vehicle monitoring	Environmental Protection	Active/passive noise suppression	Software	MTBF, MTBR	Vibration crash worthiness	Alternate fuels	Material selection	Manufacturability
Operational Reqs.	Cruise speed 200 km/h	5	3.8	5	4.2	3	3.8	4.2	5	4.2	5	3	5	3.8	3.8	4.2	5	2.2	2.2	3	2.2	2.2	3	3.8	3.4	2.6	3.8	3.8
	Payload 50 kg, package dimensions	4.6	5	5	2.6	3.8	3.4	4.6	3.8	3.4	5	3.8	5	3	3	2.6	5	4.6	3.4	2.2	2.6	2.2	1.8	2.6	4.2	2.2	3.8	4.2
	Range 200 km	4.6	5	4.6	3.8	3	5	5	5	3.4	5	3	5	4.2	4.6	4.2	5	2.6	3.4	3	2.2	1	2.6	3.4	1.8	3	3.8	3.8
	Operational size limits	4.6	3.8	3	3.4	4.2	4.2	4.6	3	1.8	3	3.8	3	3	4.6	3.8	5	3.4	3	1	1	1.4	1.4	1	1.8	1.8	3	3.4
	Interchangeability	3	3.8	3	1.8	1.8	2.6	4.2	3	3	3.8	2.2	4.6	3.8	4.6	4.2	4.2	2.6	2.6	1.8	1.4	1	3.4	3	3	1.8	3.4	3.4
Design Consideration	Operation in disaster areas	3.4	3	2.6	2.6	4.2	3.8	3.8	3.8	3.4	3.8	4.2	3	3	3.8	3.8	3.8	4.2	4.6	3.8	3	4.6	4.2	3.8	4.2	4.2	3.8	3.8
	Precision hover and landing/Maneuverability	3.2	4.6	1.8	5	5	4.2	3	1.8	5	5	3.4	1.8	2.6	3	3	3.4	2.2	4.2	3.4	2.2	2.6	4.2	2.2	2.2	2.6	2.6	1.8
	Rapid loading/unloading	4.4	2.2	3	1	1	1.4	1.8	1	1	1.4	1	3	1.8	2.6	2.6	4.6	4.6	3.4	1.4	1.8	1.4	4.2	3	3	1	2.6	2.6
	Low system complexity	2.8	4.2	3.8	2.6	2.6	2.6	3.4	2.2	2.6	3.8	3.4	3.4	3.4	5	5	4.2	5	4.6	4.2	2.2	3.4	3.8	3.4	3.8	3	3.8	5
	Initial operational capability IOC in 2025	4.8	1.4	1	1.8	1.8	1.8	4.2	3.4	1	3.8	3	2.6	4.2	5	4.2	3.4	3.8	5	5	3	5	5	4.6	4.6	3.8	4.2	4.2
	Minimum operational noise	3	2.6	3.8	4.6	4.6	4.6	4.6	3.4	3	4.2	2.6	3	3.4	3	1.8	3.4	1.8	1.8	1.4	4.2	2.2	2.2	1.4	2.6	4.2	3.4	3.4
	Logistical footprint	3.6	4.6	1.8	1.8	2.6	1.8	4.6	2.6	2.6	3.8	2.6	4.2	3.4	5	5	4.6	4.2	3.8	3	3.4	2.2	3	3.4	3.4	3.8	3	3.4
	Vibration reduction	3.4	3.8	4.2	5	5	4.6	4.2	3	4.6	5	2.6	4.2	3.4	3.8	3	5	3.8	2.6	3.4	1	4.2	3.4	3.4	4.2	1.8	4.2	4.6
	CG tolerance	3.4	4.2	3.4	1.8	3.8	3.8	2.2	2.2	3.4	4.2	2.2	2.2	2.2	3.8	2.2	5	4.6	2.2	3.4	1	1	3	2.2	3	1.4	2.2	3.4
	Payload fraction optimization	4.6	5	3.8	3.4	4.2	4.2	4.6	5	2.2	3.8	2.6	4.2	3.8	3.8	3.4	5	4.6	3.4	2.2	2.2	2.6	2.6	2.6	3	3.8	5	4.6
Minimum downwash	3	5	2.6	5	5	4.6	2.6	1.4	2.6	4.6	3.8	1.8	1.4	4.6	1.8	4.2	2.6	1.8	1.4	1.4	2.2	1.8	1.8	3	2.2	2.2	2.2	
Cost and energy	Selling Price	1.4	5	4.6	1.8	2.6	3.4	5	4.6	2.6	4.2	3	2.2	4.6	4.2	4.6	4.2	5	4.6	4.6	5	5	3.8	4.6	4.6	5	5	
	Total life cycle costs	2	5	4.6	2.6	2.2	3.4	5	4.6	2.2	4.2	2.2	3	4.2	4.2	4.2	4.6	3	4.6	4.6	4.6	4.2	4.6	4.2	4.6	4.2	5	4.6
	Operational costs	2	5	4.6	3	2.6	3.4	5	4.6	2.2	3.8	1.8	3	4.2	4.6	4.6	4.6	3	4.6	4.6	4.2	5	4.6	4.2	4.6	4.2	5	4.2
	Energy consumption: hover	3.6	5	1.8	4.6	4.6	4.6	5	5	3	5	3.4	3	2.2	4.6	2.2	4.2	1.8	2.6	2.6	1.4	3.4	2.6	2.2	2.6	4.2	4.6	3
	Energy consumption: cruise	4.6	5	5	4.6	4.2	4.6	4.2	5	3	5	2.6	5	4.2	4.6	4.2	5	3.4	2.6	2.6	1.4	3	3.4	2.2	3	4.2	4.6	3
	Low maintenance	3.4	3.8	3.4	4.2	3.8	3	4.6	3.4	3	4.2	2.2	1.8	3.4	4.2	4.6	4.2	3.8	3.8	4.6	3.4	3.4	3.8	4.6	4.6	3.8	5	4.2
Safety	Pollution	2.4	3.8	4.6	4.2	3.8	3.4	4.6	3.8	1.4	2.2	1	3.8	3.4	2.6	2.2	3.8	1.8	1.4	2.6	1.8	1.8	1.8	1.8	1	4.2	5	4.6
	Operational safety	5	4.2	4.6	5	5	3.8	5	3	3	4.2	5	2.2	4.2	2.6	5	3.8	3.4	2.2	5	1.8	1.4	5	4.6	5	3.8	4.2	3.4
	Crash worthiness	5	5	3.4	4.2	3.8	2.6	5	4.2	2.6	4.2	5	2.2	3	2.2	4.2	4.6	4.2	3.4	3	2.2	1	3.8	3	5	3.4	4.2	3.8
Summary	Post-impact survivability	3.8	3.4	3	1.8	2.2	1.4	5	2.6	1.8	2.2	3.4	1.4	3	1.4	2.6	3.8	2.6	1.8	3	2.2	1	2.2	2.6	3.4	3.4	4.2	3
	Raw Score		385	333	319	333	327	400	331	263	382	290	312	314	354	340	418	323	298	290	208	233	311	290	320	290	369	345
	Percent score		4.6	3.97	3.81	3.97	3.9	4.78	3.95	3.13	4.56	3.46	3.72	3.74	4.22	4.06	4.99	3.86	3.55	3.47	2.48	2.78	3.71	3.46	3.83	3.47	4.41	4.12
	Relative score		0.92	0.8	0.76	0.8	0.78	0.96	0.79	0.63	0.91	0.69	0.75	0.75	0.85	0.81	1	0.77	0.71	0.7	0.5	0.56	0.74	0.69	0.77	0.69	0.88	0.83
	Relative rank		3	10	15	9	12	2	11	24	4	22	17	16	6	8	1	13	19	20	26	25	18	23	14	21	5	7

i. System safety

System safety was identified from the very beginning to be one of the most important design drivers. System safety covers the safety of the entire system including the air vehicle, payload, ground personnel, ground infrastructure and environment. It considers all aspects of human, environmental and vehicle risks, including but not limited to blade strike, bird strike and emergency landing. The configurations that are inherently safer than others, such as those that have autorotative capability score higher in this category.

ii. Block Time

Block time is defined as the time from the start of package loading to end of package unloading. As the productivity index is inversely proportional to block time (Eq.1), it was identified that to increase productivity, both cruise and unloading times had to be reduced. In high speed flight, the cruise speed is mainly driven by the equivalent flat plate drag area of the vehicle because parasitic power dominates over the induced and profile power of the rotor/propeller. Therefore, less draggy configurations scored more in this category. Rapid unloading capability was also considered as equally important in minimizing block time.

iii. Logistics Footprint

The aircraft is designed to operate in a pandemic or natural disaster. Therefore, the logistical support needed by the aircraft including ground transportation, refueling/recharging, and recovery from emergency landings are considered in this category. An aircraft with a lower logistics footprint benefits from being able to easily operate in a pandemic or disaster without incurring a logistical burden.



iv. Payload Handling

The capability of the system to handle the payload safely and carefully during the loading, cruising and unloading phases of the design was considered under payload handling. Configurations that facilitate easy package loading and unloading scored more points.

v. Ease of Certification

The ease and likelihood of the vehicle obtaining FAA certification were considered under this category. Aircraft configurations which have already been certified and are in operation perhaps in another weight class were favorably evaluated. Technology readiness level (TRL) was another key factor in this category.

vi. Payload Fraction

The ratio between the payload and the gross take off weight (GTOW) was considered in this section. Productivity increases with higher payload fraction. Therefore, inherently heavy configurations scored less in this category.

vii. Maintainability and Reliability

This is primarily driven by the longevity of the system components and simplicity of repair. This mainly addresses the ease of maintaining the aircraft. A lower number of moving parts was considered beneficial.

viii. Acoustics

The potential delivery sites of the mission could be hospitals and other health centers, where noise level is of primary concern. Therefore, lower noise emissions become favorable for the successful completion of the mission.

3.1.2 Analytical Hierarchy Process (AHP)

The design drivers were compared against each other to determine the relative importance each driver has in driving the final aircraft configuration. Analytical Hierarchy Process (AHP) was used to quantitatively identify the relative weights of each design driver. Each design driver was assigned a score spanning between 1/9 and 9 depending on the relative importance compared to the others. The score increases with the relative importance and equal importance is denoted by a score of 1. Table 3.2 presents the final scores, which were obtained by averaging the scores of the team members, while maintaining the standard deviation within the acceptable limits. The normalized priority vector was obtained by normalizing each column by its column sum and taking the average of those values.

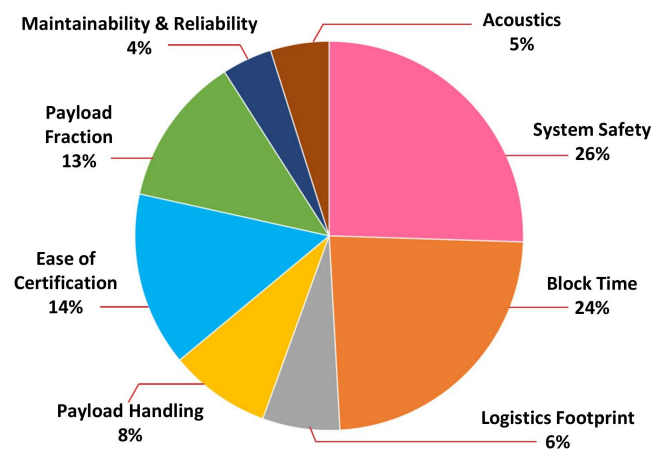


Figure 3.1: Normalized driver weights

Table 3.2: AHP Matrix

	System Safety	Block Time	Logistics Footprint	Payload Handling	Ease of Certification	Payload Fraction	Maintainability & Reliability	Acoustics	Normalized Priority Vector
System Safety	1	1	4	3	2	3	5	5	0.255
Block Time	1	1	4	3	2	2	4	5	0.236
Logistics Footprint	1/4	1/4	1	1/2	1/2	1/3	2	2	0.064
Payload Handling	1/3	1/3	2	1	1/2	1/2	2	2	0.084
Ease of Certification	1/2	1/2	2	2	1	2	3	3	0.145
Payload Fraction	1/3	1/2	3	2	1/2	1	3	3	0.125
Maintainability & Reliability	1/5	1/4	1/2	1/2	1/3	1/3	1	1/2	0.042
Acoustics	1/5	1/5	1/2	1/2	1/3	1/3	2	1	0.049

Figure 3.1 shows the normalized driver weights highlighting the relative importance of each driver in determining the final aircraft configuration. System safety receives the highest percentage weight, being consistent with the RFP requirement of a “safety first” design philosophy. Block time carries the second highest weight, acknowledging the constraints set by the RFP. Ease of certification is in third place, complying with the weight given by the RFP to certify the vehicle and start initial operations in 2025. Payload fraction comes in fourth as it directly affects the productivity of the missions. Payload handling is ranked higher than the remaining drivers due to the sensitivity of the potential payloads. Logistic footprint, acoustics, and maintainability and reliability get 6%, 5% and 4% in accordance with their importance in the mission.

3.2 Configurations Considered

Seven major aircraft configurations were considered as potential candidates in the evaluation process. As the productivity index favors high speeds, thrust compounding was considered in some of the configurations leading to a total of 15 configurations. However, since the accuracy of the evaluation process declines as the number of candidates exceeds a certain level, only the following major configurations were considered in the Pugh matrix, recognizing their thrust compounding capability as a strength.

1. Single Main Rotor (SMR)

Being the most widely used configuration in the VTOL world, the single main rotor (SMR) configuration is best known for its reliability and efficiency in hovering. It uses a single rotor for lift generation and a tail rotor to counteract the torque generated on the main rotor. For enhanced safety during loading and unloading phases, a Fenestron was considered instead of a conventional open tail rotor. The SMR has a higher safety standard due to its autorotative capability and simplicity, however, it suffers from retreating blade stall in high-speed forward flight. Moreover, as rotor performance decreases with high edgewise flow, various thrust compounding arrangements were considered such as adding propellers on the two sides as



(a) Single main rotor (SMR)



(b) Coaxial rotor



(c) Tandem rotor



(d) Tiltrotor



(e) Multicopter



(f) Tailsitter

Figure 3.2: Configurations considered

in the Eurocopter X3 [9] or having a pusher propeller at the back. Two variations of pusher propellers were considered: the tail-mounted thrusting propeller as in Lockheed AH-56 Cheyenne and the Rotoprop concept which was used in the S-61A Demonstrator [10]. Tail rotor failure is also one of the major failure modes seen in a SMR, and becomes a threat for low altitude flight due to wire strike. The tail rotor can also be a concern for the safety of the ground personnel during loading and unloading.

2. Coaxial rotor

Coaxial rotor helicopter consists of two vertically separated counter rotating rotors sharing the same rotational axis. Therefore, it eliminates the need for a tail rotor, which is beneficial in loading and unloading as well as meeting the operational space constraints. However, the counter-rotating rotors increase the mechanical complexity of the rotor hub. The larger hub leads to a significant increase in drag compared to the SMR configuration, which is detrimental for a cruise-dominated mission. Thrust compounding can be used to achieve higher speeds more efficiently.

3. Tandem rotor

Tandem rotor configuration comprises of two longitudinally-separated counter-rotating rotors and therefore, has a higher CG tolerance, which is beneficial for package delivery, especially in a crisis. It provides good lateral gust tolerance and low ground crew vulnerability due to not having a tail rotor. The elimination of a tail boom supports placing a ramp for loading and unloading. The rear rotor is located higher than the front rotor to reduce interaction with the front rotor wake. The two rotors overlap with each other to make the aircraft compact at the expense of some degradation in both hover and forward flight performance.

4. Tiltrotor

A tiltrotor aircraft has tilting proprotors at the tips of the wings. The tiltwing variation, where the entire wing tilts, was discarded due to the mechanical complexity and the instabilities developed in hover. As the tiltrotor behaves as a fixed wing aircraft in forward flight, it would be well positioned for this cruise-dominant mission. However, it would be difficult to meet the operational space limitations as the proprotors are located at the edge of the wing. It would also have a lower payload fraction due to the robustness required for the wing and proprotors. Moreover, the ranges of the missions are too low for a tiltrotor to be efficient.

5. Multicopter

The multicopter, a popular configuration choice in the drone industry, flies using multiple powered rotors mounted on arms. Most package delivery drones are multicopters but their range, speed and load carrying capacity are extremely limited. As there is no aerodynamically shaped fuselage, the multicopter incurs an enormous drag at high speeds. However, as multicopters are already in use for this vehicle class, the certification process would not be difficult. Additionally, its light-weight design would be beneficial in having a higher payload fraction, which would increase productivity. The ease of flight stability and the elimination of swashplate are also seen as added advantages.

6. Fixed Wing with Ducted Fans in Body

As a larger portion of the mission is in forward flight, it was quickly identified that fuselage drag is going to play a major role in the vehicle design. Edgewise flow and exposed rotor hubs reduce vehicle performance in cruise by decreasing propulsion efficiency and increasing drag, respectively. Therefore, a novel design idea was brought up by placing two rotors inside aircraft and covering them with an aperture mechanism in forward flight. A forward mounted propeller provides the propulsion force in forward flight, while the fixed wings provide lift. The rotors are uncovered during take off and landing phases to provide the required lift. Figure 3.3 shows the conceptual drawing of the configuration.

The vehicle would be extremely efficient in forward flight as the fuselage can be shaped to incur the least amount of drag. The elimination of exposed moving blades during take-off and landing would be one of the biggest strengths of this design as it significantly improves the safety of the ground crew. However, placing the rotors inside the airframe consumes the internal volume of the aircraft, which is detrimental, especially considering the bulky payload requirement. Moreover, it would hardly be able to get certified and start operations in 2025 due to its low technology readiness level (TRL).

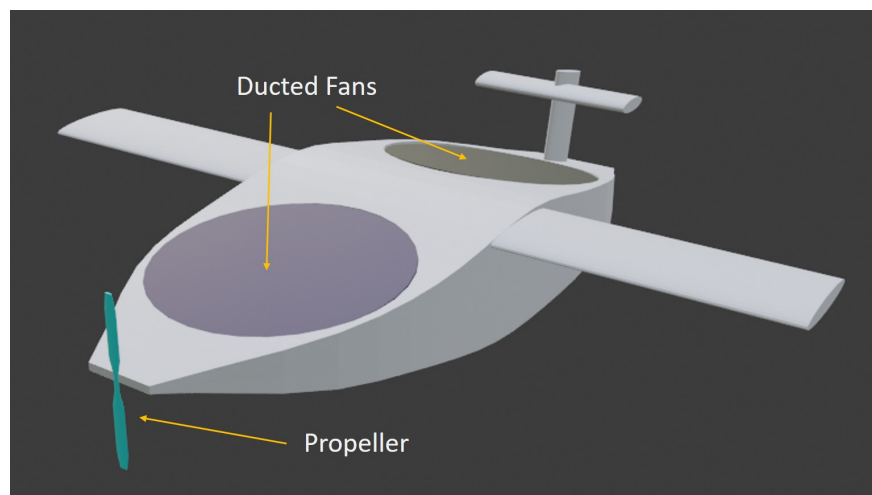


Figure 3.3: Conceptual drawing of fixed wing aircraft with ducted fans in body

7. Tail sitter

Tail sitter is a type of fixed wing aircraft with a propeller at the front. It lands on its tail after tilting 90° from the cruise attitude. Since the propeller has axial flow during the entire mission, it increases the performance of the vehicle resulting in greater productivity. Not having hubs and rotors will help reduce the drag. However, as some of the potentially sensitive payloads such as vaccine vials need to be transported upright, a tail sitter would not be suitable for the medical equipment delivery.

3.3 Selection of Configuration using Pugh Matrix

A Pugh matrix was constructed as shown in Table 3.3 to evaluate the configurations based on the selected design drivers. SMR was used as the baseline and the others were graded on a scale from -4 (much worse) to +4 (much better) and 0 being the neutral point.

Table 3.3: Pugh Matrix

Design Driver	Weights	SMR	Coaxial	Tandem	Tiltrotor	Multicopter	Ducted Fan in Body	Tail Sitter
System Safety	0.255	0	0	0	-4	-2	-2	-3
Block Time	0.236	0	0	0	4	-2	3	2
Logistic Footprint	0.064	0	-1	-1	-4	-2	-4	-2
Payload Handling	0.084	0	0	2	-1	0	-2	-4
Ease of Certification	0.145	0	-1	0	-1	0	-4	-2
Payload Fraction	0.125	0	-1	-1	-3	-1	-3	-1
Maintainability & Reliability	0.042	0	-1	0	-3	-1	-4	0
Acoustics	0.049	0	0	0	-2	1	2	0
Score		0.00	-0.38	-0.02	-1.16	-1.23	-1.25	-1.17
Rank		1	3	2	4	6	7	5

The Pugh matrix ranked SMR and tandem as the top two configurations, giving SMR a slight edge over tandem. Tandem scored higher in payload handling compared to SMR but was determined to be much heavier and has a slightly larger logistic footprint. Hence, it was decided to further analyze these two configurations to make a selection.

3.4 SMR vs Tandem

As one of the primary factors of the design is drag reduction it was decided to generate fuselage shapes for both SMR and tandem in accordance with the mission requirements of operational size limitations and loading/unloading considerations. Both fuselage outer mold lines (OML) were designed to meet the vehicle operational size objective of 4.6 m x 4.6 m. The longitudinal axis of the fuselage was aligned with the diagonal of the limiting operational size square to obtain larger rotor radii for better performance. SMR was able to be designed with a larger rotor disk area of 16 m^2 compared to tandem's effective disk area of 13.6 m^2 .

3.4.1 Implications of Loading and Unloading Mechanism

The other driving factor of the fuselage design was the loading and unloading mechanism. An initial idea brought up by the design team was to have a hole in the fuselage bottom for unloading. However, given the two sizes of the payload, the size of the hole needed to be a significant proportion of the fuselage area, and hence, can lead to a substantial decrease in the torsional stiffness of the fuselage. Therefore, a torsional analysis was performed on a semi-monocoque cylindrical structure with and without a hole at the bottom as shown in Figure 3.4. The structure with the hole was thickened from the outside to have the same torsional stiffness as the one without the hole and the increase in the weight and the outer radius was found to be 62% and 6.2%. Therefore, it was decided to abandon the hole at the bottom and have a ramp at the rear end for loading and unloading.

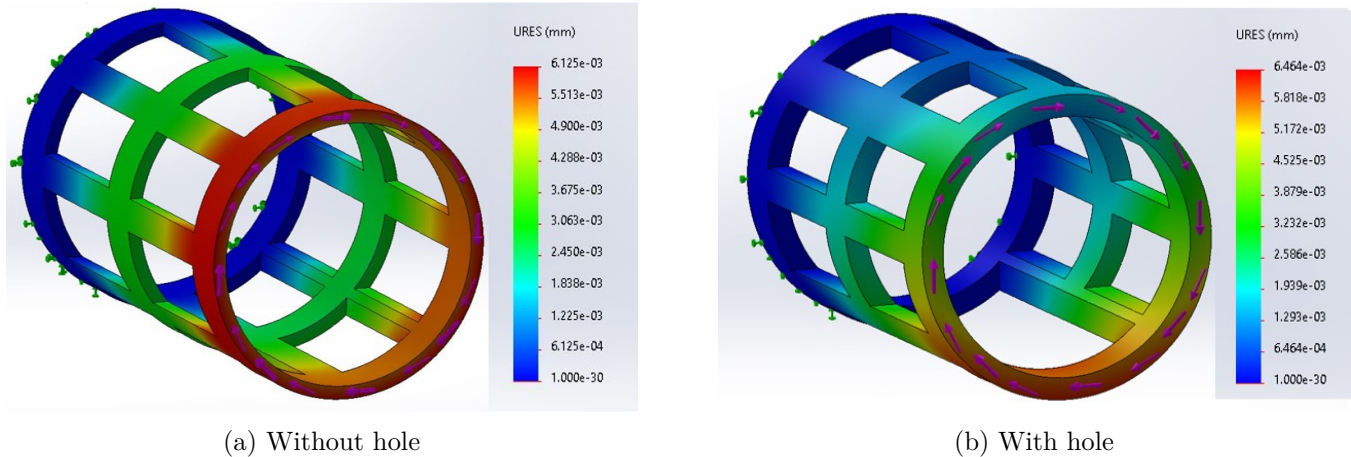


Figure 3.4: Displacement plots for semi-monocoque structure

3.4.2 Outer Mold Line (OML) Development

The outer mold lines (OML) for the two configurations were developed to incorporate a ramp at the rear end. The tail boom of the SMR had to be raised in order to have sufficient clearance from the payload during loading and unloading. This caused the SMR cross section to be slightly larger than the tandem. The resulting OMLs for SMR and tandem are given in Figure 3.5.

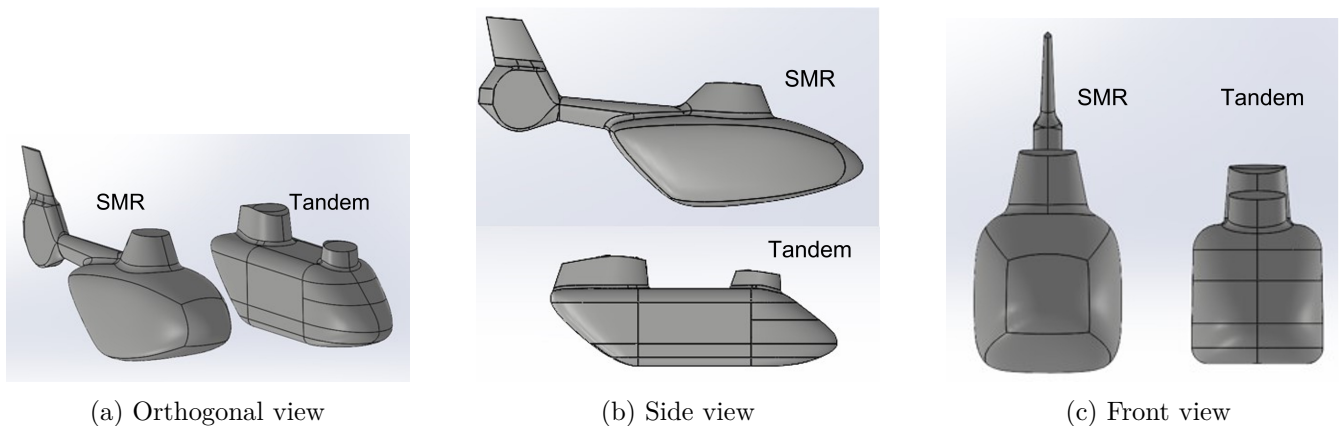


Figure 3.5: Side by side OML comparison of SMR and tandem configurations

3.4.3 Aerodynamic and Performance Analysis

An aerodynamic analysis was performed to identify the drag characteristics of the two geometries using Ansys Fluent [11] CFD program, which is based on Reynolds-averaged Navier Stokes (RANS) equations. The resulting flowpaths are given in Figure 3.6, which clearly shows the two vortices trailing off the rear end of the fuselages. These trailing vortices are the main source of pressure drag. The equivalent flat plate drag areas estimated for the SMR and tandem geometries including the estimated hub drag were 0.436 m^2 and 0.371 m^2 , respectively. Based on these values, the forward flight performance of the two configurations was analyzed using modified momentum theory and the resulting power variation with airspeed is given in Figure 3.7. An estimated GTOW of 300 kg was used for both configurations. The tandem rotors were penalized by an interference factor of 1.1 for hover and 1.75 for forward flight [12].

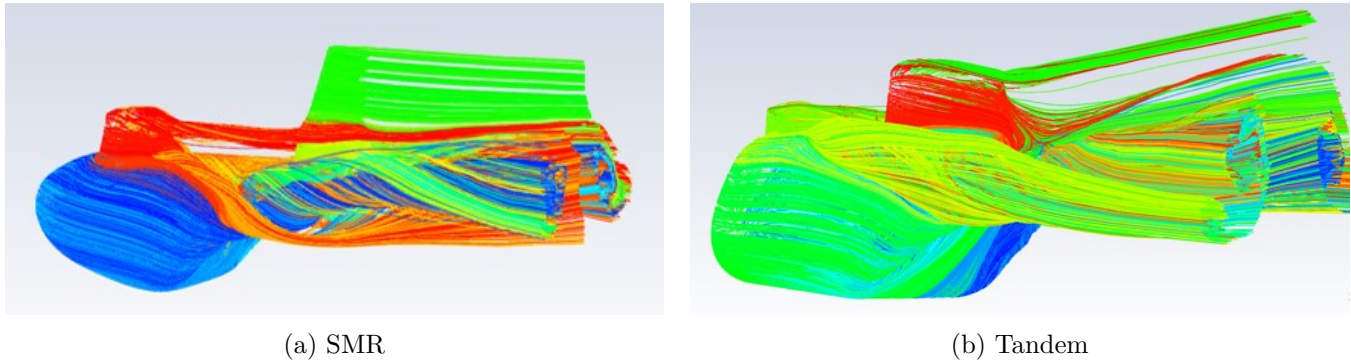


Figure 3.6: Flowpaths for SMR and tandem configurations

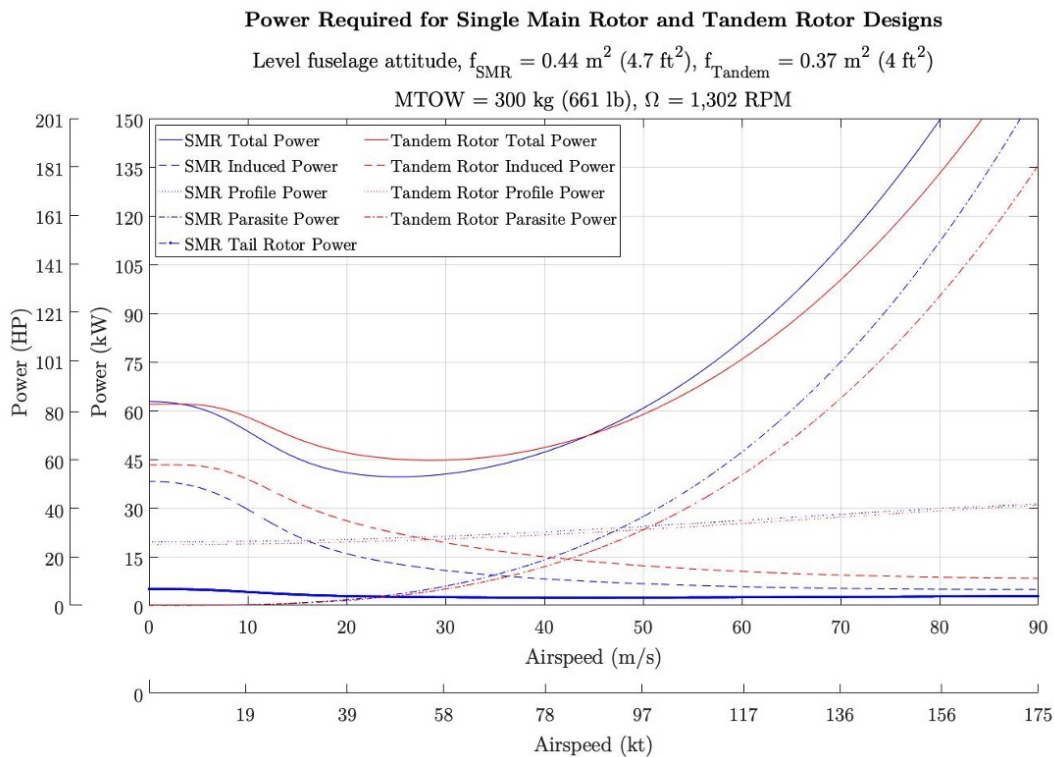


Figure 3.7: Power vs airspeed for SMR and tandem

Even though the tandem configuration shows a higher power requirement than SMR at low speeds due to higher induced power as the rotors are penalized for overlapping, its 15% lower drag compared to SMR benefits it at speeds higher than 55 m/s, where the air vehicle is designed to operate. At the preliminary design cruise speed of 80 m/s, the SMR requires 12% more power than the tandem. This was seen as the deciding factor of the aircraft configuration selection and led the team to choose the tandem configuration over SMR.

3.5 Thrust Compounding Assessment

Because of the high speed required to reduce block time and increase productivity, a thrust compounding system like a propeller could potentially improve performance. A device producing axial thrust can prevent the undesirable nose down pitch attitudes common to helicopters in high speed forward flight because the rotor's requirement to provide forward thrust is offloaded. However, there are many issues with thrust compounding systems on helicopters. Firstly, there is the safety issue of blade clearances between the rotors, fuselage, ground, and personnel. A propeller installation would also increase weight, mechanical complexity, and parasite drag. Because of their higher blade loading, propellers are less efficient than larger diameter rotors in axial flow; a lower amount of the propeller's power required may be needed to overcome the parasite power. Additionally, small diameter fans with higher blade numbers (typical for helicopter thrust compounding) have lower efficiencies.

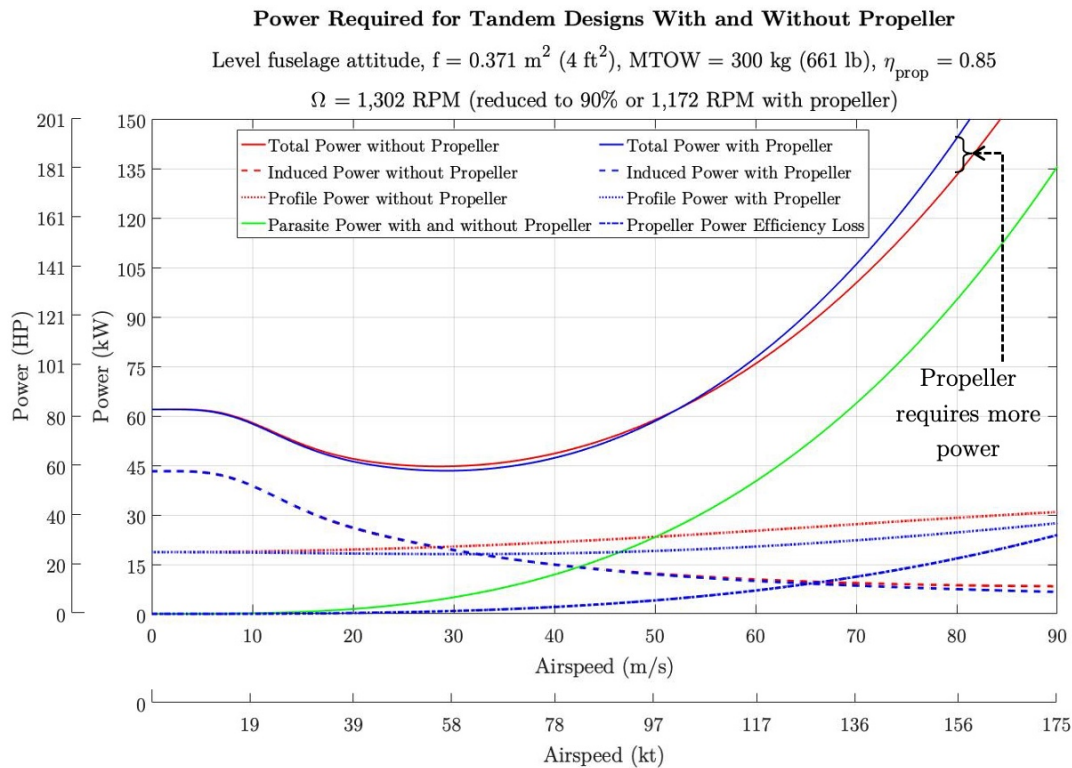


Figure 3.8: Power required for propeller thrust compounding vs. conventional tandem rotor configuration

For a tandem rotor configuration, the nose down attitude required to produce propulsive thrust is easily mitigated using forward rotor shaft tilt and differential collective trim to minimize the fuselage drag at the design cruise speed. The resulting nose up pitch attitude in hover and on the ground, potentially problematic for manned aircraft requiring a good field of view, is actually desirable for this unmanned design because it supports a simple gravity cart unloading system as discussed in Section 4.

Figure 3.8 shows the power curves for a tandem rotor helicopter with and without a propeller, assuming

a realistic 85% propeller efficiency. In other words, 18% ($1/0.85-1$) of the parasitic power is added to the power required (the “efficiency loss”) to account for the propeller’s profile power and other losses not converted to thrust. The rotors were assumed to have an overall induced power factor of 1.1 (κ_{ff}) and overlap factor of 1.75 (k_{ov}) in forward flight as determined from wind tunnel tests for the same tandem geometry [12]. Even with no weight penalty for the thrust compounding installation, a propeller drive clutch to reduce hover power requirements, and decreasing the speed of the main rotors due to their lower thrust requirement, Figure 3.8 shows greater power requirement for a thrust compounding design. Therefore, a tandem rotor configuration without thrust compounding is better suited for the Alicorn.

4 Loading and Unloading Mechanism

Alicorn is designed for delivery missions and therefore, its loading and unloading mechanism deserves a detailed design process with careful considerations to its impact on payload safety, mission performance, overall vehicle design and sensitivity to uncertain conditions. This section describes the selection process of the loading/unloading mechanism by establishing appropriate requirements, designing feasible mechanisms, evaluating its performance and finally choosing the best alternative.

4.1 Mechanism Requirements

Examining the RFP as well as the overall aircraft and mission specifications revealed the following requirements for the design of loading and unloading mechanism.

- **Automation:** The unloading process has to be fully automated. The loading may be semi-automated.
- **Safety:** The designed mechanism should contain the least amount of moving parts to decrease its chances of failure. Structurally, the mechanisms should have a sufficient factor of safety. Extra care must be taken to ensure the safety of the payload during the loading and unloading process. Motion sensitivity of the payload should also be taken into consideration.
- **Weight:** As productivity is impacted by the overall vehicle weight the mechanism needs to be lightweight. 6 kg was considered as the upper limit.
- **Unloading Time:** As the missions are time sensitive, mechanisms that allow faster unloading is preferred. Unloading process starts after the ramp is deployed and ends when the payload clears the aircraft. An unloading time of 18 s was considered as the upper limit.
- **Convenience:** The payload was identified to be too heavy for a human to lift and carry. Hence, mechanisms that assists ground handling were preferred.
- **Ground conditions:** As unloading occurs in a disaster-zone, the ground may be unprepared and hence, the designed mechanisms must take ground conditions into consideration. Wet, soft, uneven or grassy terrain can severely impact the unloading process and can lead to failures.

4.2 Mechanisms Considered

The requirements demand that the efficiency of the unloading process is more important than that of the loading procedure. Therefore, the unloading operation was the primary concern for comparing the performance of different mechanisms. It was identified that loading or unloading from the sides or the bottom of the fuselage with a hole was detrimental to the torsional strength of the fuselage, and therefore results in a significant increase in structure weight (see Section 3.4.1). Therefore, the rear end of the fuselage

was utilized for loading and unloading. Most of the mechanisms that were considered involved utilizing a wheeled cart to unload the payload from the rear door. The only other mechanism that circumvents the use of a cart is the Roller-track mechanism inspired by conveyor belts. The simpler cart options needed the payload to be tightened to the cart and will have the cart left at the unloading site with the package. This leads to carts being accumulated at the unloading site. However, having the payload on a cart increases the convenience of ground handling. The design team considered this to be an added benefit, considering the ease it provides at the unloading site to quickly move the payload to its end location. The design team also considered several alternative cart mechanisms with a higher level of automation to retrieve the cart after unloading, in order to avoid the cart accumulation problem. The following paragraphs present a summary of all the mechanisms considered.

Pure gravity cart: This mechanism (Figure 4.1(a)) involves a cart that rolls along the cargo-bay floor and down the ramp due to gravity during the unloading process. For payload loading, the package has to be secured to the cart, and has to be manually pushed up the ramp. After unloading, the cart remains with the package. This mechanism is the simplest as it involves the least number of parts; a cart frame and four wheels. The wheels have a radius of 76.2 mm and the cart has a ground clearance of 71 mm for better handling and traction characteristics on wet, soft, uneven, or grassy terrain. This mechanism weighs 3.7 kg, and is the lightest mechanism among all the designed alternatives. The unloading time with this mechanism is the least among all the designed alternatives as it accelerates under gravity without any additional mechanism to restrict its momentum. A motion study revealed that the cart takes 4 seconds to clear the aircraft. However, it poses a significant safety hazard for both the package and ground personnel as it has no control during unloading.

Winch-assisted gravity cart: This mechanism (Figure 4.1(b)) includes a winch system attached to the pure gravity cart that enables automated loading and controllability during the unloading process. However, it increases the weight, the number of parts, and the overall unloading time when compared to the pure gravity cart. The weight of this mechanism is 4.3 kg. The cart accelerates down the ramp and the winch restricts its momentum from increasing beyond a threshold, which leads to an unloading time of 6 seconds. This mechanism addresses all the major problems of the pure gravity cart. This solves the problems with the pure gravity cart but the cart remains with the package after unloading.

Winch-assisted electro-permanent magnet cart: This mechanism (Figure 4.1(c)) was designed based on the LogiMover Independent Fork System [13] which involves a ground vehicle with the ability to change its height in order to lift palletized payloads and transport them to its destination. The mechanism uses permanent magnets and electro-permanent magnets (EPM) mounted on the cart chassis and wheel base respectively to change the height of the cart. The designed electro-permanent magnet consumes 1W of power while it is magnetizing/de-magnetizing, which only lasts for around 2 seconds. Its continuous power consumption is negligible and its repulsion force is extremely high when paired with N52 grade Neodymium magnets making it suitable for lifting the cart up by an estimated 5 mm displacement. The winched version of this mechanism pulls the cart into the cargo bay using a winch system while loading and retrieves the cart while unloading. Since this mechanism needs a pallet to work, the pallet will have to be left behind creating a logistics issue. However, the major problem with this mechanism is its small wheels which are needed for the cart to slip under the pallet during its retrieval. This necessitates a prepared flat surface at the delivery site — a demand that may not be satisfied always. The weight of this mechanism 4.3 kg, and its unloading time is 14 seconds. Approximately 40% of the unloading time is due to the cart retrieval process.

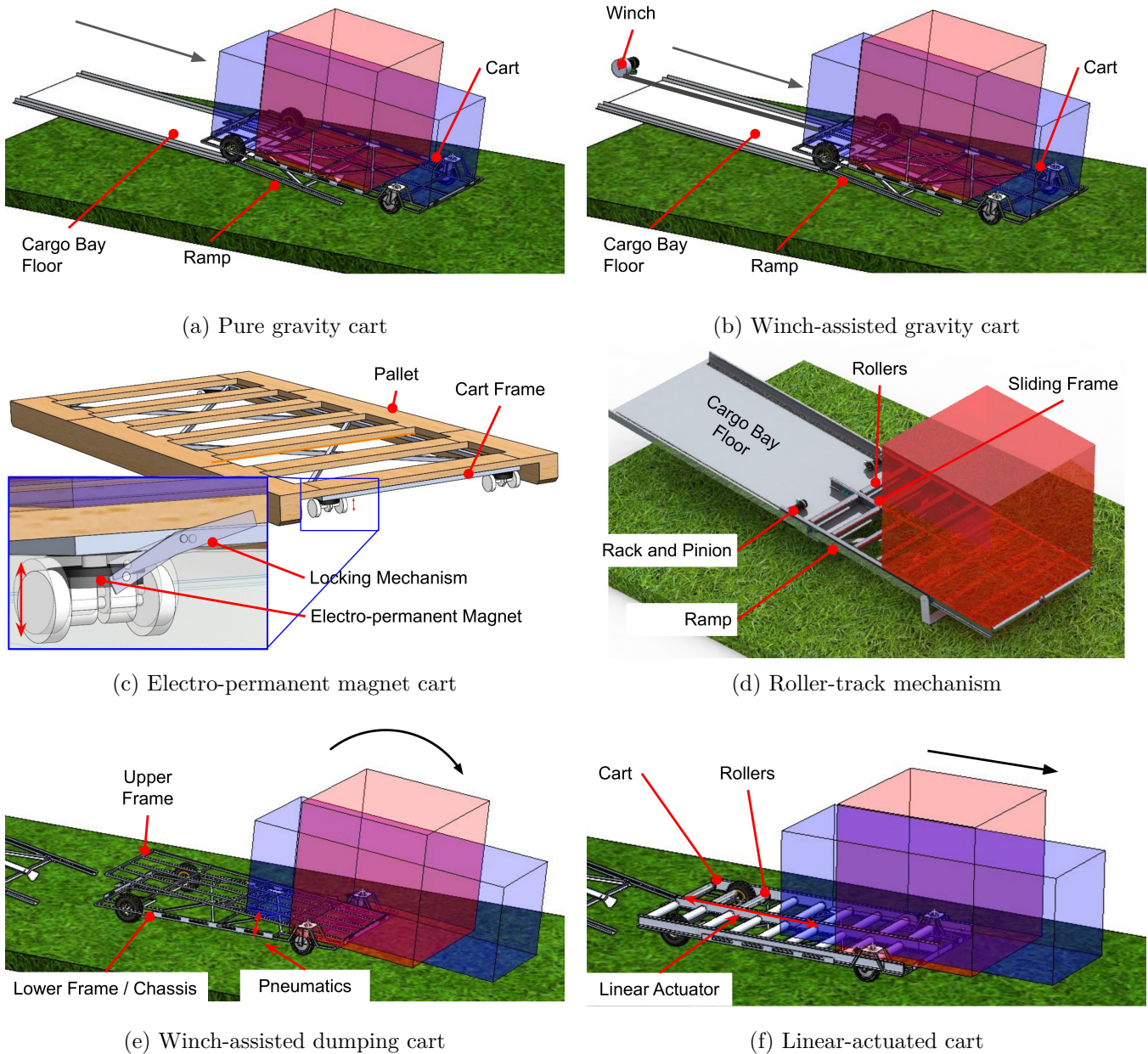


Figure 4.1: Designed mechanisms for loading and unloading

Motorized electro-permanent magnet cart: This mechanism is a motorized version of the Electro-Permanent Magnet Cart. In this version the winch system is replaced by motorized wheels giving the cart a self-driving ability. This fully automates the loading and unloading process. Adding a battery and associated electronics lead to a weight of 4.7 kg. The motors and the battery were selected based on 10° incline conditions and 10 min operation requirements.

Winch-assisted dumping cart: This mechanism (Figure 4.1(e)) was designed with the objective of leaving nothing else but the payload at the delivery site. It adds a dump-truck mechanism and an upper frame on the Winch-Assisted Gravity Cart’s chassis. The mechanism changes the orientation of the upper frame using pneumatics that are powered using a compressed air canister. Three pneumatic cylinders of

20 mm bore and 50 mm stroke are mounted on the bottom frame which requires a minimum of 87 psi of compressed air to lift the payload. The upper frame has passive rollers to assist the payload in sliding down during unloading. After the payload makes contact with the ground, a winch mechanism pulls the cart into the cargo-bay. This mechanism solves the low-clearance issue of the electro-permanent magnet cart mechanism with less number of parts. However, the mechanism weighs 6.4 kg and its unloading time is 16 seconds. Since its weight has already crossed the upper limit, its motorized version is not considered for the selection process as motorizing 76.2 mm radius wheels requires much heavier motors compared to the small wheels of the electro-permanent magnet cart.

Roller-track mechanism: This mechanism (Figure 4.1(d)) consists of multiple rollers mounted below a frame that slides on tracks mounted to the cargo-bay using a rack and pinion arrangement. The tracks are aligned with the frame using small alignment rollers. The ramp acts as an extension to the cargo-bay floor so that a sufficient clearance of the payload with the aircraft is maintained for closing the ramp and clam-shell doors. The mechanism's analysis revealed that the frame will experience a momentary cantilever load when the payload is rolling-off the end. Hence, the frame had to be designed with two C-beams at the sides and an I-beam at the middle to handle the cantilever load. Therefore, total weight of this mechanism goes up to 8.2 kg. After selecting the pinion-gear motor and performing a motion study, the resultant unloading time is 20 seconds. Both the weight and time exceed the upper limits. Additionally, the total number of moving parts is 101, which creates a very high risk of failure.

Linear-actuated cart: This mechanism (Figure 4.1(f)) fuses the roller track and the winch assisted gravity cart mechanisms. The cart frame is modified so that it contains rollers for the payload to slide on. It also has a linear actuator to force the payload out during unloading and a locking mechanism to longitudinally restrain the payload during the loading processes. The linear actuator consists of a motor with a lead-screw gear attachment. This mechanism solves majority of the issues with the roller track mechanism but its estimated weight is 5.9 kg and unloading time is 18 seconds which meet the upper limits.

4.3 Comparison, Evaluation, and Selection

A performance summary of all the loading/unloading mechanisms that were analyzed is presented in Table 4.1. The pure gravity cart is the lightest and fastest among all the alternatives, but its payload damage probability is high and hence it was rejected. The mechanisms utilizing electro-permanent magnets have too low ground clearance and hence they were also rejected. The winch-assisted dumping cart, the roller track mechanism, and linear actuated cart mechanisms are heavy, slow, and pose a subjectively medium damage risk to the payload as they involve dropping the payload from a height of about 50 mm. Therefore, the winch assisted gravity cart was selected as the loading and unloading mechanism as it is the second lightest, second fastest, with enough ground clearance and relatively low payload damage probability. Additionally, it also provides the personnel at the delivery site with the convenience of having the payload on wheels. Figure 4.2 shows the payload unloading sequence of the winch assisted gravity cart mechanism. A detailed design of the selected mechanism i.e., the winch assisted gravity cart is presented in Section 6.6.

Alicorn is primarily designed to use the winch assisted gravity cart mechanism, but it also allows the use of the other cart mechanisms without any modification to the cargo bay. If a customer prefers not to have the cart left at the landing site, the design team recommends the use of the linear actuated cart mechanism, because of its lower weight and better efficiency compared to the others. Figure 4.3 shows the payload unloading sequence of the linear actuated cart.

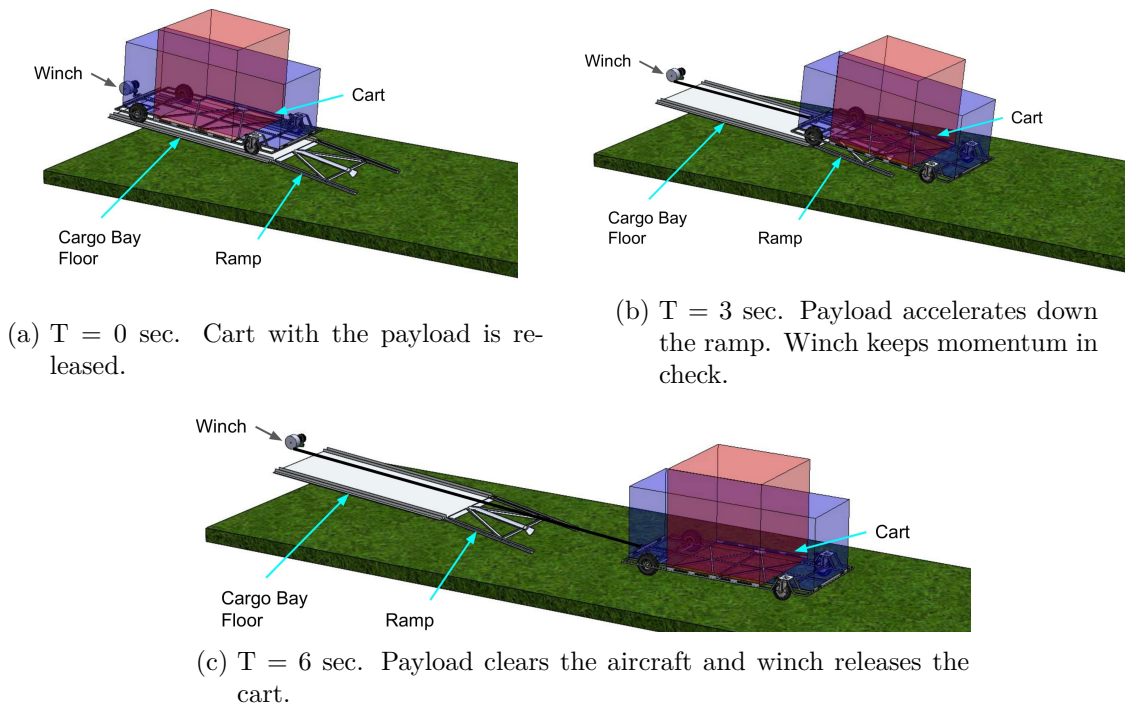


Figure 4.2: Unloading sequence of the winch-assisted gravity cart mechanism

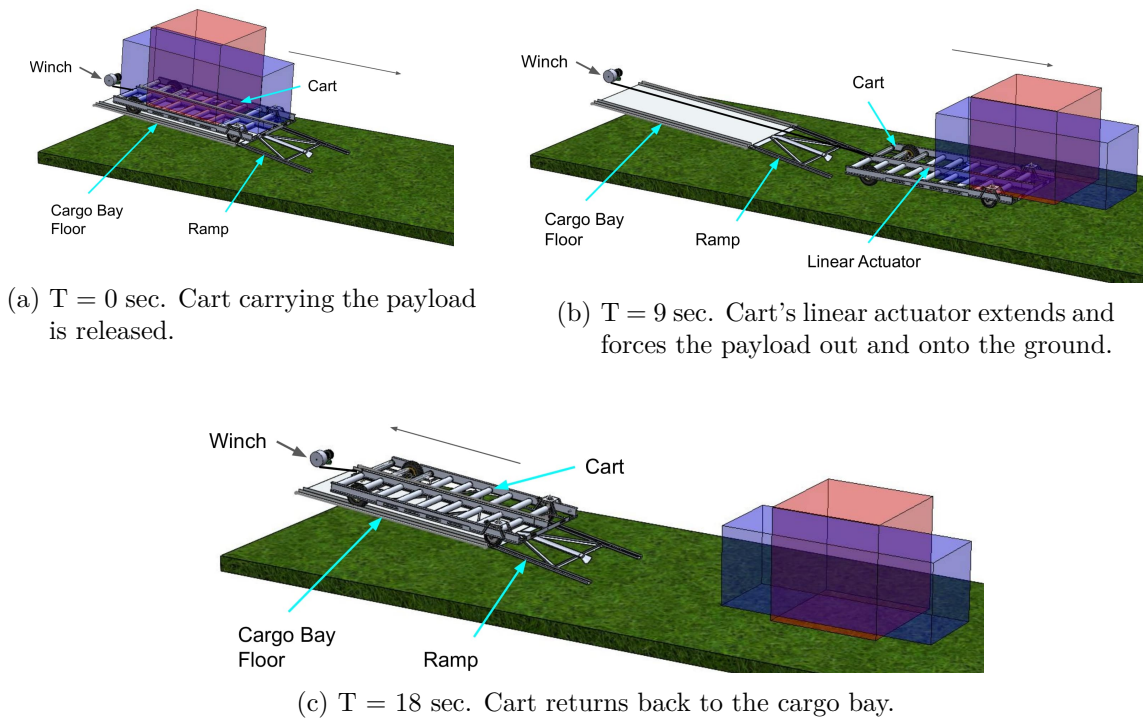


Figure 4.3: Unloading sequence of the linear-actuated cart mechanism

Table 4.1: Summary of the unloading mechanisms considered

	Pure gravity cart	Winch assisted gravity cart	Winch assisted EPM cart	Motorized EPM cart	Winch assisted dumping cart	Roller track mechanism	Linear actuated cart
Weight(kg)	3.7	4.3	4.3	4.7	6.4	8.2	5.9
% of GTOW	1.22 %	1.42 %	1.42 %	1.55 %	2.11 %	2.7 %	1.95 %
Unloading Time (s)	4	6	14	14	16	20	18
% of Block Time (Local Delivery)	0.2 %	0.3 %	0.77 %	0.77 %	0.88 %	1.11 %	1 %
Ground Clearance (mm)	71	71	2.5	2.5	71	N/A	71
Number of Parts	5	6	15	19	11	101	9
Damage Risk	High	Low	Low	Low	Medium	Medium	Medium

5 Vehicle Sizing

Having determined that the aircraft was a 1.565 m (5.13) rotor radius tandem rotor helicopter in the 300 kg (660 lb) class in Section 3, NASA's Design and Analysis of Rotorcraft method was used to initially size the component masses [14]. The values are presented in Table 5.1.

The performance model initially used for configuration selection in Section 3 was used to analyze engine sizing in Section 8.

Although it was expected that through structural and aerodynamic optimization the mass and performance requirements would decrease, this 383 kg (845 lb) gross weight was used to design the rotor and airframe. Only after the individual components were designed did the mass decrease to approximately 300 kg. However, a result of this initial sizing is that the aircraft can carry payloads over 100 kg, well in excess of the 50 kg RFP payload.

6 Airframe Design

6.1 Outer Mold Line (OML)

The fuselage shape was identified as a key design driver because of the bulky payload, and therefore, work on the fuselage outer mold line (OML) was begun at an early stage. Preliminary fuselage shapes were created to evaluate the drag characteristics using RANS based CFD. Early iterations focused mainly on containing the package and creating an aerodynamic shape while accounting for notional component and structure sizes. As the interior design and package loading and unloading mechanism was refined the OML design was able to be refined as well.

Table 5.1: NDARC mass estimate

System/ Component	kg	lb
Rotor Blades	11.6	25.6
Rotor Hubs	9.9	21.7
Basic Aircraft	61.8	136.3
Crashworthiness	3.7	8.2
Landing gear	12.4	27.4
Engine	89.0	196.2
Fuel System	3.7	8.2
Gearboxes	7.8	17.2
Driveshafts	8.4	18.6
Rotor brake	0.5	1.1
Rotor shafts	2.5	5.6
Flight Controls	14.1	31.0
Actuators	5.9	13.0
Electrical, avionics, loading sys, etc.	44.5	98.1
Empty weight	303.5	669.1
10% contingency	30.3	66.9
GTOW: empty weight + fuel + payload + contingency	383.4	845.2

Because the fuselage shape was critical to the success of the vehicle design, a workflow that facilitated rapid iteration of the fuselage OML was required. Working with surfaces in a typical computer aided design (CAD) package such as SolidWorks [15] was determined to be too slow and cumbersome given the schedule constraints. Instead, the main fuselage shape was determined using mesh-based subdivision surfaces in a mesh-modeling program called Blender [16]. Structural requirements and internal components, such as the primary package, could be easily positioned and iterated in Blender, and the fuselage shape was refined to contain these shapes. The cage mesh could then be exported to Fusion 360 [17] and converted to T-splines. This resulted in a solid model with nearly the same geometry as the subdivision surface from Blender but in a solid model format that could then be used to produce the geometric input files for CFD or for further detailed design.

6.2 Aerodynamic Optimization

As fuselage drag was determined to be one of the most important design factors, more emphasis was placed on obtaining the optimum fuselage OML that results in the least amount of drag. Ansys Fluent [11] was used as a quick analysis tool in addition to the in-house CFD platform, Mercury Framework [18]. Fluent has a limited accuracy due to its limit on the number of mesh elements in the student version, however, it was still useful as a quick comparison tool.

As the first step, a CFD simulation was performed using both Mercury Framework and Ansys to understand the aerodynamic characteristics of the geometry. Figure 6.1 shows the resulting vorticity contours, freestream momentum and coefficient of pressure (CP) contours, and flow lines for the initial analysis.

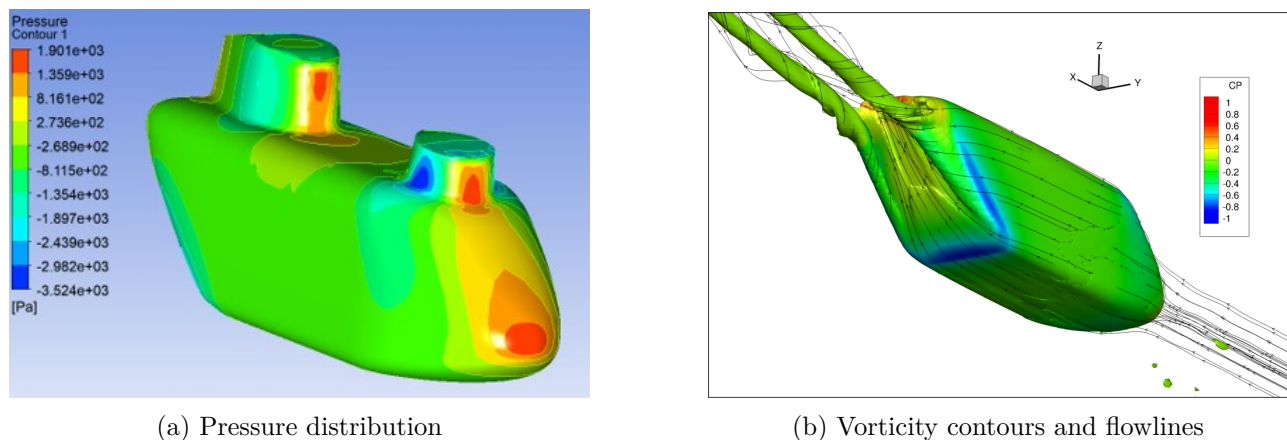


Figure 6.1: CFD results for the initial fuselage geometry

As observed in Figure 6.1 the flow that comes from the bottom of the fuselage does not separate at the rear end and stays attached almost up to the upper end of the rear ramp, possibly due to the shallow ramp angle. This is beneficial in maintaining a low pressure drag. It was also observed that there are two trailing vortices generating at the two edges of the ramp due to the pressure difference between flows coming from the sides and the bottom. These vortices create suction at the ramp surface increasing the pressure difference between the front and rear sides of the fuselage, leading to an increase in drag. On the other hand, these vortices are useful in keeping the flow attached to the middle portion of the ramp. The attached flow on the ramp causes an upward movement in airflow, resulting in a downward force on the fuselage. The equivalent flat plate drag area and downforce area are 0.239 m^2 and 0.257 m^2 , respectively.

It was quickly identified that the strength of the two trailing vortices had to be reduced in order to reduce the drag and downforce. After studying a number of methods, it was decided to use vortex generators [19] to produce a counter rotating vortex to shrink the trailing vortex. Inspiration was found in Formula-1

aerodynamics, where a vortex (Y-250 [20]) is purposefully generated to guide the airflow through the vital components of the vehicle to ensure low drag. The same strategy was used in this situation to control the trailing vortices. However, this would increase the friction drag due to the resulting turbulent boundary layer. Figure 6.2 shows two types of vortex generators analyzed and their resulting vortices and flow patterns. However, none of them showed a decrease in drag as the pathlines clearly show that the flow originating from the vortex generators mixing with the two trailing vorticity due to their dominance. The vorticity generated by the vortex generators is too small to affect the trailing vortices. Generating a larger vortex would increase the friction drag. Therefore it was concluded that vortex generators could not reduce the fuselage drag.

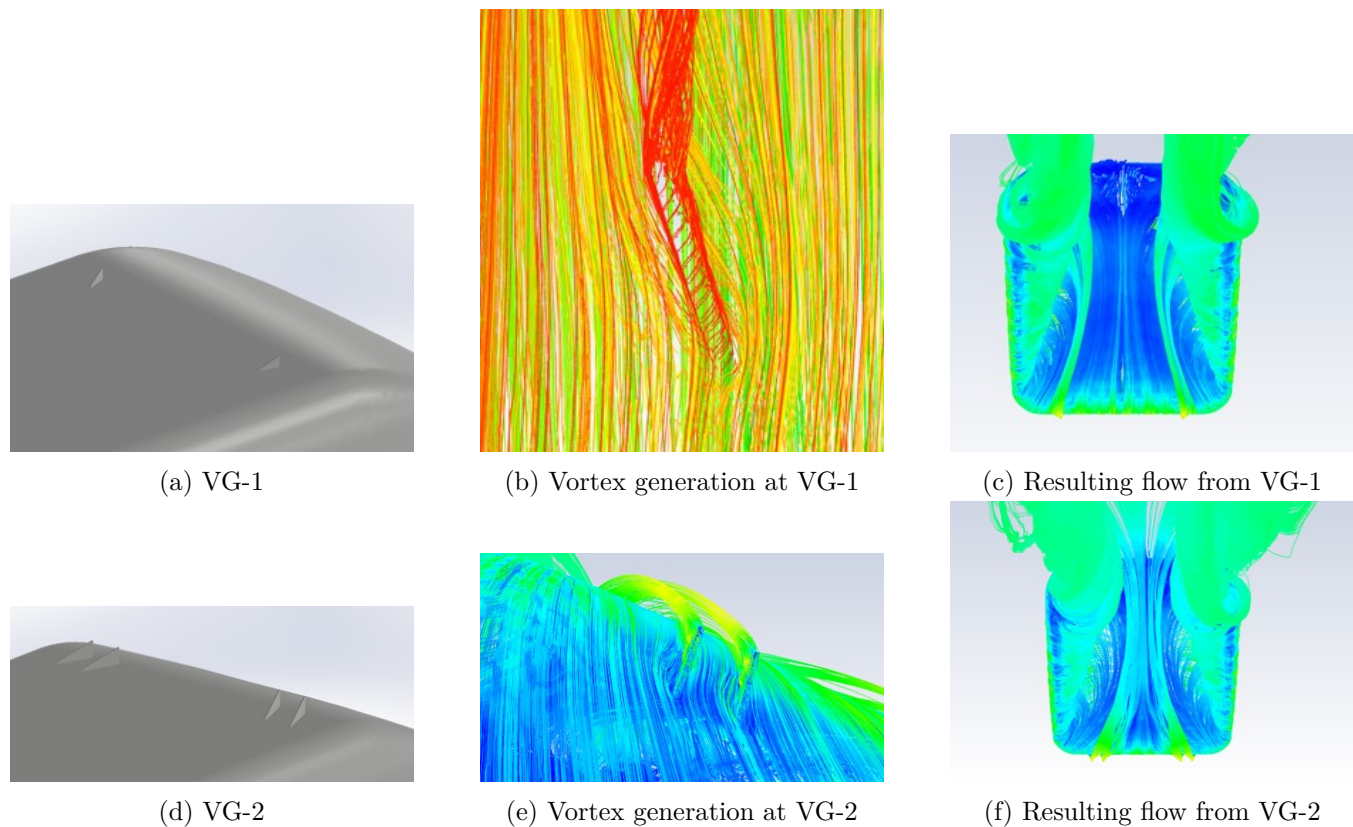


Figure 6.2: Vortex generators (VG) and the resulting vorticity and airflow

The next approach was to smoothen out the bottom edges of the fuselage to reduce the pressure difference between the two flows that interact, producing the vortex. This would essentially lengthen the fuselage, increasing the friction drag. But this was deemed affordable as friction drag was found to be only 15% of the total drag. The cross sectional area had to be slightly increased as well to facilitate the curvature. The rounded rear end made it difficult to accommodate a ramp due to the difficulty of having a hinge at the rounded bottom edge and in ensuring the top edge touches the ground evenly, when the ramp is open. Therefore, four fuselage models were produced with different rear end shapes and was called the “Long Oval” fuselage family. The side views of these models are shown in Figure 6.3. Long Oval A has the most rounded rear end, whereas Long Oval B has rounded bottom edge but sharp side edges, to accommodate a ramp. Long Oval C is somewhere in between A and B. Long Oval D was built to be symmetrical around the middle horizontal plane to incorporate a perfect “tear drop” shape, in order to have better aerodynamic characteristics. The resulting drag and downforce are given in Table 6.1.

As expected, smoothening out the edges has resulted in a significant reduction in drag and downforce. Long Oval D incurs the lowest drag force while producing no downforce due to its symmetry. However,

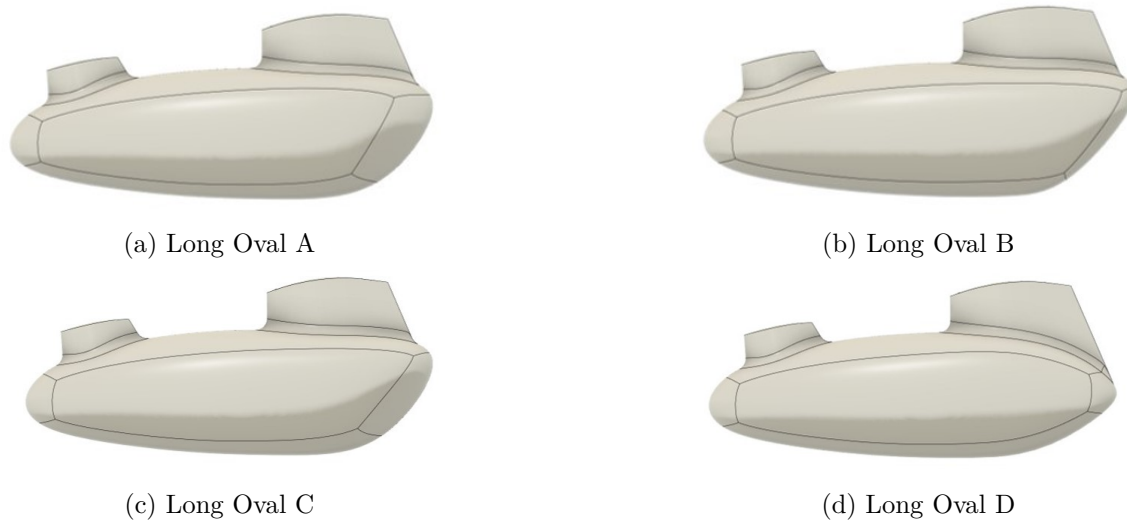
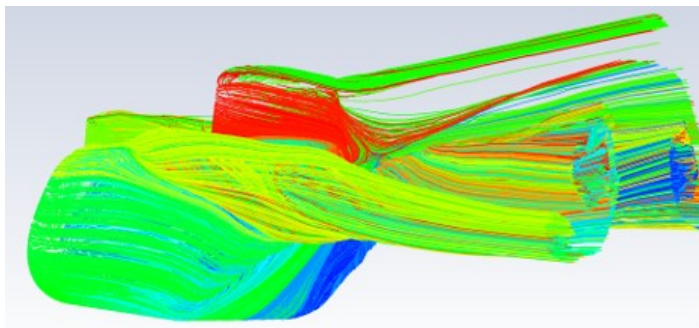


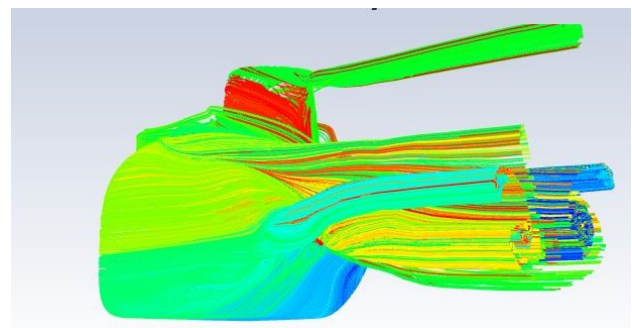
Figure 6.3: Long Oval fuselage family

Table 6.1: Comparison of fuselage drag and downforce characteristics of Long Oval fuselage family with original model

Model	Drag Area / m^2	Percentage Change	Downforce Area / m^2	Percentage Change
Original model	0.239	-	0.257	-
Long Oval A	0.151	-37%	0.104	-60%
Long Oval B	0.189	-21%	0.228	-12%
Long Oval C	0.166	-31%	0.153	-41%
Long Oval D	0.135	-44%	0.000	-100%



(a) Long Oval A



(b) Long Oval D

Figure 6.4: Wake of Long Oval A and D

as the rear end of the aft pylon comes so far down, it is extremely difficult to design a mechanism that opens the rear end of the fuselage. Long Oval A comes second with a 37% reduction in drag. Even though it is difficult to design a ramp, the rear end could be opened with a clamshell mechanism. At this stage, after a careful consideration of the customer requirements, it was identified that the drag reduction is more important than having a rear ramp. Therefore, Long Oval B and C were discarded.

Figure 6.4 shows the difference between the wake of Long Oval A and D. The curvature has reduced the strength of the trailing vortices moving along the side edges of the rear surface. The symmetrical Long Oval D model has two pairs of counter rotating vortices coming from the upper and lower surfaces of the

fuselage weakening each other's vorticity. Therefore, this constitutes the perfect fuselage shape from an aerodynamic perspective. Hence, it was seriously considered to see whether there is any way of designing a mechanism to open the rear end of the fuselage to facilitate loading and unloading. But after a rigorous discussion it was decided that having part of the pylon being able to move on a clamshell door would drastically reduce the structural integrity and result in an extremely heavy fuselage. Therefore, Long Oval A was chosen as the preliminary shape for the fuselage and was subjected to further analysis to reduce drag and downforce.



Figure 6.5: Pointed nose versions of Long Oval A

Table 6.2: Drag area for the variations of Long Oval A model

Model	Drag Area / m^2	Percentage Change
Long Oval A	0.151	-
Long Oval AP	0.140	-7%
Long Oval ASP	0.151	0%

The bluntness of the fuselage nose was observed to be contributing towards drag and therefore, two more models were developed with a pointed (Long Oval AP) and a super-pointed (Long Oval ASP) nose as shown in Figure 6.5. The resulting drag areas obtained for these two models are given in Table 6.2. The pointed version further reduces the drag by 7% whereas the super-pointed version doesn't make much difference. Therefore, Long Oval AP was chosen as the optimum fuselage shape for the design.

As the structural design and internal layout were refined, it was possible to shrink the fuselage OML further by having a tunnel arrangement for the sync shaft and reducing the pylon sizes. The equivalent flat plate drag area was reduced to $0.175 m^2$ and this was verified by both Ansys and the in-house CFD code. The final flat plate drag area was estimated to be $0.182 m^2$, factoring in the effects of the LiDAR (see Section 10), the air inlet, and exhaust pipe. The final fuselage shape is shown in Figure 6.6 and the resulting flow pathlines are shown in Figure 6.7.

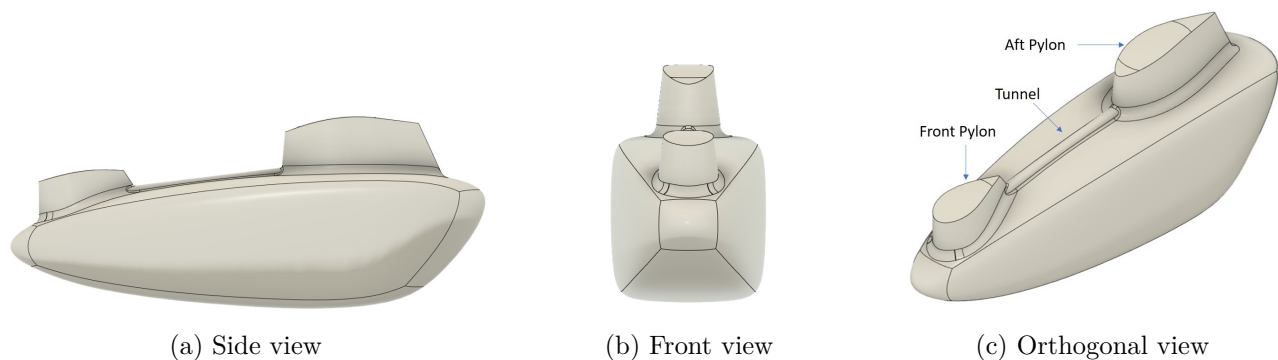


Figure 6.6: Final fuselage shape

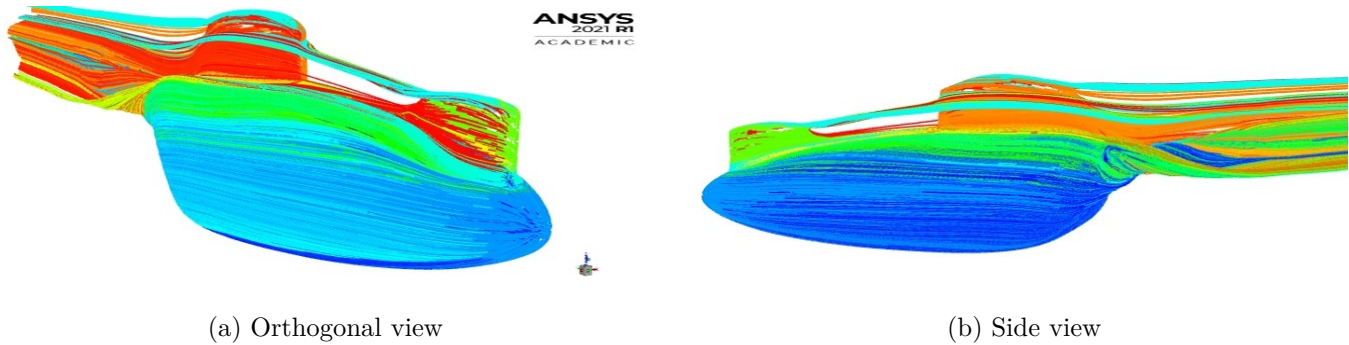


Figure 6.7: Airflow around the final fuselage

6.3 Material Selection

The unique design in the fuselage along with the necessity to keep the structure as light as possible were the driving factors in the material selection. The design team identified a broad set of materials for consideration in the design of the fuselage. These materials are listed in Table 6.3 with pros, cons, and Table 6.4 provides a safety assessment for each material.

Table 6.3: Fuselage material pros and cons.

Material	Pros	Cons
Steel Alloy	<ul style="list-style-type: none"> • High Young's modulus • High yield Stress • Great in applications with high loading (landing gear etc.) • Inexpensive/easily machined into components 	<ul style="list-style-type: none"> • Heaviest solution • Lower fatigue resistance
Aluminum Alloy	<ul style="list-style-type: none"> • Lightest metal • Inexpensive/easily machined into components • Inexpensive material to purchase 	<ul style="list-style-type: none"> • Low Young's modulus • Low yield stress • No fatigue resistance
Titanium Alloy	<ul style="list-style-type: none"> • Highest strength to density of all metal alloys • Highest fatigue resistance for metal alloys • High temperature resistance 	<ul style="list-style-type: none"> • Difficult to weld • Expensive/difficult to machine • Expensive material
Composite	<ul style="list-style-type: none"> • Highest strength to density for all materials. • Lightest weight solution • Highest fatigue resistance 	<ul style="list-style-type: none"> • Expensive/difficult to manufacture • Expensive solution • No deformation and explosive failure

Table 6.4: Fuselage material safety analysis

Material	Safety Analysis
Steel Alloy	<ul style="list-style-type: none"> • High Young's modulus • High yield stress • Yielding provides warning of failure.
Aluminum Alloy	<ul style="list-style-type: none"> • lightweight low/moderate loading • Avoid areas of cyclical loading no fatigue resistance. • Yielding provides warning of failure.
Titanium Alloy	<ul style="list-style-type: none"> • Moderate/higher loading where structure still needs to be light. • At high temperatures corrodes if exposed to oxygen. • Ideal for high cyclic loading due to it's fatigue resistance. • Yielding provides warning of failure.
Composite	<ul style="list-style-type: none"> • Ideal for high cyclic loading is applied for it's high fatigue resistance. • Ideal for moderate/high loading due to its High tensile strength. • Provides no warning of impending failure. • Recommend not applying this material to drive shafts or dynamic components .

The design team focused on using materials that would provide the lightest structural weight while providing the required factor of safety. Due to the lightweight requirement, both titanium and steel alloys were discarded. This left the design team with aluminum and composite materials. Table 6.5 provides the density (ρ), Young's modulus (E), yield strength (σ_y), ultimate tensile strength (σ_t), and ultimate compressive strength (σ_c) for Aluminum 2024-T361 and Celion 3000/E7K8.

The design finalized on Celion 3000/E7K8 plain weave carbon fiber/epoxy. This decision was strongly influenced by the need to make a lightweight vehicle. To get an advance warning of catastrophic failure, strain gauges were fixed at vital structural points to monitor the loads applied. If the strain measured exceeds $8800 \mu\epsilon$, the system will alert through HUMS to replace the vital structure. Aluminum 2024-T361 were used for the drive shafts and landing gears, and Titanium inserts were applied to the carbon fiber epoxy structure to prevent galvanic corrosion between carbon fiber and Aluminum.

Table 6.5: Properties for Al 2024-T361 and Celion 3000/E7K8

Material	ρ ($\frac{kg}{m^3}$ ($\frac{lb}{ft^3}$))	E (GPa(Msi))	σ_y (MPa(Ksi))	σ_t (MPa(Ksi))	σ_c (MPa(Ksi))
Al 2024-T361	2780 (173.55)	72.4 (10.5)	395 (57.29)	495 (71.79)	495 (71.79)
Celion 3000/E7K8	1550 (96.76)	68.67 (9.96)	N/A	910.1 (132)	717.0 (104)

6.4 Landing Gear Design

Because parasite drag was a significant design driver, landing gear design was considered to be critical. A lightweight skid design common to rotorcraft of this size would not be the optimum configuration for drag. Several landing gear configurations were considered: fixed skids, retractable skids, fixed wheels, fixed main wheels with a retractable nose wheel, and fully retractable wheels. Rough landing gear configurations were mocked up in CAD and analyzed using CFD to evaluate the impact on drag. Table 6.6 shows the equivalent flat plate drag areas obtained for the fixed skids and fixed wheel designs and are compared with the retractable option. These numbers were then used in the initial performance code to evaluate the impact on vehicle productivity.

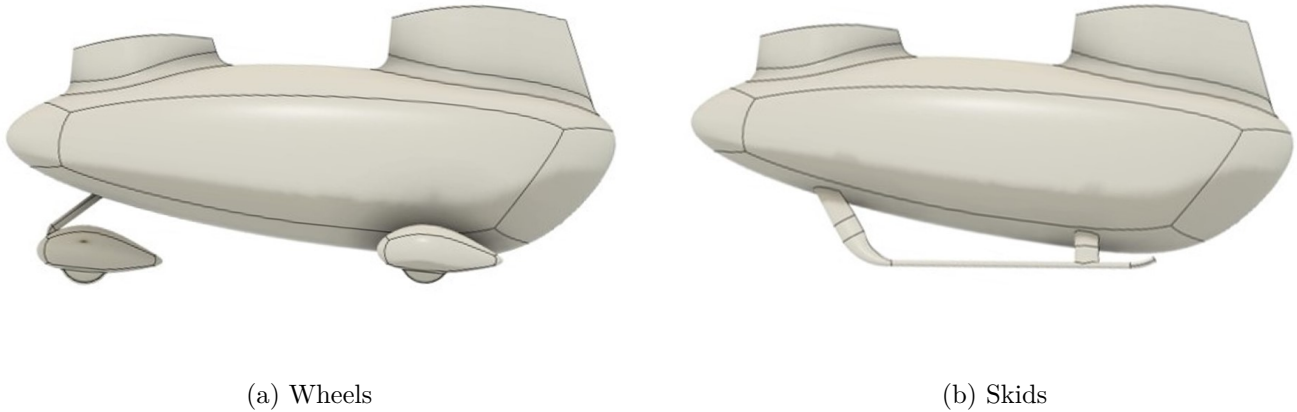


Figure 6.8: Fixed landing gear options considered

Table 6.6: Equivalent flat plate drag areas for various landing gear designs

Model	Drag Area / m^2	Percentage Increase
Fixed skids	0.304	27%
Fixed main landing gear	0.283	19%
Fixed landing gear	0.318	33%

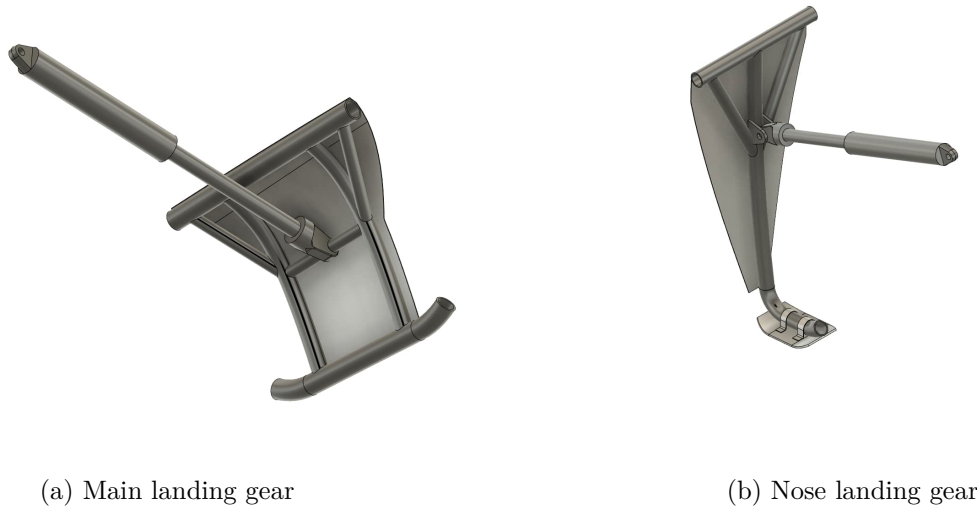


Figure 6.9: Final retractable landing gears

Ultimately, any drag penalty associated with fixed landing gear (skids or wheels) was deemed less attractive. The design team decided to develop a lightweight retractable solution for landing gears. As there is no requirement for autonomous taxi operations, the wheeled landing gear was considered unlikely to provide a competitive advantage due to its weight and complexity. The operational benefits of wheels would only be realized during manual ground operations, during which, small lightweight wheels could be attached to the aircraft. Wheeled gear would also necessitate brakes for safe landing and ground operations on surfaces that are not perfectly level. The braking mechanisms would require additional complexity and weight, making wheeled landing gear increasingly undesirable. With these design considerations in mind,

lightweight retractable skids were chosen as the ideal solution for this mission.

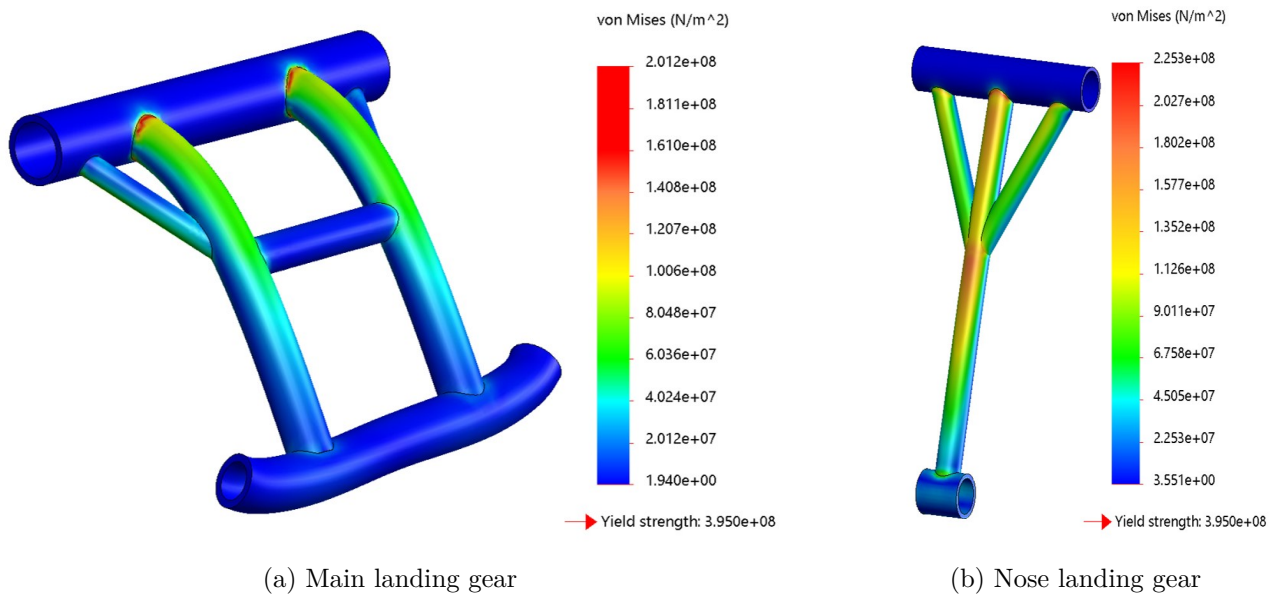


Figure 6.10: Stress diagrams for landing gears

The landing gear was designed such that the aircraft maintains a 5° nose-up attitude while on the ground to facilitate the gravity assisted unloading method. This requires the main gear to be quite short and the nose gear to be comparatively long. The nose gear is positioned far forward such that the main gears carry approximately 62% of the aircraft's weight. When deployed, the static roll over angle of the aircraft is 36° , well above the rule of thumb of 30° .

Two design approaches were considered for the main landing gear. The first involved integrating the outer skin covering the landing gear into the actual landing gear structure. The landing gear itself would be constructed from welded aluminum plates. This approach was eventually abandoned due to the complexity of the structure and difficulty with retraction. Instead, a more traditional welded-tube approach was taken, which proved to be a more compact and lightweight option, and the landing gears developed are shown in Figure 6.9. They are deployed and retracted using linear actuators.

Once deployed, the landing gears are restrained from further rotation effectively providing a fixed restraint at the hinges connecting them to the main structure. Therefore, the actuators do not take any load other than the load coming from the self weight of the landing gears during deployment and retraction. The main landing gear axis is at 35° to the vertical axis, whereas the nose landing gear axis is at 10° . The nose landing gear was designed to tolerate up to 10° of ground inclination both ways.

The landing gears were designed to withstand a 3G (three times gravitational acceleration) load during a possible hard landing. Aluminum 2024-T361 alloy was used for the structure. The stress, strain and displacement were analyzed using Solidworks [15] and the landing gear structure was optimized to take the maximum allowable load at a minimum self-weight. Figure 6.10 shows the stress distribution in the main and nose landing gears due to the maximum allowable load. The factor of safety for the main and nose gears were kept at 1.6 and 1.58, which are greater than the 1.5 limit. Both main and nose landing gear actuators were designed to take the load coming from the landing gear self weight during the 3G loading situation. This resulted in lightweight main and nose landing gears weighing only 2.7 kg and 2.5 kg, respectively, including the 1 kg actuators.

6.5 Fuselage Structure

The extreme importance placed on the fuselage aerodynamic design made the structural design challenging. The structure not only has to support the weights of the internal components and the external loads but also has to accommodate the aerodynamic OML. The dominant loads arise from the weight of the internal components, especially the engine and payload, once the structure is restrained at the rotors. After several iterations the bulkheads and beams were located to efficiently diffuse the load. The initial structure is given in Figure 6.11.

The structure consists of seven bulkheads held together by two keel beams running along the top and bottom of the fuselage. Two side beams are included for better structural integrity. The bottom keel beams are truncated closer to the main landing gear allowing it to be retracted. One middle beam and two side beams are put in place to carry the load of the truncated keel beams.

The engine is mounted in between the two rotors using a frame (Figure 6.12) that attaches to the third bulkhead from the front. As per the mounting arrangement of the engine, which is discussed in detail in Section 8, it applies a considerable cantilever load on the bulkhead. An insulated firewall is placed behind the engine to safeguard the payload and other equipment from the high temperature of the engine. Two keel beams are placed at the top and bottom to hold the bulkheads together and support the bending moments between the two rotors, arising mostly from the weight and the torques applied on the two rotors. The forward portion of the structure is bolted to the engine bulkhead so that it can be removed for engine maintenance. The bottom keel beams are truncated at the rear to accommodate the retractable main landing gear. Two more beams are placed at the sides to improve structural integrity. The rearmost bulkhead is at an angle to accommodate the OML, and hold the clamshell doors and the internal ramp.

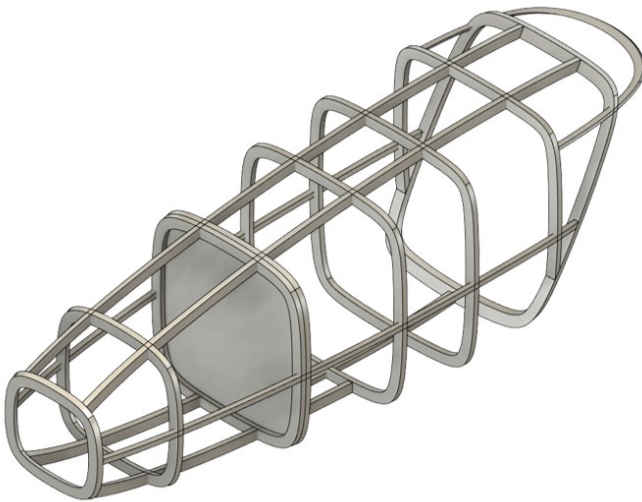


Figure 6.11: Preliminary Structure



Figure 6.12: Mounting frame of the engine

To reduce the weight of the structure, hollow rectangular sections are used for both bulkheads and beams as they are more efficient against bending. The structure was designed to withstand a 3G (3 times the gravitational loading) during flight, maintaining a minimum safety factor of 1.5. Structural analysis was performed for both airborne case and landing case, where the weight was taken by the rotors and landing gears, respectively. It was identified that 3G landing becomes the limiting case for the structure in terms of strain. Figure 6.13 shows the stress diagrams for the limiting case of 3G landing. The factor of safety for the airborne and landing cases in terms of stress is 14.3 and 2.8 with respect to the ultimate strength of Celion 3000/E7K8, which is well above the limit of 1.5. The respective maximum strains are $1387 \mu\epsilon$

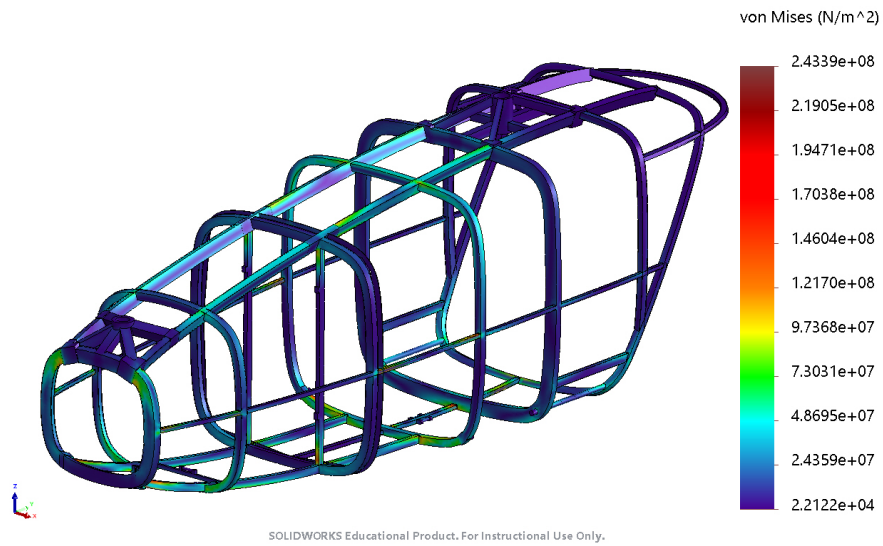


Figure 6.13: Stress diagram for limiting case

and $2963 \mu\epsilon$, which are also below the $3000 \mu\epsilon$ endurance limit. The maximum displacements measure as 4.2 mm and 11.0 mm for the two cases, respectively. The structural weight was reduced to 22 kg by properly identifying the load paths, having the optimum structural members to handle the load, and using the strong lightweight material.

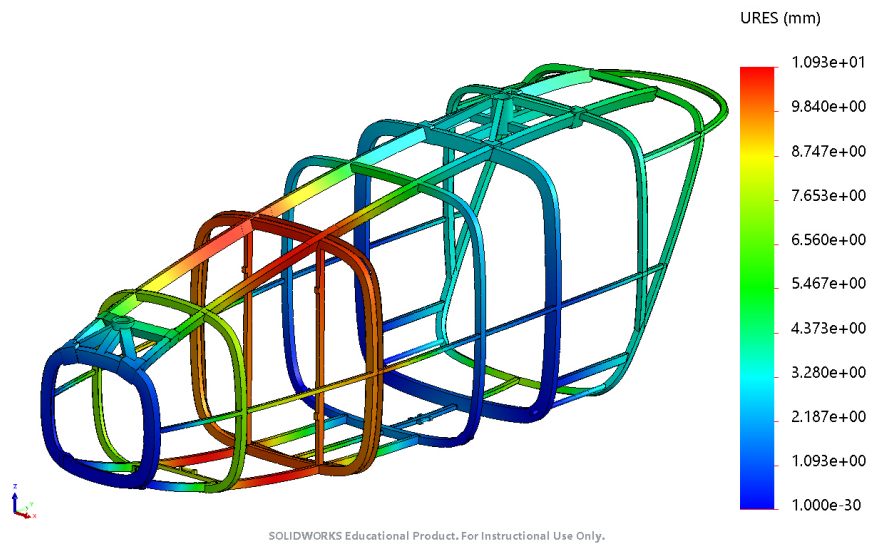


Figure 6.14: Displacement diagram for limiting case

6.6 Payload Handling

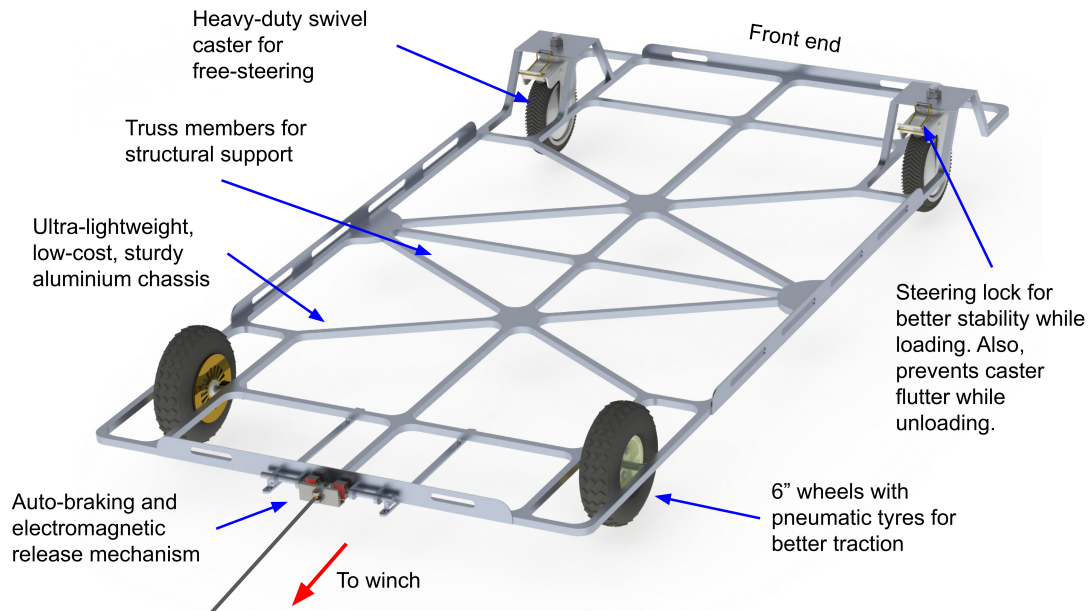


Figure 6.15: The winch assisted gravity cart

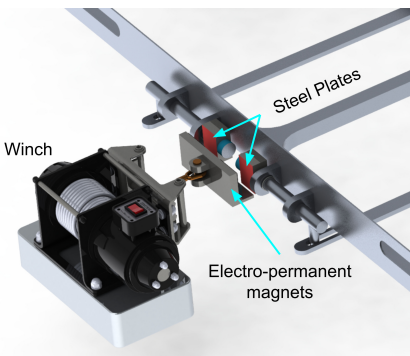


Figure 6.16: Electromagnetic Release

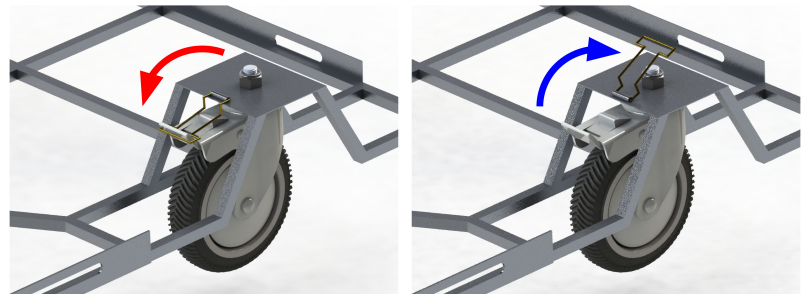


Figure 6.17: Caster steering lock hook

Alicorn uses the winch assisted gravity cart mechanism introduced in Section 4 for loading and unloading the 50 kg payload. The primary features of the designed cart are shown in Figure 6.15. The cart chassis can accommodate both the payload sizes of 70 cm × 70 cm × 70 cm and 140 cm × 50 cm × 50 cm. The payload is tightly secured to the cart chassis via Kevlar straps. An overview of the unloading sequence is given in Section 4. At the end of winch cord is an electro-permanent magnet (EPM), shown in Figure 6.16 that tightly attaches itself to the steel plate with a force of 600 N when magnetized and detaches if demagnetized. The EPM is powered with cables running inside the winch cord and it takes approximately 20 W of power while magnetizing/demagnetizing. In addition to this, the caster's steering can be locked in place with the help of wire hooks as shown in Figure 6.17.

During loading, the caster steering is locked and the EPM is attached to the steel plates on the rear-end of the cart frame. A signal is then sent to the EPM to magnetize itself. Another command to the aircraft will start the winch motor and pull the cart inside the aircraft's cargo-bay. Tracks on the ramp as well as in

the cargo-bay floor help in aligning the cart with the aircraft's heading. It is estimated that this procedure should take less than 10 seconds. The aircraft's rear cameras also monitor the loading process. The cart with the payload stops when the rear-end of the cart comes close to the fire-wall. This is detected by proximity sensors placed on the fire-wall. Four force transducers located on the cargo-bay floor measures the weight and center of gravity of the cart with the payload in order to determine if their values are within the tolerance. This completes the loading sequence and the ramp can now be closed.

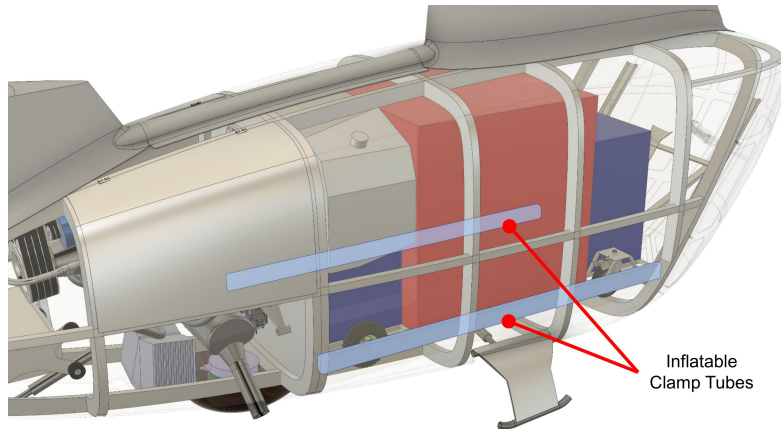


Figure 6.18: Cargo Bay

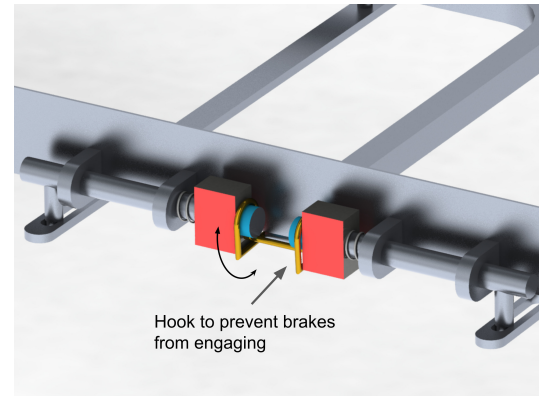


Figure 6.19: Anti-braking hook

While in flight the cart is constrained longitudinally with the ramp-door from the back and fire-wall from the front. The cargo-bay walls, roof, and floor are also lined with inflatable clamp tubes as shown in Figure 6.18 to secure the cart and payload. The clamp tubes are inflated at the end of the loading sequence using an air pump. The estimated inflation time is around a minute. At the delivery site before the start of the unloading procedure the clamp tubes will start deflating. The estimated deflation time is around 4 seconds.

During unloading, the ramp-door opens and the winch gradually releases the cart down the ramp as depicted in Figure 4.1(b). The cargo-bay floor is inclined downwards by 5° towards the rear so that the cart can accelerate under gravity. The cart is designed to clear the aircraft in 4 seconds. This is detected by the aircraft's rear cameras at which point the winch stops turning and the EPM is demagnetized which releases the cart. To further prevent the cart's motion due to uneven terrain, disturbances, or downwash an auto-braking mechanism depicted in Figure 6.20 automatically engages as soon as the hook is detached. The braking force can be adjusted by changing the spring constant. This completes the unloading sequence and the aircraft is now free to close its ramp and take-off. To disengage the auto-braking mechanism a simple anti-braking hook as shown in Figure 6.19 can be moved to its place by the personnel at the delivery site after which the cart becomes free to move forwards or backwards. Caster's steering lock hook can also be moved to allow free steering of the cart and the payload.

Cart Structure: The chassis is component that experiences the maximum stress while it is carrying the 50 kg payload. The cube payload of size 70 cm \times 70 cm \times 70 cm has the lesser contact area and hence the chassis will experience the maximum stress while carrying it. To support this load as well as to keep the weight and cost low, the chassis is made up of hollow square aluminium extrusions arranged in a truss pattern and welded together. The extrusions has outer dimension of 10 mm and wall thickness of 1 mm. This design leads to the chassis weighing only 1.5 kg while being able to support more than twice the payload weight. The von Mises stress acting on the chassis is shown in Figure 6.21.

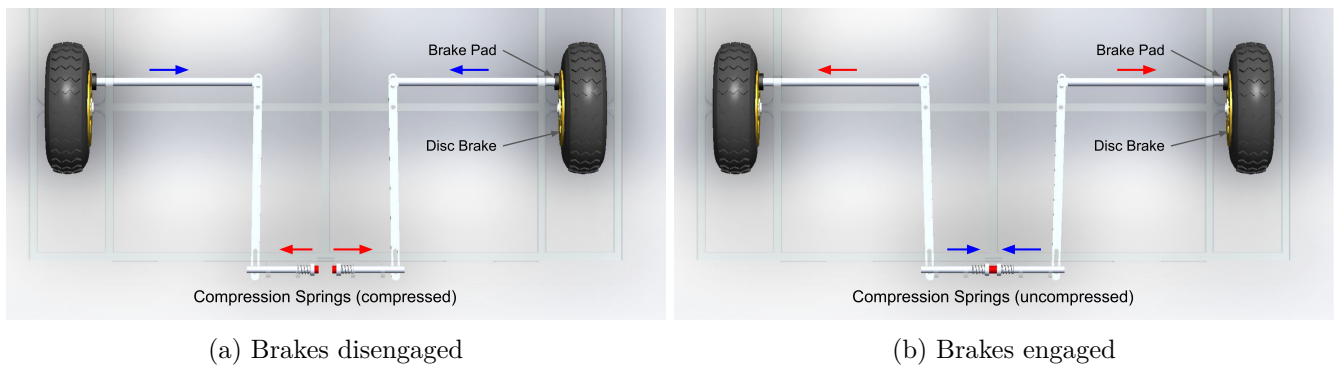


Figure 6.20: Auto-braking Mechanism

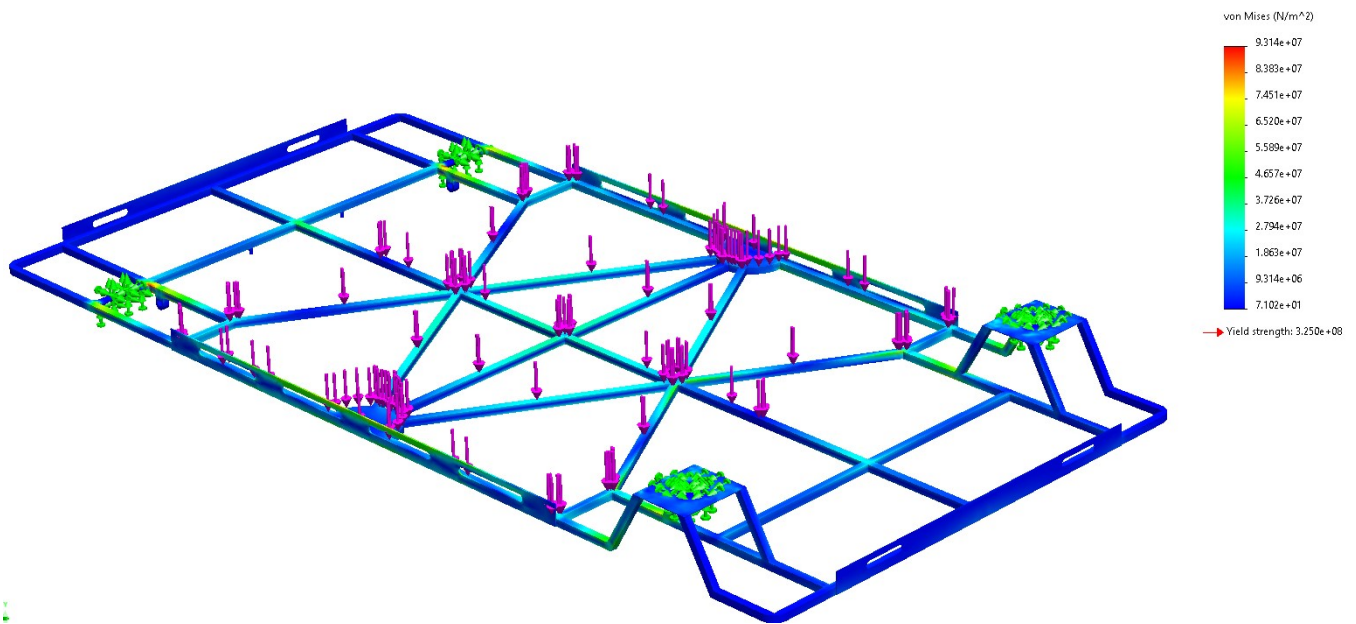


Figure 6.21: Chassis stress analysis

Ramp and Clamshell Doors: The aft of the airframe contains a lightweight internal ramp structure and two clamshell doors with linear actuators for automated deployment. In the loading procedure after the payload with the cart is pulled inside the cargo bay, the ramp closes followed by the clamshell doors. In the unloading procedure, after landing at the delivery site, the clamshell doors open, followed by the deployment of the ramp. A ground clearance flap located underneath the ramp also automatically deploys simultaneously. Figure 6.22 shows the deployed state of the ramp and clamshell doors.

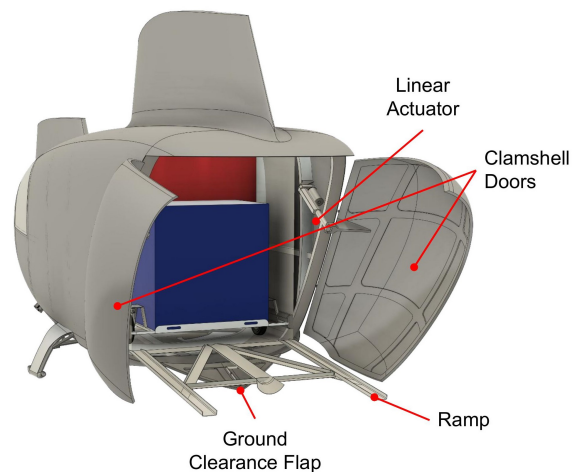


Figure 6.22: Ramp and Clamshell Doors

6.7 Internal Layout

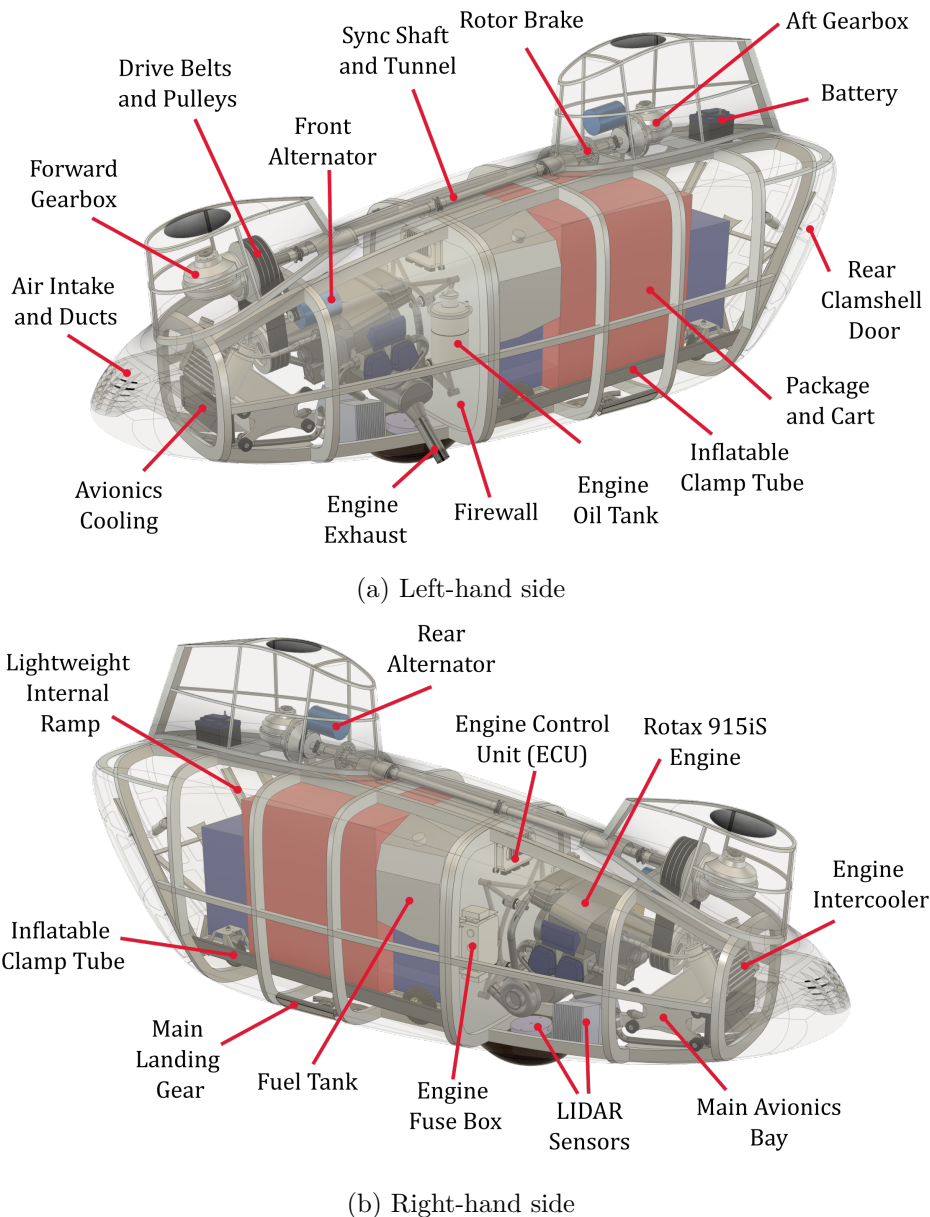


Figure 6.23: Internal layout overview

Considerable effort was put into determining the internal layout of the vehicle ensuring safety and meeting other design requirements of the RFP. The internal layout had to reflect requirements such as maintaining an adequate center of gravity location, maintaining clearance for package loading and unloading, allowing for inspection and maintenance, and reducing the vehicle cross section to reduce drag. Fuselage outer mold line development and the internal layout directly impacted each other, especially as the vehicle sizing matured and engine was selected. Therefore, the two designs were done in parallel.

Figure 6.23 provides an overview of the internal layout of the aircraft. The aircraft is separated in the center by the main firewall. The engine is mounted immediately forward of this location on shock mounts for vibration isolation and to permit flexibility for engine de-clutching. The engine is positioned such that

enough space remains for the main drive belts. The pulley mounted to the engine propeller shaft flange “overhangs” the propeller reduction gearbox to allow the necessary longitudinal space between the engine and the forward gearbox.

The cargo winch is positioned forward of the firewall in an enclosed case and runs aft, through a hole in the firewall into the engine compartment. Necessary engine accessories such as the engine fuse box, engine control unit (ECU), and oil fuel tank are mounted to the forward side of the firewall. Immediately below the engine are the three LiDAR sensor positions. The main avionics bay is positioned forward of this, above the nose landing gear. The engine inter-cooler, an integral part of the selected Rotax 915iS engine, is positioned above the avionics. The inter-cooler and avionics radiator are fed fresh air through the intake in the nose of the aircraft. The intake has fixed louvers that are angled downward to help reject precipitation from entering the aircraft.

The main payload bay dominates the aft half of the aircraft. Besides the internal package itself, the payload bay also contains inflatable clamp tubes on the sides to secure the package. Both package sizes are carried in the center of the payload bay, which allows the forward ceiling to be lowered to provide space for the fuel tank.

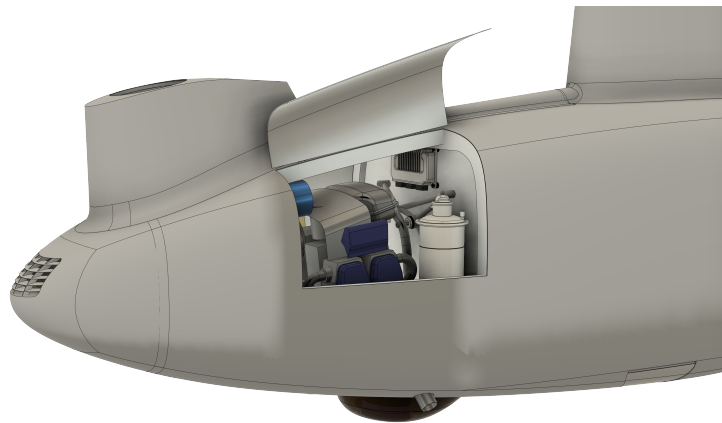


Figure 6.24: Engine bay inspection doors

The fuel tank is positioned immediately aft of the firewall and is shaped to occupy the space not required by either package size. Despite utilizing a single combined fuel tank, two fueling ports are provided, one on each side of the aircraft for convenience and to better access fuel quantity in the uniquely shaped tank.

The retractable main landing skids are located centrally below the payload bay, and extend down and outward about a pivot outboard of the payload bay floor. The two clamshell doors and the lightweight ramp are located aft of the payload bay to permit loading and unloading.

The aft pylon is mostly empty except for the aft rotor gearbox, the rear alternator, rotor brake and battery. This unusual battery position was determined to satisfy center of gravity requirements. Otherwise, the pylon's size was driven by a desire to improve the aircraft's inherent directional stability, not internal packaging requirements.

Two engine-bay doors are provided for inspection of the engine and other components forward of the firewall before flight. Engine exhaust exits the aircraft through the stick exhaust tube included with the engine through a hole in the lower left skin of the engine compartment. The engine's turbocharger is located laterally opposite the engine exhaust, and a NACA inlet is provided in this location to provide the necessary air.

7 Rotor Design

Rotor design was considered an important aspect of the aircraft design process because it affects most of the other design components and the dynamic and performance characteristics of the aircraft. Both rotors of the tandem configuration were designed to be identical to each other except for the direction of rotation, where the front and rear rotors rotate counter-clockwise and clockwise, respectively, looking down from above the rotor.

The rotor radius (R) was based on the operational size limits given for the aircraft. Three blades per rotor were selected to simplify blade spacing and inter-meshing. The flap hinge offset was minimized to about 2.5%, to reduce hub moments and permit large flapping angles necessary for adequate yaw authority. The aircraft GTOW was initially estimated to be 383 kg using the AFDD weight model developed by the U.S. Army Aeroflightdynamics Directorate at NASA Ames Research Center [14]. As the design matured this reduced to 298 kg (657 lb), however, the rotors were designed for the higher gross weight. The design cruise speed was set at 90 m/s (175 kt) in order to reduce block time and maximize productivity, while maintaining a lower gross weight. The flat plate drag was estimated to be 0.182 m^2 (1.96 ft^2). The forward and rear rotor shafts were tilted forward by 12° and 7° , respectively, to provide the propulsive force for cruise with a level body attitude while also maintaining sufficient clearance between the two rotors and the fuselage. The blade tip speeds are maintained at 213 m/s (700 ft/s) and 202.3 m/s (664 ft/s) under maximum and continuous engine power, respectively, considering both rotor and transmission efficiency. An aerodynamic analysis was performed to optimize the blade geometry for maximum performance.

7.1 Blade Aerodynamic Optimization

As both missions are primarily focused on cruise and the performance of the aircraft is measured by its productivity, reducing the block time was considered a vital aspect of the design. Therefore, the rotor design was focused on obtaining the highest lift to drag ratio, while maintaining an acceptable figure of merit in hover.

The first task was to select an airfoil or a combination of airfoils for the blade. The following 10 airfoils were considered in the selection process considering their suitability to be used as inner and outer airfoils.

- | | | | |
|----------|-----------|-----------|-----------|
| 1. VR-7 | 4. SC1095 | 7. SSCA09 | 10. OA209 |
| 2. VR-12 | 5. SC2110 | 8. RC510 | |
| 3. VR-15 | 6. SSCA07 | 9. OA206 | |

In order to obtain more accurate estimates for the sectional lift (c_l) and drag (c_d) coefficients, the Mach and Reynolds (Re) number distributions along the blade span and azimuth locations were calculated using a preliminary aspect ratio of 18. The calculated distributions are given in Figure 7.1. Mach number remains less than 0.6 in hover and increases to 0.8 in forward flight. Reynolds number remains at or below 0.9 million in hover, which is below the 1 million boundary for turbulent flow. In cruise, outboard sections the advancing blade increase to 1.2 million, reaching turbulent conditions. Therefore, the c_l and c_d values used for the analysis of each airfoil must not only be functions of the airfoil angle of attack (α) but also Mach and Reynolds number (Re). 2-D RANS based CFD simulations were carried out on each airfoil to determine c_l and c_d values as a function of both angle of attack and Mach number. In these simulations, α and Mach number were varied between -20° to 20° and 0.2 to 0.8, respectively. Data for high angles of attack was taken from the high angle tables for NACA0012 [21]. Re number correction [22] was performed to account for the differences in actual and table Re number using Eq. 2, 3, and 4. The subscript t refers



to the table values of the drag and lift coefficients.

$$c_d = \frac{c_{dt}}{K} \quad (2)$$

$$c_l = K c_{lt} \quad (3)$$

K is calculated as,

$$K = \left(\frac{Re}{Re_t} \right)^{0.5} \quad (4)$$

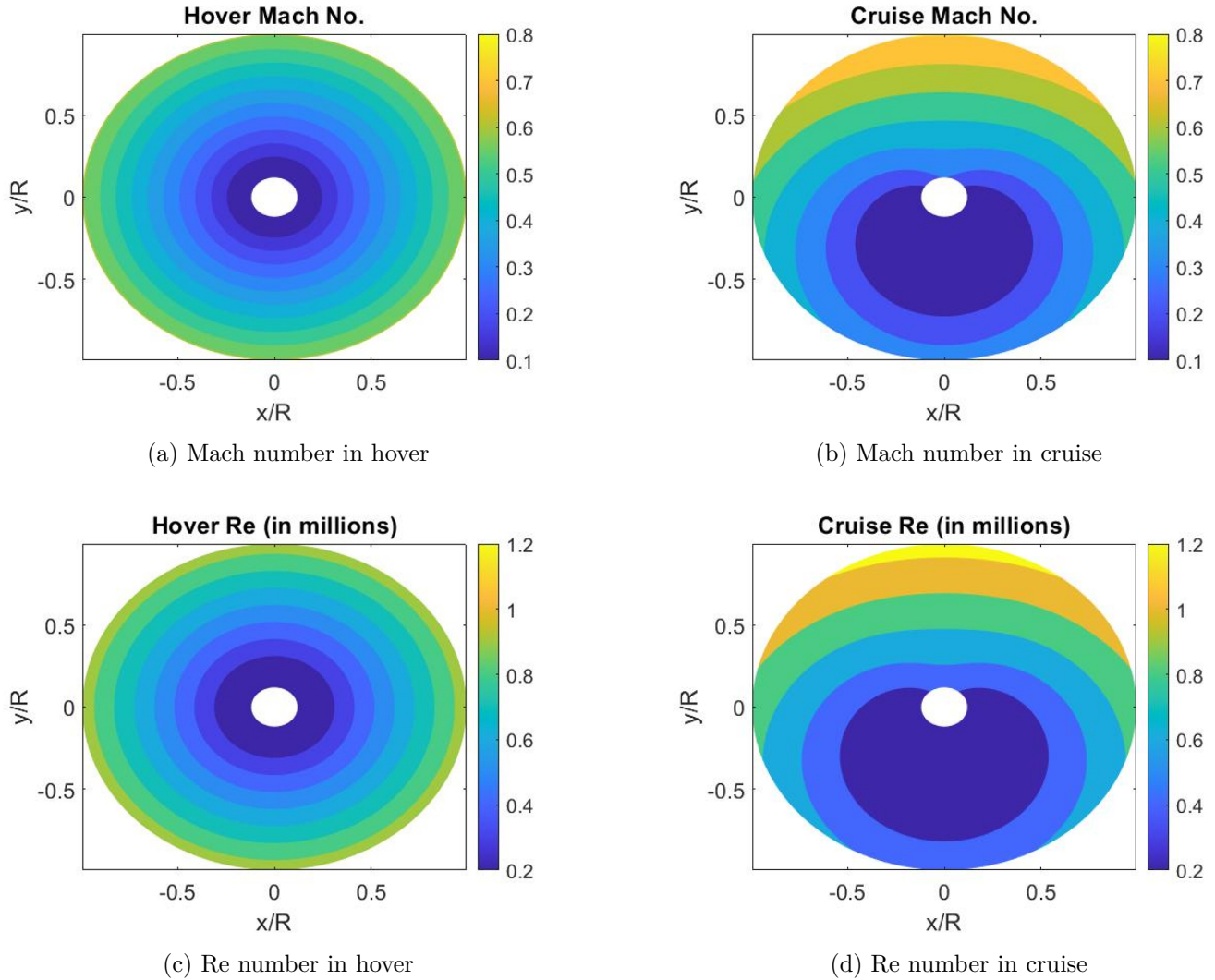


Figure 7.1: Mach and Re number distributions in hover and cruise

Figure 7.2 presents the variation of maximum c_l/c_d with Mach number for the considered airfoils. Based on these results, the Boeing VR-7 airfoil was selected for the inner airfoil as it shows the highest $(c_l/c_d)_{max}$ values below Mach 0.66. For higher Mach numbers, the thinner Sikorsky SSCA07 and SSCA09 airfoils appear superior. Considering the thickness transition from the relatively thick VR-7 to these thinner airfoils and potential blade design and manufacturing concerns, the slightly thicker SSCA09 airfoil was selected for the outer portion of the blade. Figure 7.3 shows the maximum sectional lift coefficient $(c_l)_{max}$,

the sectional drag coefficient at zero lift c_{d0} and $(c_l/c_d)_{max}$ for the selected airfoils. The VR-7 shows a higher $(c_l)_{max}$ than the SSCA09 for the range of Mach numbers but the SSCA09 shows a lower c_{d0} . The airfoil with the superior $(c_l/c_d)_{max}$ value transitions from the VR-7 to the SSCA09 at Mach 0.7, which corresponds approximately with the non-dimensionalized span location (r/R) of 0.8. For this reason, the airfoil transition was placed at this location; the transition would occur over 5% of the blade span.

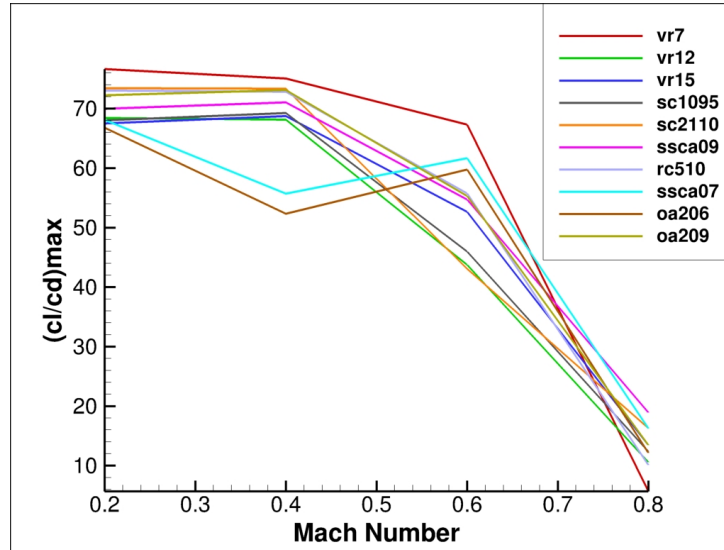


Figure 7.2: Variation of $(c_l/c_d)_{max}$ with Mach number for different airfoils

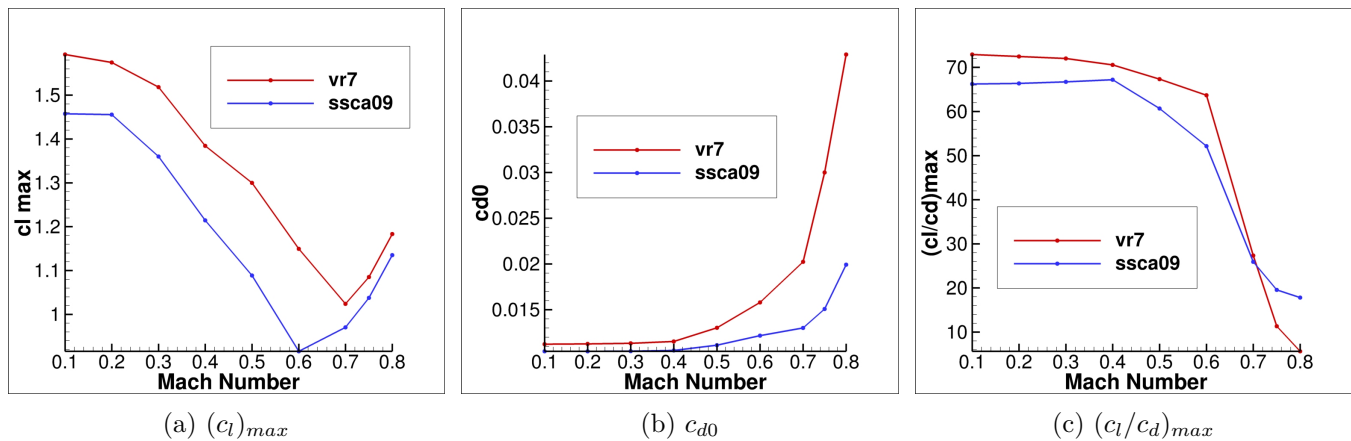


Figure 7.3: Lift and drag characteristics for the selected airfoils

The drag divergence Mach number for SSCA09 airfoil was determined to be around 0.78. The blade tip is swept such that it remains below Mach 0.75, leaving a margin for variations in atmospheric conditions and forward flight speed. This results in a 22° tip sweep beginning at $r/R = 0.9$. The swept tip also avoids transonic effects allowing the aircraft to maintain higher tip speeds in forward flight.

A blade element momentum theory (BEMT) code was developed by the design team to identify the optimum twist and taper for the blade. The effect of tip loss was accounted for by Prandtl's tip loss correction [23]. This code was used to perform a parametric sweep on different blade geometries, including variations in linear and bi-linear twist and taper, twist and taper transition locations, and blade aspect ratio. Blade twists of up to $-20^\circ/\text{span}$ and taper ratios (c_{root}/c_{tip}) of up to 3.5 were considered, resulting in more than 2000 different blade geometries. A rectangular planform was maintained at the inboard section

Table 7.1: Rotor Characteristics

Parameter	Value
Radius	1.565 m (5.13 ft)
Root chord	155.8 mm (6.13 inches)
Tip chord	56.7 mm (2.23 inches)
Solidity	0.0634
Tip speed (5 min limit)	212 m/s (695.5 ft/s)
Tip speed (Continuous)	202 m/s (662.7 ft/s)
Inner airfoil	VR7
Outer airfoil	SSCA09
Flap frequency	1.023/rev
Lag frequency	0.373/rev

as the inboard taper is found to not make much difference in rotor performance [24]. A tip anhedral was also considered in order to reduce blade vortex interaction (BVI) noise. The resulting figure of merit (FM) and helicopter lift to drag ratio (L/D_e) for the best combinations considered are given as a Pareto plot in Figure 7.4.

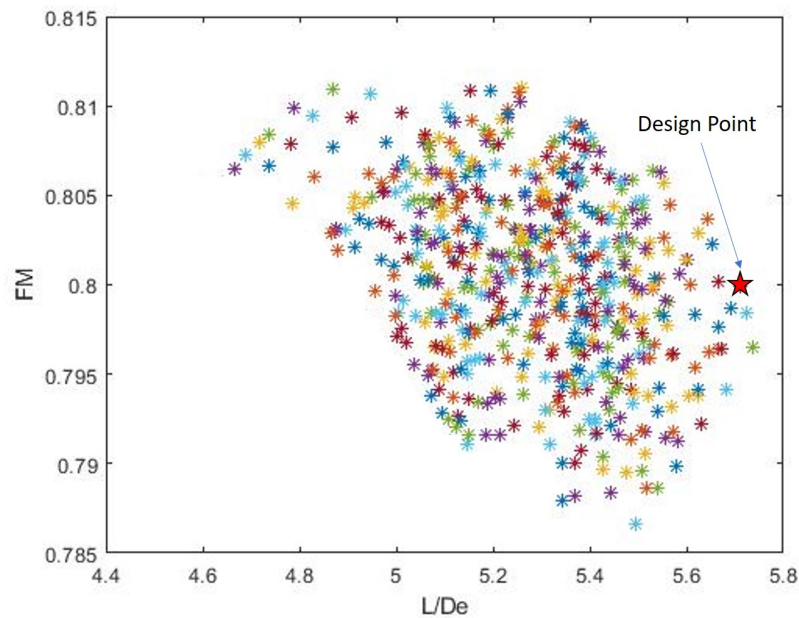
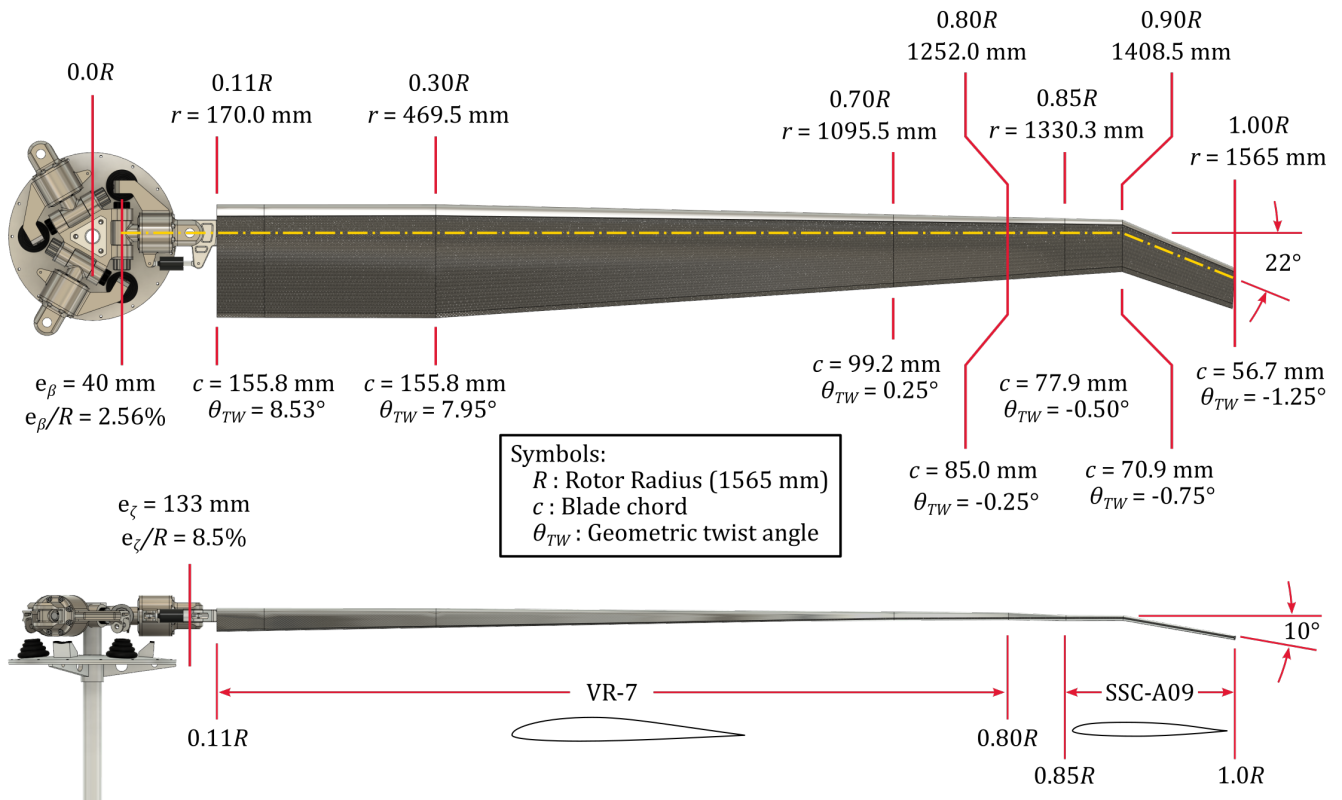


Figure 7.4: Refined Pareto plot for rotor blade design

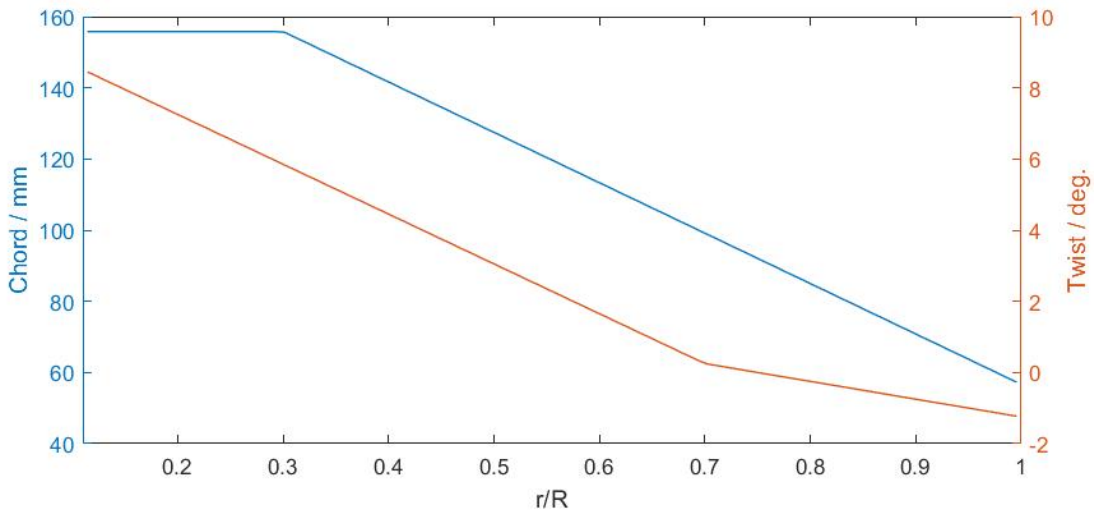
Since the aircraft is designed to spend more time in forward flight, a higher weight was placed on maximizing L/D_e , in selecting the design point from the Pareto front, while maintaining a decent FM. The selected design point has a L/D_e of 5.7 and a FM of 0.8, and the resulting blade geometry is given in 7.5.

7.2 Blade Structural Design

The blade designed for both rotor systems is shown in Figure 7.5. The blade consists of a constant-chord inboard section where the main mounting cuff is attached, a tapered mid-span region, and a tip section. The blades of the front and rear rotors are mirror images of each other but are otherwise identical. The



(a) Blade geometry



(b) Chord and twist distribution

Figure 7.5: Final blade design

internal structure, material selection, and root structure were designed to be lightweight structures that could withstand centrifugal forces and bending loads applied during flight while providing the necessary control.

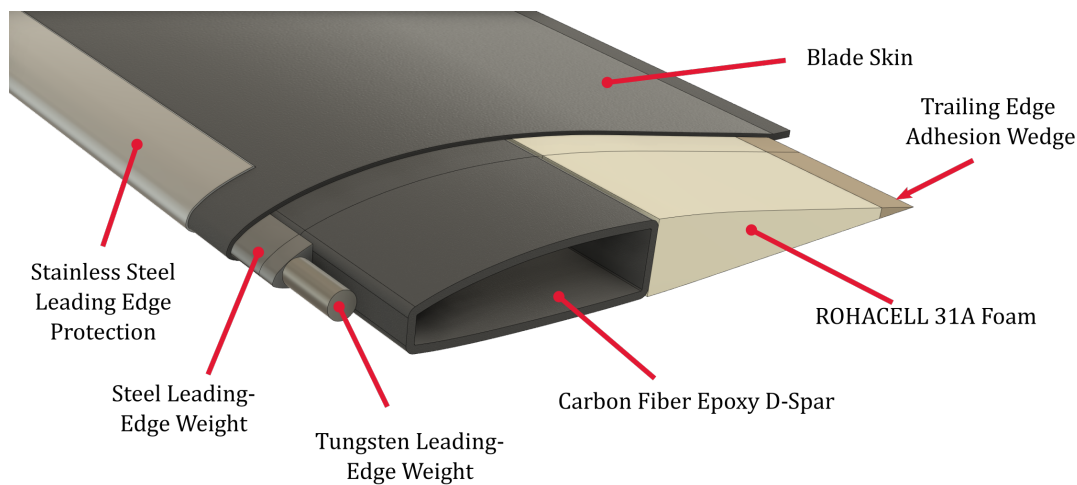


Figure 7.6: Internal blade structure

7.2.1 Structural Design

To determine the internal structure layout and type of beam, the design used an in-house code to determine the ideal shape and thickness of the beam. The elastic axis is maintained at or near the quarter chord by utilizing an appropriate material distribution. In order to transfer the centrifugal forces from the blade to the hub, titanium inserts are used to keep the carbon fiber epoxy continuous. The material for the spar was chosen through a lightweight carbon fiber epoxy material that provided the necessary strength to account for the centrifugal load as well as other aerodynamic loads transferred through the blade to the hub.

Figure 7.6 presents the final rotor blade internal structure. From the in-house code it was determined that a D-spar with a thickness of 1.7×10^{-3} m (0.067 inches) was appropriate for this application. The D-spar is ideal in its simplicity, ideal for confined spaces, and the fact the shape keeps the elastic axis at the quarter chord. The material decided was the CELION 3000/E7K8 for its low density and relatively high strength properties. The plies chosen were $[0_3 \pm 45_2 0_3]$. To increase stiffness and prevent instability, ROHACELL 31A was selected to fill the blade between the D-spar web and trailing edge due to its relative lightweight compared to other ROHACELL and similar foams. ROHACELL was selected over the common NOMEX honeycomb structure due to its greater ease of use and shapeability for small-scale applications. A tungsten leading edge weight is placed along the inboard and mid-span sections of the blade, where space permits. A larger solid tungsten weight is placed at the 75% radial station and is embedded into the spar so that it is restrained against the large centrifugal forces. This weight also acts as a barrier to restrain the tungsten leading edge weight inboard. In combination, these leading edge weights bring the blade CG 0.3% forward of the quarter chord line, ensuring torsional stability. A bonding wedge is placed at the trailing edge to provide adequate surface area to bond the upper and lower skin together.

The outer skin was composed of AS4 3K/E7K8 composite fiber epoxy with plies of $[\pm 45_4]$. The aircraft will only be operated in Visual Meteorological Conditions (VMC) where the cloud ceiling will be 1,000 ft with 3 statute miles of visibility per the FAA regulations. As such, lightning protection and blade de-icing systems were determined to be unnecessary, and would not provide a competitive advantage when considering the weight and complexity such systems would add.

7.2.2 Fan Plots

Fan plots were calculated for the flapping and lag axes using 20 finite elements. Each section's mass, material, and geometric properties were used to determine the natural frequencies of the entire blade for varying rotor speeds. It was determined that the normal operating rotor speeds were free of resonance conditions. The combined fan plots are shown in Figure 7.7.

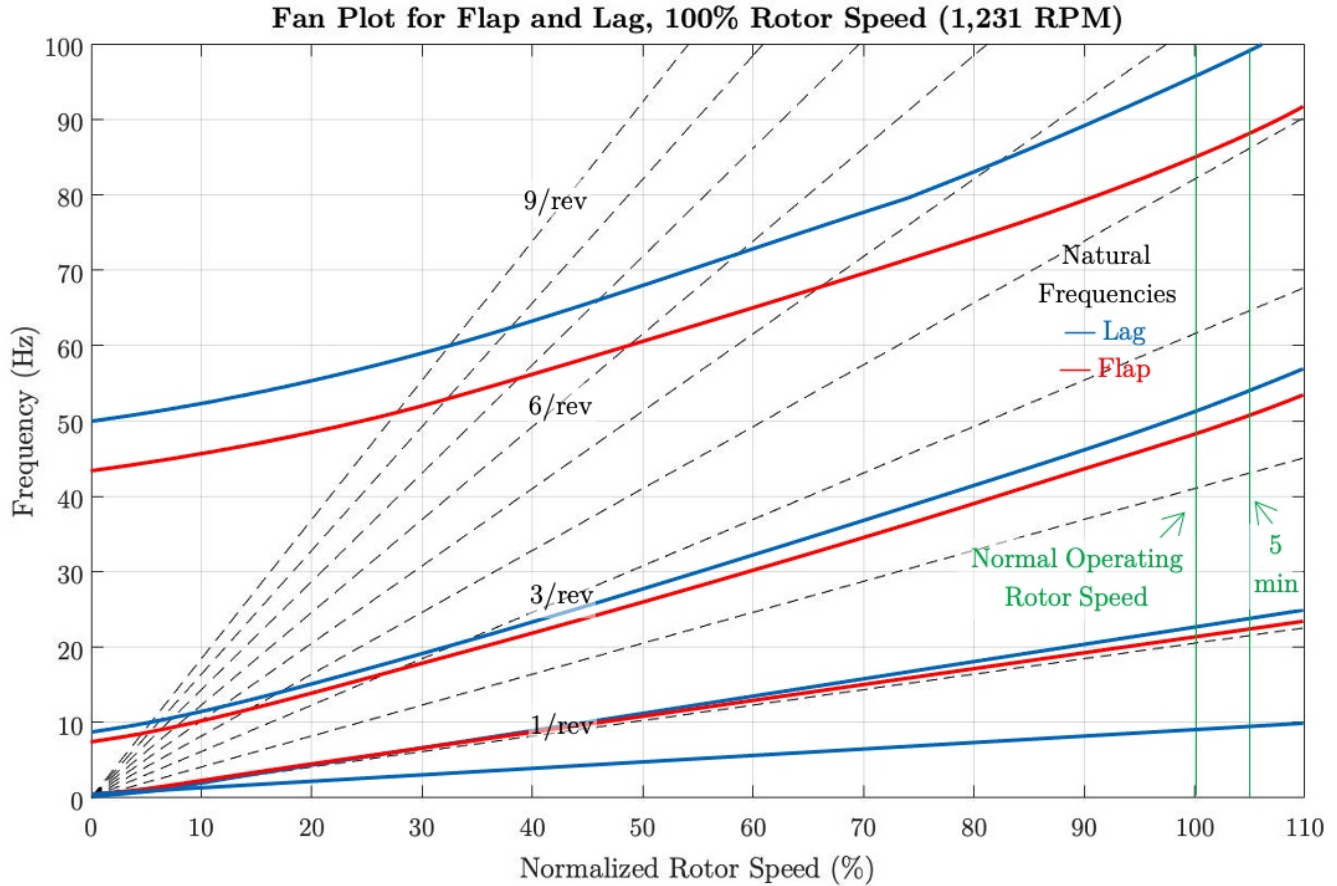


Figure 7.7: Fan plot for flap and lag

7.3 Actuator Design

Electro-Mechanical Cylinders (EMCs) and Electro-Hydraulic Actuators (EHAs) were considered to actuate the swashplate. Using the geometrical data derived from the blade design combined with desired control speed and authority a set of requirements for the actuators as shown in Table 7.2 were calculated. Table 7.3 shows a comparison of the two actuators' properties. Miniature EHAs such as the one described in [25] perfectly matches our requirements, provided two of them are mounted in series so as to achieve twice the output speed, power and stroke. Mounting two EHAs in series also improves safety by providing dual redundancy. In case, one of the actuator fails, the other one will still be able to move the swashplate, albeit at lower control speeds and authority. If two or more actuators fail then the aircraft will abort its mission and either return back to home or safely land, depending on its condition. Table 7.4 lists the component weights of the EHA actuator. It is capable of generating forces of up to 295 N (66.3 lb), 70% more than our requirement. A total of twelve such EHAs (six EHAs per swashplate) weighing 6 kg (13 lb) with total maximum power consumption of 360 W is utilized by Alicorn to meet its high performance and

safe actuation needs.

Table 7.2: Actuator Requirements

Parameter	Value
Maximum Force	172 N
Maximum Stroke	67 mm
Actuation Speed	300 mm/s
Weight	< 1 kg
Power	< 100 W
Redundancy	> 1

Table 7.3: EMC vs EHA

Property	EMC	EHA
Size	Small	Large
Power/Weight	Low	High
Maintenance	Nil	Seldom
Cost	Low	High
Backlash	Yes	No
Shock loading	Bad	Good
Temperature Issues	No	Yes

Table 7.4: EHA Breakdown

Name	Weight
Pump and Motor	205.6 g
Valve	14.8 g
Pressure Transducers	100.5 g
Hydraulic Cylinder	64.8 g
Drive Electronics	78 g
Total Weight	463.7 g



Figure 7.8: Two EHAs in series

7.4 Hub Design

A tandem helicopter achieves yaw authority through differential lateral tilt of the rotor tip-path-plane, and thus thrust vector. To achieve this, the rotor hub must provide sufficient flapping response. This requirement eliminates truly rigid rotors and hubs like those of Sikorsky's advancing blade concept and X2 aircraft. Sufficiently soft hingeless or bearingless rotors could be considered, but the higher hub moments and associated additional structure make them less desirable than a traditional articulated hub with a small hinge offset. The flap hinge offset was minimized to about 2.5% of the rotor radius in order to maximize flap response and reduce hub moments. A titanium alloy (Ti-6Al-4V) due to its high specific strength. The other materials considered were either too weak (in the case of aluminum), too heavy (in the case of steel), or would feature a catastrophic failure mode (in the case of various composites with no noticeable yield before failure). Figure 7.9 depicts the rotor hub design.

A lag damper is sized to reduce the lag frequency to 0.37/rev. The damper is mounted to the pitch casing and connects to the rotor blade. Inside the pitch casing both ball bearing and thrust bearings transfer the centrifugal forces from the blade to the main rotor hub. The thrust bearings were sized to handle 81.8 kN (18,400 lb). Ball bearings were sized to handle 4.3 kN (966 lb). Figure 7.10 provides the detailed design of the pitch casing.

7.5 Swashplate Design

A conventional swashplate mechanism was chosen for Alicorn's control actuation rather than experimenting with novel ideas, due to reliability and safety concerns. The swashplate system of Alicorn is connected to the static mast at the bottom using an anti-rotation rod and at the middle with the spherical bearing as



Figure 7.9: Rotor hub

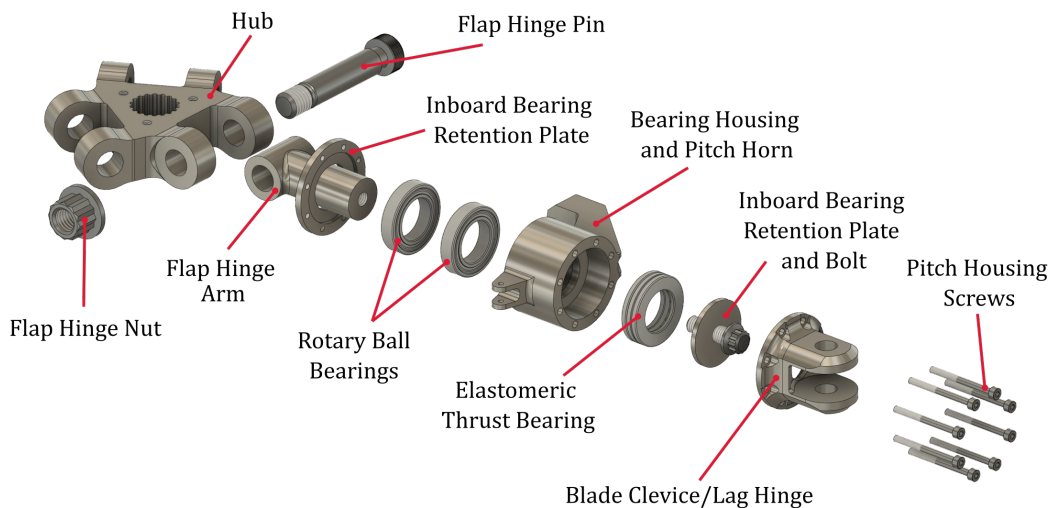


Figure 7.10: Articulation arm assembly

shown in Figure 7.11. The anti-rotation rod prevents the non-rotating swashplate from rotating with the rotating swashplate and minimizes the bending loads on the actuators. The spherical bearing is mounted on the mast using a low friction sleeve made of steel coated Kevlar, allowing it to move up and down smoothly. The actuators are mounted on the gearbox with a 120° angle between each other. The front and rear swashplate actuators are located such that one actuator is at the opposite side of the sync shaft, allowing the sync shaft to run between the two gearboxes. The non-rotating swashplate is connected to the actuators for it to be moved up and down and tilted.

The rotating swashplate is connected to the non-rotating swashplate with a tapered roller bearing, which allows it to rotate while transmitting the pitch link loads to the rest of the swashplate system. It is also connected to the shaft with rotating scissors using a splined collar. This transmits the torque from the shaft to the rotating swashplate, leaving the pitch links to carry only the axial loads. The pitch links connect to the pitch horns on the flapping axis and 60° off from the pitching axis to maintain symmetry.

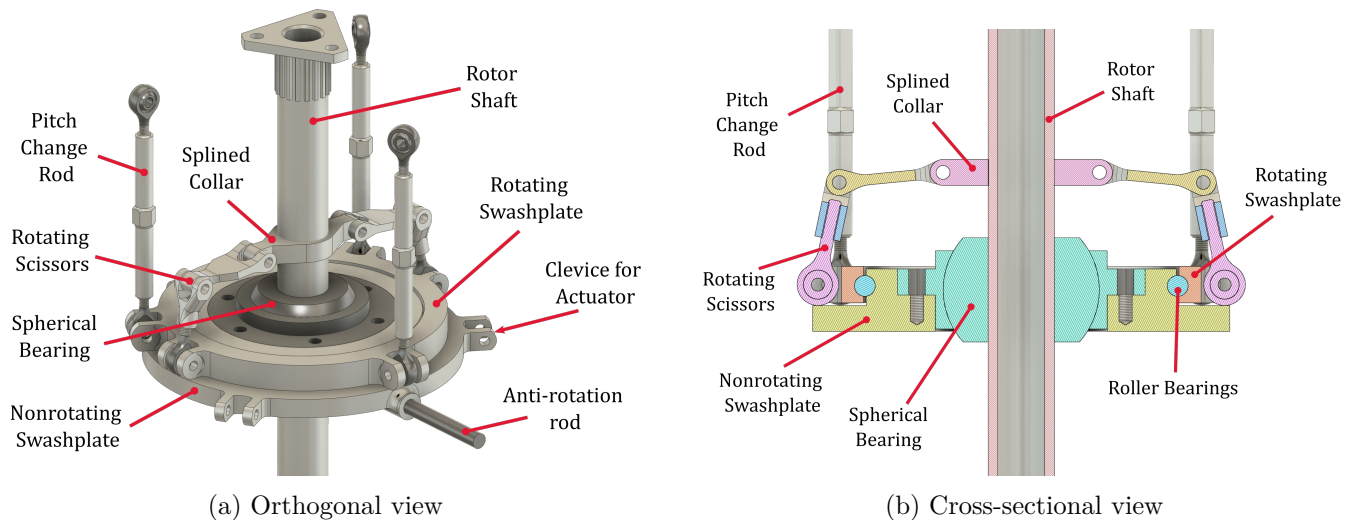


Figure 7.11: Swashplate assembly

8 Propulsion System Design

8.1 Candidate Engines

Due to the Alicorn's low disk loading and reduced tip speed, a maximum continuous power of 97 kW (132 HP) could provide a 90 m/s (175 kt) cruise speed, potentially increasing the productivity of the engine. Thus, engines in the 100 kW (136 HP) class were considered.

Because of the requirement to achieve aircraft certification before 2025, mature powerplants were preferred for the Alicorn. Emerging technologies such as Liquid Piston's X4 combined cycle rotary engine [26] and small turbine startups offered promising specifications, but would have introduced excessive technical risk into this aircraft's development timeline. Established engines used in slightly smaller UAVs initially appeared promising, but proved under powered. For example, in the case of the Austro Engine AE50R powerplants used in the Schiebel S-100C, three of them would be needed for this design, partially due to the 20% performance reduction from the sea level power rating (35.8 kW/ 48 HP MCP) [27][28].

Although promising for shorter range applications, electric propulsion was quickly eliminated as unfeasible. Most electric aircraft currently flying are either short range unmanned aircraft or general aviation trainers that spend most of their time near airfields [29]. Even assuming the integration of a cutting-edge Lithium-ion polymer battery with a 265 kW-hr/kg gravimetric energy density [30], the gross weight would quickly escalate. For example, if the aircraft had a lightweight 14 kg (31 lb) motor and 102 kg (225 lb) battery with a 300 kg (662 lb) total mass, it would only be able to fly 57 km (31 nmi) at 54 m/s (105 kt) under the RFP conditions, including hover requirements and 20 min reserve. To fly the full 200 km Logistics Mission profile at 67 m/s (130 kt), the battery would need to have a mass of 366 kg (807 lb), and the aircraft would weigh 564 kg (1,244 lb). Hybrid electric systems were also ruled out due to the flight profile not being conducive to recharging (i.e. a long range constant cruise profile instead of repeated climbs and descents in a traffic pattern).

Taking into consideration these factors, five promising engines were evaluated for this design, and are shown in Figure 8.1 [31][32][33][34][35].

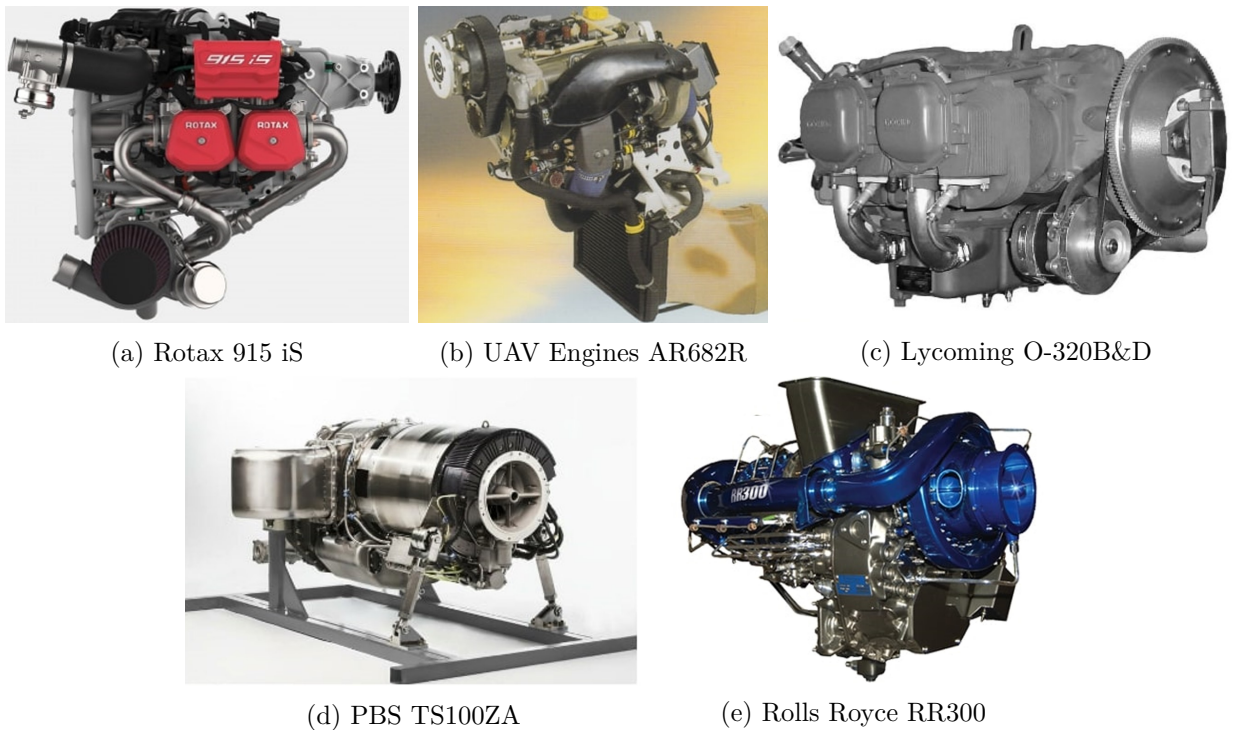


Figure 8.1: Powerplant selection finalists

The Rotax 915 iS is an oil-cooled, turbocharged, four cylinder reciprocating aircraft engine, the latest in a series of lightweight designs from this Austrian company. Its predecessors, the naturally aspirated 912 and turbocharged 914 models, have a significant maturity [36]. In addition to popular applications in the light conventional airplane market in Europe and elsewhere, Rotax engines are used in the Dynali H3 two-seat helicopter and MQ-1 Predator. The Rotax 914 has a continuous power rating of 73.5 kW (100 HP), well below the 915's 99 kW (135 HP), but it is only 10 kg (22 lb) lighter. As this indicates, the specifications of the 915 show that it has the manufacturer's highest power-to-weight ratio, and because it is turbocharged, it can easily maintain its full Maximum Rated Power and Maximum Continuous Power under the high-hot conditions listed in the RFP requirements. Its critical altitude is approximately 4,600 m (15,000 ft) [37]. It has been certified since the end of 2017 by EASA [38]. Rotax recommends a conservative time between overhaul of 1,200 hours for the 915 [39], but this is expected to be extended to 2,000 hours in the next few years based upon the history of its earlier models [40]. The engine is being sold for approximately \$40,350 [41].

The Lycoming O-320 is part of a family of venerable engines that have powered general aviation mainstays such as the Cessna 172 and Robinson R22 for decades. It is more powerful at sea level than the Rotax 915 iS, but is air-cooled and naturally aspirated. While it is relatively heavy and suffers at altitude because it is naturally aspirated, it is certified worldwide to be safe and reliable [33]. New versions of the engine retail for over \$51,000, but there is also a significant market for less expensive rebuilt and overhauled models [42].

UAV Engines is a United Kingdom based company that manufactures the AR682R, a dual rotor Wankel engine that was based on a previously certified single rotor version [32]. As noted previously with Austro Engines, although rotary engines are promising, it was difficult to find many in the power range needed for this aircraft. Thus, two of these engines would be required to power the Alicorn at high speeds, thus adding complexity, weight, and volume. However, the advantage of redundancy in the event of an engine failure made this an option worth investigating. Pricing information was not readily available, although

UAV Engines seems to have a presence at industry trade shows.

The Rolls Royce RR300 is a modernized, down-rated version of the Allison Model 250 (civilian) and T63 (military) turboshaft designs which have accumulated millions of flight hours. Certified in 2008, it is used in the Robinson R66 and other rotorcraft [35]. Engine performance and specific fuel consumption were based upon publicly available flight test reports for the T63 [43]. The price for this engine is approximately \$300,000 [44].

PBS, a Czech small engine manufacturer with experience in powering UAVs, has introduced a new turbine, the TS100ZA. It is compact but features high fuel consumption, a typical problem for small gas turbines, and has only flown in one experimental manned helicopter [34]. A price for this engine was not readily available.

8.2 Engine Selection

The performance data for these engines are shown in Table 8.1. Performance was calculated for the RFP flight conditions, not simply at sea level. As in the earlier configuration trade studies, modified momentum theory performance calculations with compressibility and mach divergence corrections were used for engine comparisons. Breguet range and fuel consumption were modeled for the 200 km (108 nmi) Logistics Mission from the RFP. Total aircraft weights were corrected for each engine's installed weight and the required fuel.

Rotax and Lycoming provided the dry weight of their engines and all accessories in their documentation, so the mass was increased slightly to account for fluids such as oil and coolant. UAV Engines provided a full installed weight for their Wankel motor, and all data provided is for two of these power plants. Both of the turbine manufacturers only provided dry weights with minimal accessories and mounting equipment, so their masses were increased by 15% to reflect more accurate installed weights. Rotax, Lycoming, and UAV Engines designs could all consume motor vehicle gasoline (MOGAS) in addition to aviation gas (AVGAS). Note that the AKI value is the standard $(R+M)/2$ octane rating used in the U.S., so both the Rotax and Lycoming engines require "premium" 91 octane gasoline. 10% ethanol content is generally acceptable in these fuels. In any case, MOGAS is more widely available and less expensive than AVGAS or jet fuel.

Like the aforementioned Austro Engines design, it was immediately clear that the non-turbocharged or non-turbine models produced by Lycoming and UAV Engines have performance penalties, as they each lost approximately 20% of their power available compared to sea level under standard day conditions. The dual engine concept of the AR682R had a potential single engine hover envelope, but integrating two engines into a common transmission would pose significant challenges, in addition to being three times of a larger volume than a single Rotax configuration. The Rotax, PBS, and Rolls Royce engines featured critical altitudes above 3,000 m (10,000 ft), and considering that the density altitude according to the RFP requirements is above 2,000 m (6,600 ft), these had higher specific powers.

Because the analysis showed that the Lycoming O-320 installation resulted in a 6 m/s (12 kt) slower cruise while being the most massive engine, it was eliminated from further consideration. Higher power and/or turbocharged engines produced by Lycoming and other manufacturers did not appear to address this problem. Though there were numerous larger engines available with better specific power, their much greater cross-sectional areas, and being significantly more massive would degrade productivity and require bolstering the aircraft's structure, iteratively compounding the weight penalty.

Both of the turbine designs showed the potential for higher speeds, but because of the additional loads imposed on the rotor system and Mach drag divergence at such a high advance ratio, this extra power availability provided fewer advantages. Only the immature PBS turboshaft could provide a superior speed and lower weight compared to the Rotax installation, but only marginally.



Table 8.1: Powerplant performance data for 200 km (108 nmi) Logistics Mission at 1,350 m (4,430 ft), ISA+20 °C (RFP conditions)

	Rotax 915 iS	Lycoming O-320B&D	UAV Engines AR682R	PBS TS100ZA	Rolls Royce RR300
Engine Type	4 cylinder, oil cooled, turbo reciprocating	4 cylinder, air cooled reciprocating	Twin rotor Wankel, water-cooled	Turboshaft	Turboshaft
Number of Engines	1	1	2	1	1
Max Rated Power, kW (HP)	104 (141)	104 (141)	112 (152)	177 (241)	177 (241)
Max Continuous Power, kW (HP)	99 (135)	88 (120)	100 (136)	157 (214)	155 (211)
SFC, kg/kW-hr (lb/HP-hr)	0.32 (0.52)	0.38 (0.62)	0.34 (0.55)	0.55 (0.89)	0.43 (0.700)
Volume, m ³ (ft ³)	0.12 (4.2)	0.36 (12.7)	0.33 (11.7)	0.11 (3.9)	0.29 (10.2)
Installed Weight, kg (lb)	86 (190)	131 (289)	113 (249)	65 (143)	105 (232)
Specific Power, kW/kg (HP/lb)	1.23 (0.75)	0.81 (0.49)	0.99 (0.60)	2.76 (1.68)	1.72 (1.05)
Max Cruise Speed, m/s (kt)	91 (177)	85 (165)	91 (177)	92 (179)	92 (179)
Fuel Required, kg (lb)	24 (53)	28 (62)	26 (57)	40 (88)	33 (73)
Gross Takeoff Weight, kg (lb)	298 (657)	348 (767)	328 (723)	294 (648)	327 (721)
Fuel Type	AVGAS, MOGAS (>91 AKI)	AVGAS, MOGAS (>91 AKI)	AVGAS, MOGAS (>87 AKI)	Jet Fuel	Jet Fuel

The Pugh Matrix ranking the remaining engines is shown in Table 8.2. The evaluation criteria were:

- **Productivity:** A fast, light aircraft is better than a slow, heavy one. As per the RFP, productivity is a surrogate for cost, and is an excellent combined performance metric.
- **Maturity and certification:** With the emphasis on safety and rapid certification, proven and reliable technologies are preferred.
- **Volume and integration:** Large (or multiple) engines not only displace other components and thus increase the helicopter's mass, drag, and mechanical complexity.
- **Fuel consumption:** Although a powerplant that uses significant fuel would already lose points under the productivity criterion, excessive fuel use complicates operations during disaster relief (operations from unsupported sites, fuel shortages, etc.). It also is one of the biggest expenses in aviation and can be an unnecessary strain on the environment if more efficient designs are ignored.
- **Fuel type:** The capability of utilizing low-octane MOGAS greatly expands the aircraft's reach, removing restrictions from being based at airports and decreasing costs.
- **Transient response:** Turbine engines generally have slower engine response ("spool up") times than comparable reciprocating engines.



Table 8.2: Powerplant selection Pugh matrix

Criteria	Weights	Normalized Weights	Rotax 915 iS	UAV Engines AR682R	PBS TS100ZA	Rolls Royce RR300
Productivity	5.00	0.26	0	-2	0	0
Maturity and Certification	5.00	0.26	0	0	-4	2
Volume and Integration	4.00	0.21	0	-4	1	-3
Fuel Consumption	3.00	0.16	0	-1	-4	-2
Fuel Type	2.00	0.11	0	2	-2	-2
Transient Response	2.00	0.11	0	0	-2	-2
Score			0.00	-0.47	-2.53	-0.63

The Rotax 915 iS had a better overall score than the other options, and thus was selected as the powerplant for this helicopter. Notably, it was also the least expensive engine with pricing information available.

8.3 Engine Installation and Operation

The engine is installed in the nose bay of the aircraft using its included support bracket attached to the structure surrounding the firewall. The Rotax 915 iS Configuration 3 version includes a constant speed propeller hydraulic governor which is modified to maintain constant rotor RPM. Affixing the propeller flange to the lower drive sheave will require careful calibration, dynamic balancing, and consultation with the engine manufacturer. Similar installations of Rotax engines have been demonstrated in other helicopters [39].

The Rotax 915 iS can be started with the aircraft's battery. The engine includes an internal alternator that powers the fuel pumps and ignition system, while also providing limited power (500 W) to aircraft accessories. An additional 3 kg (7 lb) external alternator is typically shipped with the engine and belted to the Propeller Speed Reduction Gearbox, but because of the high electric power requirement of the Alicorn, much larger alternators driven by the transmission will be used instead [39]. Section 10 provides additional information on the electrical system.

Air ducted through inlets in the fuselage will feed the turbocharger intake, pass over the intercooler, and pass over the engine body for cooling. The engine exhaust pipe protrudes slightly from the left of the fuselage. Fuel will proceed from the tanks behind the firewall to the fuel rail inlet for combustion. The engine fuel pumps and gravity will provide sufficient suction for reliable fuel flow [39].

The avionics and flight control system interface with the Rotax 915's Electronic Engine Management System (EMS) to control engine start, throttle position, speed governing, and shutdown. The engine can operate at 5,800 RPM and provide up to 104 kW (141 HP) for five minutes (MRP), or continuously at 5,500 RPM, producing up to 99 kW (135 HP) (MCP) [37]. A clutching bracket affixed to the engine allows for the engine to be lifted slightly, relieving the transmission load and allowing for engine start independent from the rotor system. The clutching system and transmission integration are discussed in Section 9.

8.4 Fuel System

A semi-partitioned 40 L (10.6 gal) fuel tank is located behind the engine firewall and forward of the payload. At approximately half of its depth, the tank separates into two compartments. This provides clearance over the longer-length payload as well as preventing complete loss of fuel in the unlikely event of a leak. The tank accommodates 30 kg of premium grade motor vehicle gasoline (U.S. 91 octane rating, or equivalent aviation fuel) with room for expansion in warmer temperatures. The external structure is aluminum and the interior contains a crash-worthy plastic liner. The aircraft is gravity fueled utilizing either of two caps on the dorsal side of the fuselage. The caps are equipped with vents to prevent vapor accumulation and over pressure conditions. Fuel samples can be taken from a common sump access point on the underside of the aircraft. The Rotax 915 iS fuel system provides sufficient suction to extract the fuel and inject it into the engine cylinders for combustion. Two small boost pumps located near the bottom of each side of the tank are operated during startup, takeoff and landing, and fuel priming. Two potentiometers detect the fuel level and provide data to the avionics.

9 Transmission Design

9.1 Overview

The transmission arrangement was a logical outgrowth of a reciprocating engine selection and the utilization of a lightweight belt-drive demonstrated by small manned helicopters currently in production. Typical drive systems designed produced by Dynali, a Belgian manufacturer of light manned helicopters (powered by the similar Rotax 912 and 914 engines), as well as by the Robinson Helicopter Company, are shown in Figure 9.1. Robinson's R22 and R44 clutch designs move a driveshaft using a flex coupling, whereas Dynali lifts their engines to reduce belt tension. The transmission design of the Alicorn is similar to the Dynali design, including the transmission-driven alternator [45][46][47].

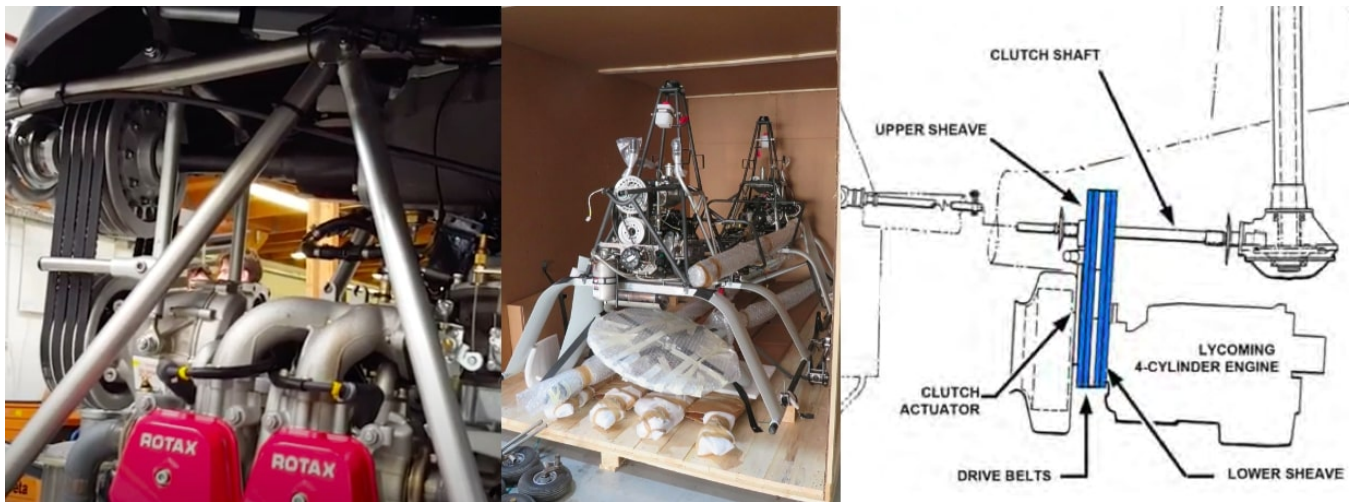


Figure 9.1: Light helicopter belt drive systems, from left to right: Dynali H3 manned helicopter, Dynali H3 UAV versions prior to shipment for agricultural/logistics/surveillance modification, and Robinson R44 Raven



Figure 9.2: Front-left isometric view of engine and transmission

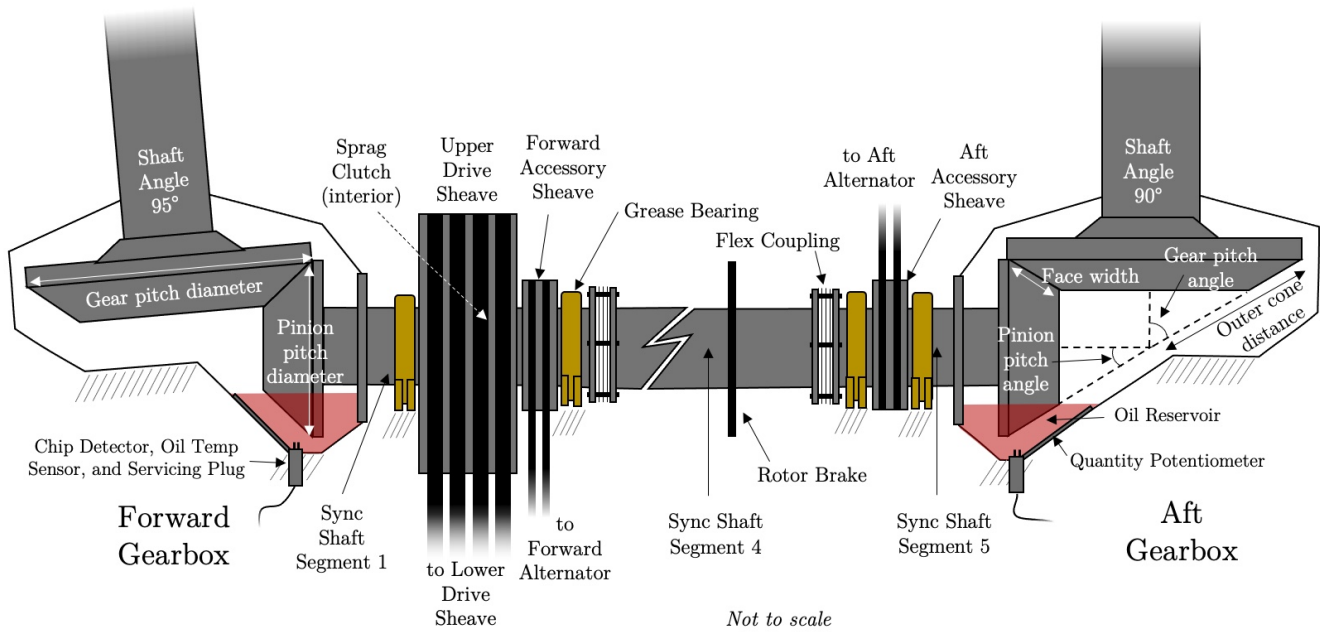


Figure 9.3: Transmission schematic

Because of the smaller rotor radius and high angular velocity requiring an overall reduction ratio of only 4.47, aside from the engine's included Propeller Speed Reduction Gearbox, there are only two additional

reduction stages needed between the engine’s output flange and the rotor system. In order to prevent damaging the engine on startup, it is unloaded from the main transmission. This also provides a safety benefit by allowing engine start before rotor system engagement. Thus a belt drive system can link the engine and the driveshaft linking the gearbox (also known as the synchronizing shaft). V-belts and pulleys can be lighter than traditional spur gear transfer cases, and require much less maintenance, and allow for a simple engine clutching method. Efficiencies for belt drives can be almost as high as traditional geared transfer cases. A view of the engine and transmission is shown in Figure 9.2.

A summary of the drivetrain component speeds are shown in Table 9.1. The Rotax 915 iS develops its maximum power at 5,800 RPM, which results in a 1,298 RPM rotor speed. However, except for maximum gross weight takeoffs and other high power situations of less than five minutes in duration, the aircraft will predominately operate at the maximum continuous rotor speed of 1,231 RPM, which is optimized for lower advance ratios in high speed forward flight.

“Equivalent gear teeth” are listed for the engine’s Propeller Speed Reduction Gearbox, where the ratio was known but the exact multiples of teeth were not readily available from the manufacturer, and to represent the relative size of the smooth upper sheave (needed for smooth engine to driveshaft clutching) compared to the toothed lower sheave shafted to the engine. Because the alternators are driven by the slower moving synchronizing (“sync”) shaft in order to maintain electrical power in the event of an engine malfunction, its reduction ratio is less than one. As is standard in gear design, speed ratios and associated tooth numbers were based on exceeding minimum values (usually 12) to prevent gear failure, and using ratios of primes (or integers that have a greatest common denominator of one) to allow for more even wear.

Table 9.1: Drivetrain component speeds at maximum continuous and maximum rated power settings

Drive Section	MCP (100%)	MRP (105.5%)	Gear Teeth	Reduction Ratio
Engine	5,500 RPM	5,800 RPM	7 (equiv)	-
Prop Reduction Gearbox	2,263.4 RPM	2,386.8 RPM	17 (equiv)	$17/7 \approx 2.43$
Lower Sheave	2,263.4 RPM	2,386.8 RPM	31	-
Upper Sheave	1,896.3 RPM	1,999.8 RPM	37 (equiv)	$37/31 \approx 1.19$
Sync Shaft Bevel Pinion	1,896.3 RPM	1,999.8 RPM	37	-
Rotor Shaft Bevel Gear	1,231.0 RPM	1,298.1 RPM	57	$57/37 \approx 1.54$
Rotor Tip Speed	201.75 m/s (662 ft/s)	212.75 m/s (698 ft/s)	-	$57/31 \times 17/7 \approx 4.47$ (overall from engine)
Alternator	4,999.5 RPM	5,272.1 RPM	57	$11/29 \approx 0.379$

9.2 Gearboxes and Synchronizing Shaft

Gear design was based upon the methods outlined in Dudley’s Handbook [48], and per American Gear Manufacturer’s Association (AGMA) guidance [49][50]. A single-stage bevel gear arrangement was used for the rotor gear boxes. Because of the 5° difference in shaft tilts, the shaft angles of the rear and forward gearboxes are 90° and 95° , respectively. The pinions (input gears) are mounted to both ends of the synchronizing shafts, and the rotor drive bevel gears are mounted with their teeth facing downwards, which has the benefit of preventing oil churn and metal particles from accumulating. Splash-type lubrication is driven by the pinion as it spins through the oil reservoir at the bottom of the gearbox. The reservoir geometry ensures constant lubrication at different aircraft attitudes, and its separation from the rest of the gearbox provides more surface area for air cooling. A combination chip detector, oil temperature sensor, oil quantity potentiometer, and servicing plug are mounted to the bottom of each gearbox. These sensors’ data are used to determine servicing and maintenance intervals. Oil temperature is designed to be below 120°C . The general gearbox installation is illustrated in Figure 9.3.



Table 9.2: Bevel gear material properties

Gear Material Properties: Carpenter Pyrowear ® 53 Tool Steel			
Characteristics	Case hardened, temperature resistant	Iron, Fe	89.50%
Brinell Hardness	334	Molybdenum, Mo	3.25%
Ultimate strength, MPa (ksi)	1,172 (170)	Copper, Cu	2.00%
Yield strength, MPa (ksi)	965 (140)	Nickel, Ni	2.00%
Elastic modulus, GPa (ksi)	200 (29,000)	Chromium, Cr	1.00%
Poisson's ratio	0.30	Silicon, Si	1.00%
Density, kg/m ³ (lb/ft ³)	7,800 (487)	Manganese, Mn	0.35%
		Carbon, C	0.10%
		Vanadium, V	0.10%

Table 9.3: AGMA bending stress for gearbox input pinion teeth

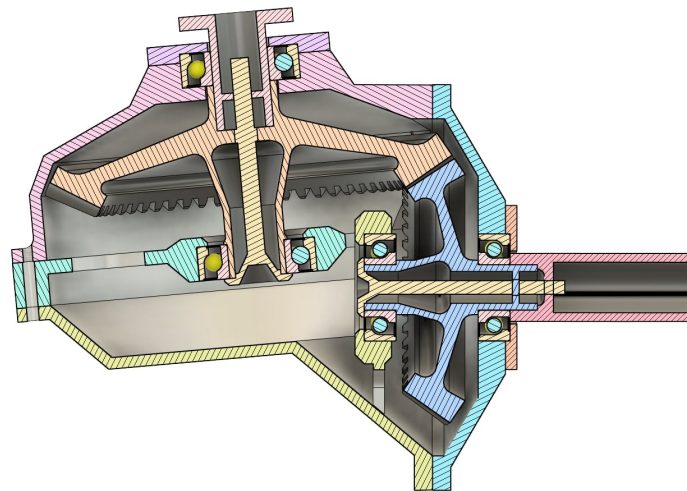
AGMA Maximum Design Bending Stress		AGMA Maximum Allowable Bending Stress	
60% MRP per gearbox, kW (HP)	84.6 (115)	AGMA bending strength, MPa (ksi)	348 (50.5)
Pinion angular speed (RPM)	2,000	Factor of safety	1.5
Torque on pinion, N-m (ft-lb)	298 (220)	Stress cycle factor (>8,000 hrs)	0.9
Tangential transmitted load, N (lb)	5,138 (1,155)	Temperature factor	1
Overload factor	1	Reliability factor (99%)	1
Quality number	12 (highest)	Allowable tooth bending stress, MPa (ksi)	208 (30.2)
Dynamic factor	1		
Size factor	1		
Load distribution factor	1.3		
Rim thickness factor	1		
Geometry factor	0.41		
Tooth bending stress, MPa (ksi)	208 (30.2)		

To ensure a lightweight, compact, and resilient gearbox, Pyrowear 53 Tool Steel was chosen as the material. It is produced through a case hardening process and is very temperature resistant, an important metric for aircraft drivetrains [51]. Its characteristics are listed in Table 9.2. The constraint in the design was tooth bending strength of the smallest gear, the pinion input bevel gear. The facewidth was increased until the teeth were large enough to support this stress. The key values for this process are shown in Table 9.3. The gearboxes were designed for over 8,000 flight hours between overhauls and will require minimal maintenance. Views of the forward gearbox's bevel gears, cross section, and exterior are shown in Figure 9.4.

Values for the AGMA contact stress calculations are listed in Table 9.4. The allowable pitting is greatly in excess of the expected value, indicating that the bending stress was still the design constraint for sizing the transmission. The general parameters of the bevel gears are shown in Table 9.5.

Table 9.4: AGMA contact stress for gearbox input pinion teeth

AGMA Maximum Design Contact Stress		AGMA Maximum Allowable Contact Stress	
Tangential transmitted load, N (lb)	5,138 (1,155)	AGMA contact strength, MPa (ksi)	1,724 (250)
Geometry factor for pitting resistance	0.097	Factor of safety	1.5
Surface condition factor	1	Stress cycle factor (>8,000 hrs)	0.7
Material elastic coefficient MPa ^{1/2} , ksi ^{1/2})	233	Hardness ratio factor	1
Overload factor	1	Temperature factor	1
Quality number	12 (highest)	Reliability factor (99%)	1
Dynamic factor	1	Allowable tooth contact stress, MPa (ksi)	803 (117)
Size factor	1		
Load distribution factor	1.3		
Tooth contact stress, MPa (ksi)	225 (32.6)		



(a) Cross section



(b) Bevel gear meshing



(c) Exterior with sync shaft

Figure 9.4: Forward gearbox

Table 9.5: Bevel gear properties

Gear Parameter	Forward Gearbox	Aft Gearbox	Gear Parameter	Common to Both Gearboxes
Shaft Angle (deg)	95	90	Pinion number of teeth	37
Pinion pitch angle (deg)	34.43	32.99	Gear number of teeth	57
Gear pitch angle (deg)	60.57	57.01	Face width, mm (in)	24.9 (0.980)
Pinion rotation	CW viewing forward	CCW viewing aft	Diametral pitch, teeth/mm (teeth/in)	0.319 (8.10)
Gear rotation	CCW from above	CW from above	Pinion pitch diameter, mm (in)	116 (4.57)
Pinion spiral handedness	Right	Left	Gear pitch diameter, mm (in)	179 (7.04)
Gear spiral handedness	Left	Right	Outer cone distance, mm (in)	75.0 (2.95)
			Pressure angle (deg)	20
			Working depth, mm (in)	5.33 (0.210)
			Clearance, mm (in)	0.589 (0.0231)
			Spiral angle, mm (in)	35
			Whole depth, mm (in)	6.96 (0.274)
			Addendum, mm (in)	1.94 (0.0764)
			Design backlash, mm (in)	0.051 (0.0020)

As in all inter-meshing helicopters, the purpose of the sync shaft is to transfer torque to each gearbox, to keep the rotors phased (preventing collision), and to transfer torque as needed during an autorotation. The forward and aft segments are not only in torsion, but also are under bending stress due to the pulley tensions. Thus, they are made of solid steel, and their short lengths are supported by grease bearings on either side. The longer segments are made of hollow aluminum, and are in addition to grease bearings are attached to flex couplings that allow for some movement and aircraft structural deformation. A rotor brake is located on the aft segment to allow for rapid shutdowns when necessitated for safety or in high winds. The overall weight is less than 7 kg, including supports. Design data for the sync shaft is shown in Table 9.6.

Table 9.6: Sync shaft data

Sync Shaft Segment	Length mm (in)	Material	Density kg/m ³ (lb/ft ³)	Yield strength MPa (ksi)	Allowable shear stress MPa (ksi)	Max bending moment N-m (ft-lb)	Max torque N-m (ft-lb)	Diameter mm (in)	Thickness mm (in)	Critical speed (RPM)	Max speed (RPM)
1 (forward)	168 (6.61)	ASTM A514 Steel	7,850 (490)	690 (100)	66 (9.6)	670 (494)	497 (367)	45 (1.8)	Solid	No factor (short solid shaft)	2,000 (well below critical speeds, avoids resonance)
2	664 (26.1)	6061-T6 Aluminum	2,700 (169)	275	27	Negligible	298 (220)	30 (1.2)	3.9 (0.15)	5,512	
3	534 (21.0)									7,905	
4	380 (15.0)									15,609	
5 (aft)	60 (2.36)	ASTM A514 Steel	7,850 (490)	690 (100)	66 (9.6)	17 (13)	298 (220)	31 (1.2)	Solid	No factor (short solid shaft)	

9.3 Drivebelt design

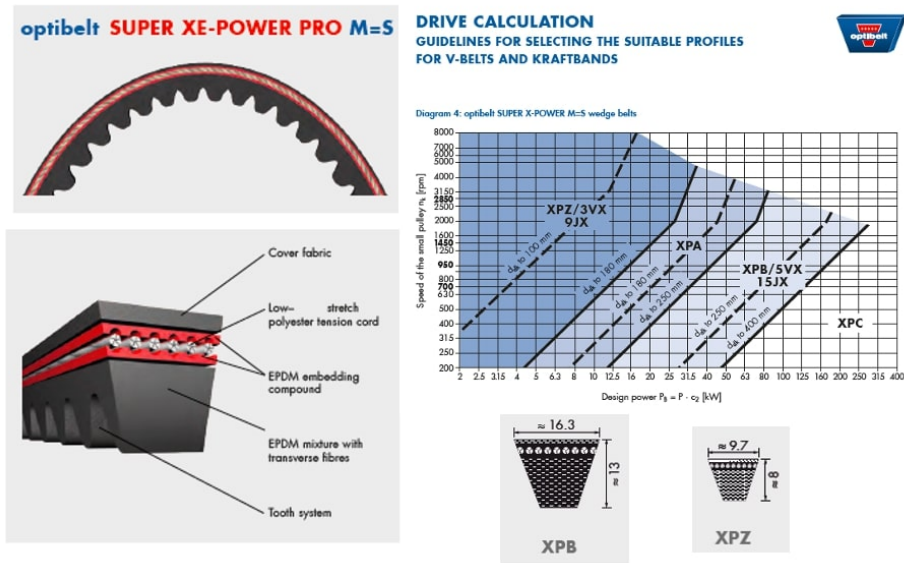


Figure 9.5: Optibelt V-Belts

Table 9.7: Sheave and belt data

	Lower Drive Sheave	Upper Drive Sheave	Forward Accessory Sheave	Forward Alternator Sheave	Aft Accessory Sheave	Aft Alternator Sheave
Pulley Location	Propeller reduction gearbox output flange	Forward sync shaft, contains sprag clutch	Forward sync shaft, aft of upper drive sheave	Below forward accessory sheave in engine bay	Aft sync shaft, between rotor brake and gearbox	Above aft accessory sheave in rear pylon
Rotation viewed from aft side	Clockwise					
RPM at 100% rotor speed	2,263	1,896	1,896	5,000	1,896	5,000
Diameter, mm (in)	188 (74.0)	224 (8.81)	112 (4.41)	43 (1.7)	112 (4.41)	43 (1.7)
Width, mm (in)	82 (3.2)		28 (1.1)		28 (1.1)	
V-Belt number and type	4 × Optibelt XPB (cogged)			2 × Optibelt XPZ (cogged)		
Cogged or smooth grooves	Cogged	Smooth	Cogged	Smooth	Cogged	Smooth
Static shaft tension, N (lb)	7,403 (1,664)		574 (129)		574 (129)	
Dynamic shaft tension, N (lb)	2,529 (569)		294 (66.1)		294 (66.1)	
Center-to-center distance, mm (in)	302 (11.9)		210 (8.3)		120 (4.7)	

V-belt and pulley design was based on data from Optibelt, a leading manufacturer of high-performance drive belts based in Germany. In addition to robust industrial applications, their belts have been used in aircraft. The belts selected were of the cogged Super XE-Power Pro type, which are constructed from ASTM standard D-1418 ethylene propylene diene monomer (EPDM) rubber and low-stretch polymer tension cords. Efficiencies for these configurations are expected to be in excess of 97%. Excerpts from their technical manual showing a cross section of the V-belts and some of the selection criteria are shown in Figure 9.5. Calculated sizing and tensions for the sheaves (pulleys) and the belts are provided in Table 9.7. Note that the dynamic tension is lower due to the centrifugal force pulling the belts away from the pulleys; the system is designed to support the static tensions. Optibelt claims belt life up to 25,000 hours if their design recommendations are followed. Although most ground vehicle and aircraft alternator installations



feature single drivebelts with similar geometry to the Alicorn, the alternator sheave sizes and separation distances are smaller than the manufacturer's recommendation for a single belt, and thus two belts are used for higher reliability. Even with an assumed belt life reduction of 50% to 12,500 hrs, the belts will only be at 64% of their design life if they are replaced when the gearboxes are overhauled at 8,000 hrs. Belts exhibit signs of impending failure by losing tension; the manufacturer provides measurement procedures and equipment to ensure safe operation [52].

9.4 Clutch System

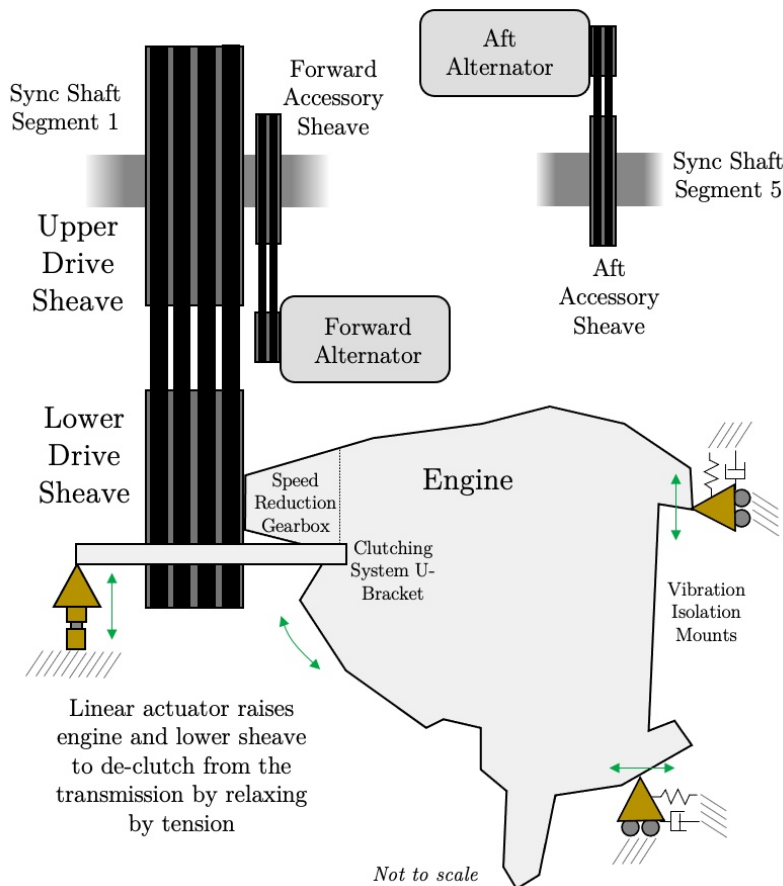


Figure 9.6: Engine, clutch, and alternator integration with transmission

An illustration of the engine and alternator integration with the V-belt drive is shown in Figure 9.6. The engine clutch actuator is designed to lift the forward engine mounts via a U-bracket by approximately 10 mm (0.39 in) to relieve the belt tension and allow the engine to start separately from the rotors. The engine shock mounts allow this small displacement. To engage the transmission after the engine start, the clutch actuator lowers in approximately 5 seconds. The V-belts spinning on the lower sheave will be pulled into the un-toothed grooves of the upper sheave. As the V-belts settle into the grooves, the resulting sidewall friction engages the sync shaft. When not powered, the clutch defaults to the engaged (down) position.

10 Avionics

Safe, reliable and high performance autonomous unmanned flight missions require an in-depth analysis of the existing state-of-the-art software frameworks and careful selection of the precise hardware. Factors such as redundancy, reliability, ability to survive extreme environments, size, weight, power, and cost informed the design and selection process of Alicorn’s avionics hardware. The software architecture follows the well-established classical robot autonomy and artificial intelligence techniques for most modules. Perception tasks utilize the more modern machine learning approaches that have higher benchmark scores and a proven track record in real-world scenarios.

10.1 Sensing Suite

Choosing the right sensors is extremely vital to the safety, stability, and performance of the autonomy framework as failures at the sensing level will cascade to failures at the control end. Selecting high-end sensing equipment will lead to an increase in processing power demand, which increases the overall weight and power requirements. On the contrary, selecting low-end or hobby-grade sensors increases the risk of failures and can put considerable strain at the estimation and control level as it now has to handle noisy sensors with high, time-varying biases. Keeping these factors into consideration Alicorn’s sensing suite shown in Figure 10.1 was optimally designed to meet the safety and performance requirements while ensuring healthy runtime of the autonomy software in non-catastrophic conditions. The following list gives an overview of all the selected sensors.



Figure 10.1: Primary situational awareness sensors

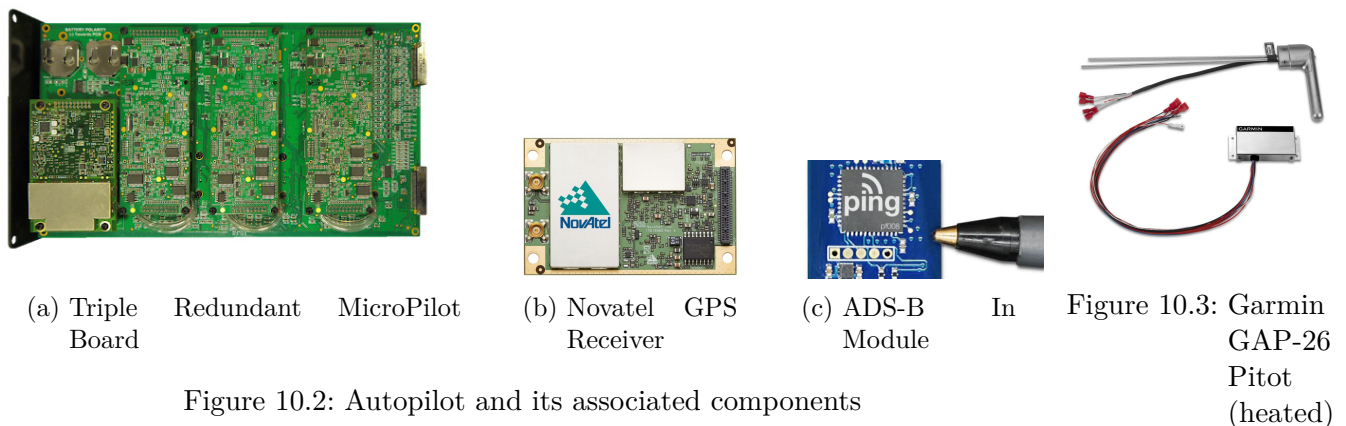


Figure 10.2: Autopilot and its associated components

- **LiDAR** determines ranges by targeting an object with a laser and measuring the time for the reflected light to return to the receiver. Since Alicorn flies at an altitude of 150 m (492 ft), LiDARs with range

ratings of more than 200 m (656 ft) at 10% reflectivity were selected. Specifications of the selected devices are shown in Table 10.1.

Table 10.1: Selected LiDARs

Name	Weight (kg)	Power (W)	Range (m)	Field-of-view	Angular Resolution
Horn X2	2.8	60	300	$90^\circ \times 30^\circ$	$0.09^\circ \times 0.083^\circ$
Velodyne Alpha Prime	3.5	22	220	$360^\circ \times 40^\circ$	$0.4^\circ \times 0.11^\circ$

Alicorn utilizes one Velodyne Alpha Prime, a panoramic scanning LiDAR for detecting objects surrounding the aircraft and two Horn X2 LiDARs from Benewake for scanning objects located on the ground as well as for precision landing tasks. Dust-penetrating (DUSPEN) filtering techniques are utilized so that LiDAR can perform mapping in occluded conditions. Since LiDARs have to protrude beyond the aircraft fuselage's OML, an aerodynamic protective glass window is required. To this end, we selected the BOROFLOAT 33 floated borosilicate flat glass due to its superior optical flatness, high transparency, chemical durability, low thermal expansion, and resistance to abrasion, scratches, and sharp impacts.

- **Cameras** being relatively small in size, lightweight, and low power consumption, they can be placed at a large number of locations to get omni-directional sensing coverage with a high degree of redundancy. They are crucial in providing situational awareness of the aircraft's surroundings. The primary selection factor is the MTBF metric and hence FLIR cameras were selected as they provide unparalleled performance with their robust camera casings and proven track record in space, military, and commercial applications. Factors such as resolution, dynamic range, external trigger capability, and any additional features that can help with processing and survivability in extreme environments informed the down-selection process. Selecting higher resolution provides longer range detection capability. A higher dynamic range is beneficial for operating in low-light and nighttime conditions. External trigger capability is essential for the tight-synchronization of multiple cameras. A summary of the selected cameras is shown in Table 10.2.

Table 10.2: Selected Cameras

Name	Weight (gms)	Power (W)	Dynamic Range	Resolution
FLIR Firefly DL	20	2.2	65.69 dB	1440×1080
FLIR Thermal Vision Automotive Development Kit (ADK)	100	4	8-14 μm (LWIR)	640×512
FLIR Blackfly S USB3 (5K Res.)	53	4.2	70.69 dB	5320×4600

The Firefly DL camera comes with an integrated Intel Movidius Myriad X Vision Processing Unit (VPU) which provides the perfect platform for offloading some Machine and Deep Learning based tasks from the primary processing hardware. Additionally, for vision based tasks VPUs are more energy efficient and lightweight, while having ample processing power. However, using Firefly camera comes at the cost of reduced resolution and thereby lower detection range. Therefore, for getting long range sensing which is essential for detecting objects in the aircraft's flight path, Alicorn uses Blackfly S cameras. Its higher dynamic range and 5k resolution help in detecting high-speed obstacles that are approaching the aircraft from front and bottom directions. Since, both Firefly and Blackfly cameras detect visible light only, Alicorn also uses Thermal Cameras for night-time operations, which are heat regulated and have an inbuilt sun protection. In contrast to Infrared (IR) cameras, these work passively, have a longer sensing range, and superior detection capability of humans and animal's

heat signatures.

- **Airspeed Probe** sensor placed on the fuselage nose provides high-quality airspeed data and angle-of-attack measurements at high-speeds. Alicorn uses a high-end fully-regulated heated version of the Garmin GAP-26 Pitot Tube, which serves as a layer of safety to vision, lidar, and GPS based ground velocity sensing. Additionally, it expands Alicorn’s versatility and its operational temperature extremes.
- **IMU, GPS, and ADS-B IN** hardware are integrated into the Autopilot. Alicorn’s Autopilot shown in Figure 10.2 is an upgraded version of the Triple Redundant MicroPilot MP2128^{3X} Autopilot. The MP2128^{3X} is comprised of three MicroPilot MP2128^{HELI2} autopilots, mounted on a redundancy board. This also enables triple redundancy for IMU and GPS receivers. The complete Autopilot system is isolated from vibrations and electromagnetic interference. Additionally, heat resistors in the Autopilot regulate the IMU temperature so that it performs optimally throughout the mission. Novatel OEM7720 GPS receivers have a very high MTBF score and hence, they are used by Alicorn as the primary localization unit. Alicorn also contains Automatic Dependent Surveillance-Broadcast (ADS-B) receivers so that it can avoid aircraft equipped with ADS-B Out.

10.2 Processing Suite

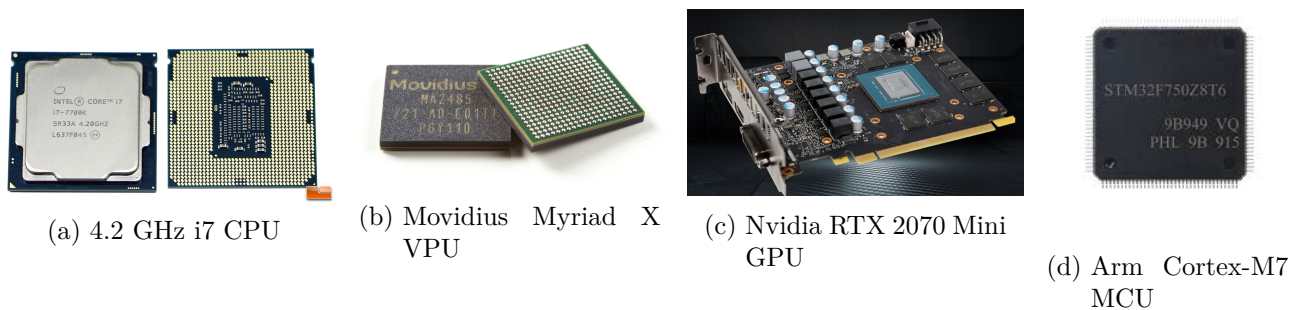


Figure 10.4: Onboard Processors

Alicorn’s processing suite contains numerous powerful processors, each one specialized for different types of tasks and processing requirements. The central avionics rack shown in Figure 10.5 houses a PC-motherboard with an Intel core i7 Central Processing Unit (CPU), dual Nvidia GeForce RTX 2070 Mini Graphics Processing Units (GPUs), three ARM Cortex M7 microcontrollers (MCUs) in Autopilot, and one in Health and Usage Monitoring System’s (HUMS) Data Processing Unit (DAPU). In addition to these, an Intel Movidius Myriad X Vision Processing Units (VPUs) comes pre-integrated with each Firefly DL Camera. Figure 10.4 and Table 10.3 provides an overview of all the Alicorn’s processing hardwares. The following list gives an overview of each processor’s specialization and the primary autonomy tasks that each processor is assigned.

- **CPU:** The desktop grade Intel core i7 processor has a clock speed range of 2.9GHz – 4.2GHz and 4 physical cores, which makes it suitable for intensive computing tasks such as sensor fusion, Simultaneous Localization and Mapping (SLAM), and motion planning. It also acts as the host for the huge amount of incoming sensor data from LiDARs and cameras. The images obtained from all the cameras are sent to GPUs for feature extraction, matching and triangulation tasks.
- **GPU:** Desktop grade dual Nvidia GeForce RTX 2070 Mini graphics cards are powered by the Turing GPU architecture and have more than 2K Nvidia CUDA (Compute Unified Device Architecture) cores, which makes it suitable for heavy parallelized tasks such as image feature extraction, matching,



Figure 10.5: Central avionics rack: Internals

and triangulation. It also handles deep-learning based object detection and classification tasks of Alicorn's front and bottom facing high-resolution cameras.

- **MCU:** The MCUs and embedded SoCs (System on Chips) of the Autopilot as well as the HUMS's DAPU contains ARM Cortex M7 processors which have very high-energy efficiency with accelerated single-precision, floating-point operations, and digital signal processing capabilities, making them suitable for performing intensive real-time tasks such as state estimation, control, and failure detection.
- **VPU:** Each Firefly DL camera contains the Intel Movidius Myriad X VPU, which have been designed to accelerate machine vision tasks and as such they are highly efficient in running machine vision algorithms such as CNN (convolutional neural networks), SIFT (Scale-invariant feature transform) and similar. Additionally, they bypass any off chip buffers and include direct interfaces to take data from cameras, making them suitable for deploying trained neural networks and making decisions on-camera thereby eliminating the need for a host system. Object detection and classification algorithms run independently on the VPU of each Firefly DL camera.

Table 10.3: Alicorn's Processing Suite

Name	Quantity	Net Weight (kg)	Net Power (W)
Intel core i7 CPU (with RAM, SSD, motherboard)	1	1	125
Nvidia GeForce RTX 2070 Mini GPU	2	0.8	350
ARM Cortex M7 microcontroller	4	0.04	4
Intel Movidius Myriad X VPU	10	0.2	20

10.3 Autonomy Architecture

Autonomy for UAVs or robots in general is its own ability of integrated sensing, perceiving, analyzing, communicating, planning, decision-making, and acting/executing, to achieve its goals as assigned. The actions may be confounded by the occurrence of unmodeled events, requiring the system to dynamically adapt or re-plan. Alicorn monitors the key elements of the dynamic world and adapts to changes in its

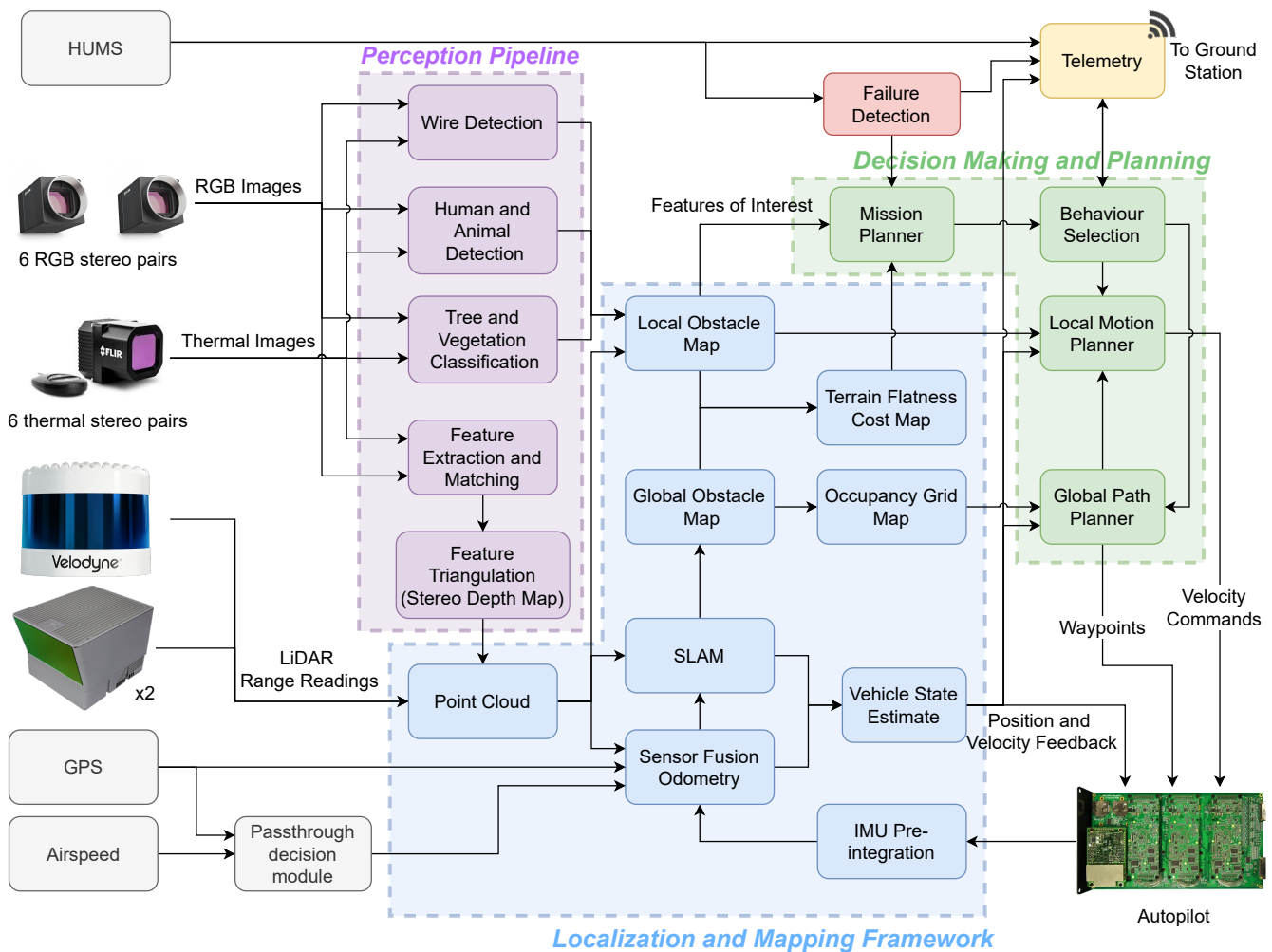


Figure 10.6: Autonomy Architecture

environment and in itself. Alicorn's autonomy stack is designed to handle open world conditions where environment is not known *a priori* and it has to generate new plans, monitor, change plans, and learn within the constraints of its bounded rationality. Alicorn follows a traditional autonomy architecture shown in Figure 10.6. Three different frameworks work in tandem to create a robust, reliable and intelligent behavior of the aircraft. The frameworks as well as the individual modules are divided according to temporal requirements (based on environmental dynamics and hardware support) which provides a coarse division of control as well as safety.

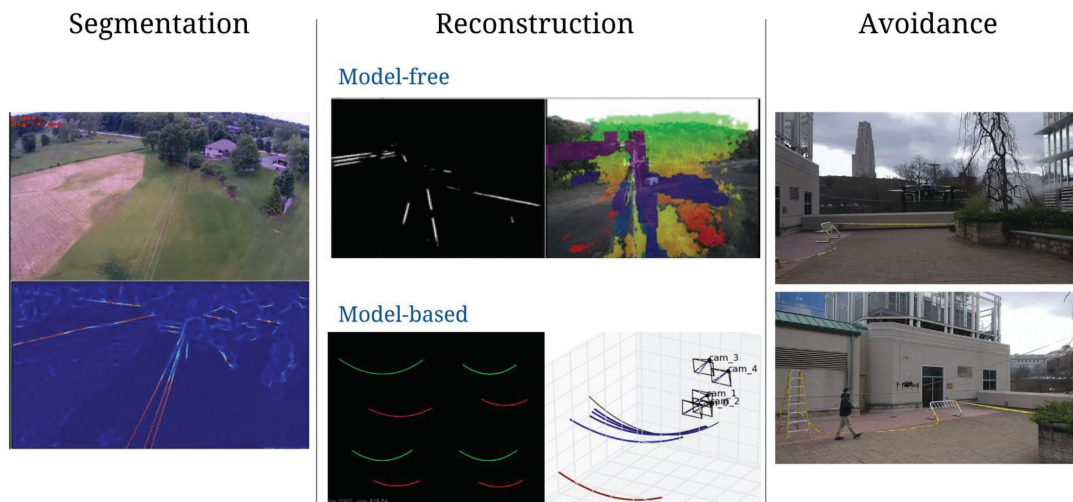
Object Detection

One of the state-of-the-art object detection methods with a high IoU (Intersection over Union) mAP (Mean Average Precision) a score of 0.5 on the Microsoft COCO (Common Objects in Context) dataset is YOLOv3 (You Only Look Once) network which is suitable for detecting objects like birds, animals, and humans from long-ranges. Figure 10.7 shows the network's detection probabilities of individual objects tested on sample aerial-images. Since the probabilities are low, Alicorn's perception pipeline utilizes YOLOv3 re-trained on COCO dataset with added labeled aerial images of animals, trees and other relevant objects.

Detection, reconstruction and avoidance of wires and power lines are extremely vital for safe operations.



Figure 10.7: Animal, human, and bird detection

Figure 10.8: Wire Detection Pipeline
Image taken from [53]

Thin wires and similar objects like power lines, cables, ropes and fences are some of the toughest obstacles to detect, and are a cause of numerous accidents each year. Compared to LiDARs, cameras are better at detecting wires from long distances. In [53, 54], the authors designed a wire segmentation framework and multi-view Reconstruction of wires using a Catenary Model. They treated pixel-wise wire detection as a binary semantic segmentation task and used a dilated CNN trained on a synthetic dataset augmented with a few real images. Figure 10.8 summarizes the wire detection and avoidance approach used by Alicorn.

10.4 Communications System

Alicorn is equipped with a triple-redundant communications system for enabling reliable communications between the UAV and ground control station, as well as providing a datalink for transmitting UAV-captured information, including images and video feeds. These sub-systems are described below.

- **Radio:** Alicorn uses pMDDL (Pico MIMO Digital Data Link) Radio for high power, long range broadband COFDM (Coded Orthogonal Frequency-Division Multiplexing) wireless communication.

It uses Maximal Ratio Combining (MRC), Maximal Likelihood (ML) decoding and Low-Density Parity Check (LDPC) to achieve robust performance. Operating in the frequency range of 2.402 - 2.478 GHz, it enables low-latency wireless control, telemetry, and video link. Additionally, it has inbuilt AES(Advanced Encryption Standard) encryption for enhanced system safety and security. Its output power is 1W and hence for 200+ km long-range Beyond Visual Line of Sight (BVLOS) operations, it is paired with a NuPower Xtender Bidirectional Amplifier which has 10W Output Power, 10dB gain while transmitting, and 13dB gain while receiving.

- **LTE:** A Botlink XRD device on Alicorn enables LTE command and control capabilities, providing a layer of safety to BVLOS flights. In case of emergency or radio link blackout, operator can monitor and guide Alicorn using a 4G LTE connection from anywhere in the world through the cloud. It also uses the 128-bit AES encryption for internet security.
- **Satellite:** Honeywell's Small UAV SATCOM enables command and control capabilities from anywhere in the world. It operates on the fast, secure and ultra-reliable Inmarsat SwiftBroadband high speed satellite network (SBB) and provides the ultimate layer of communication safety.

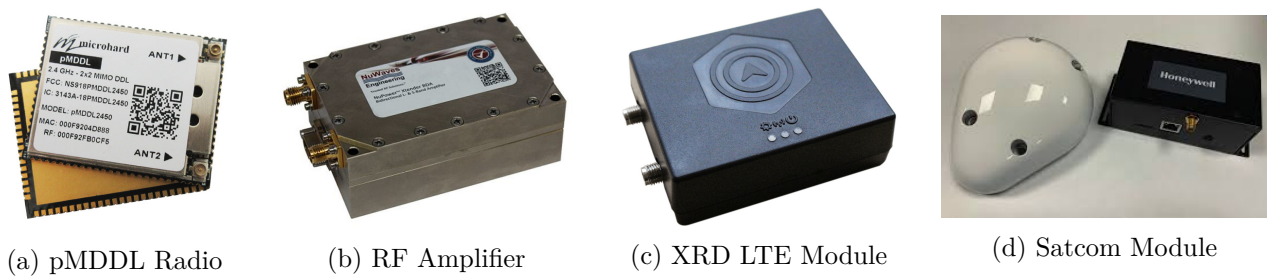


Figure 10.9: Communications System

10.5 Health and Usage Monitoring System

The Health and Usage Monitoring System (HUMS) aboard Alicorn collects data from numerous sensors located at key locations (engine, transmission, actuators, cooling system, hub, tunnel, pylons, gearboxes etc.) and analyzes the aircraft condition to ensure its availability, reliability and safety. The HUMS self-diagnoses the aircraft and characterizes the severity of failures if it occurs, so that appropriate decisions can be made by the aircraft. In addition, it performs predictive maintenance which is essential for reducing costs and aids in performing repairs when the damage is minor to increase the aircraft mean time before failure (MTBF) and decreases the mean time to repair (MTTR). Furthermore, it also performs operational data recording and reduces aircraft on ground instances.

10.6 Thermal Management System

Thermal management is crucial for safe, reliable, and long-term operations of avionics hardware. It is essential that the operating temperatures of avionics are kept within acceptable limits as they experience a wide range of rugged environments such as freezing conditions, high humidity, sand and temperature extremes. Liquid cooling the avionics is suitable for Alicorn due to its efficient heat transfer over distance with low rates of mass transfer and wide range of operating temperatures. Transporting heat away from the source to a secondary cooling surface allows for large, more optimally designed radiators.

Figure 10.10 shows the liquid cooling system of the central avionics rack. Three primary high temperature areas have been targeted: CPU, GPU, and autopilot. A custom designed liquid block shown in Figure 10.11 is used for cooling the autopilot, radio amplifier, HUMS DAPU, and other nearby mounted components.

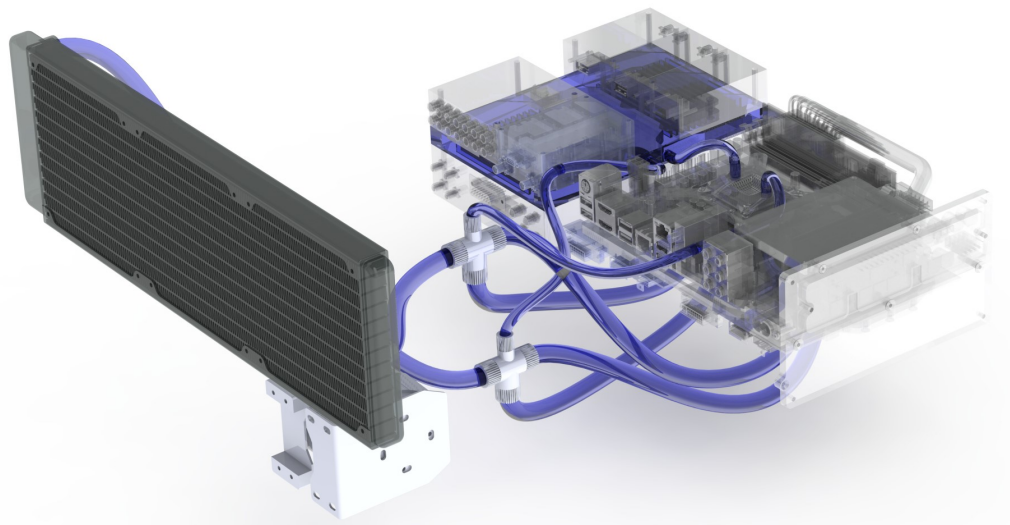


Figure 10.10: Central avionics rack: Liquid Cooling System.
Tube lengths are exaggerated for clarity.

The liquid cooling system uses micro-channels to improve the functionality, efficiency, dependability and safety of the avionics. Additionally, it regulates flow rate to different areas of a heated surface, targeting more cooling to higher power regions. Furthermore, it has a sealed design for leak-tight performance over the full temperature and pressure ranges.

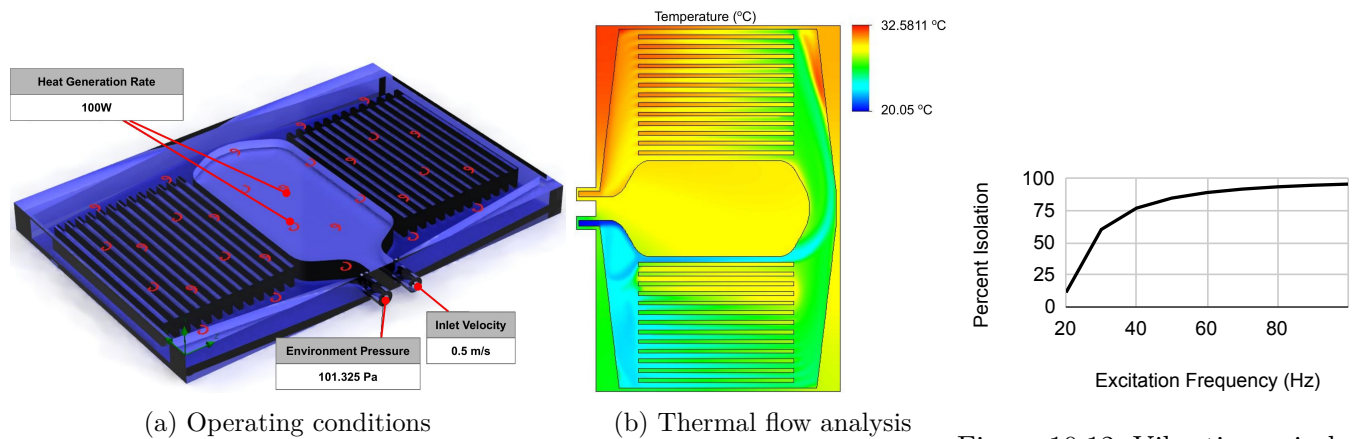


Figure 10.11: Custom designed liquid cooling block

Figure 10.12: Vibration isolation

10.7 Mounting and Vibration Isolation

Alicorn's electronics are mounted on a rugged aluminum chassis and are enclosed in an air-tight EMI protected casing. Alicorn is a relatively small helicopter and hence it experiences higher frequency vibrations of more than 40 Hz. Therefore, passive vibration isolation mounts are sufficient for isolating engine and rotor vibrations. The central avionics rack is mounted to the aircraft body using eight M12 vibration isolating studs. The studs contain Sorbothane disk isolation pads of 30 durometer hardness and are mounted under 20.4 kg (45 lbs) of compression load. Figure 10.12 shows the vibration isolation characteristic of the selected Sorbothane mounts.

10.8 Weight, Power and Cost Summary

A breakdown of the Alicorn's avionics components and their weight, power and cost estimates are presented in Table 10.4. Since, some components do not have their current prices listed online, their costs were adjusted to account for diminution. The total weight of the avionics is 18.871 kg. The total maximum continuous power consumption is 957 W. The total cost estimate is 131,100 USD.

Table 10.4: Avionics Breakdown

Name	Quantity	Net Weight (kg)	Net Power (W)	Cost (USD)
Autopilot (incl. ADS-B IN, radio telemetry, and GPS Receivers)	1	0.859	25	5K
HUMS Data Processing Unit	1	0.3	5	0.5K
Radio Amplifier	1	0.3	25	1K
LTE comm	1	0.3	25	0.5K
SatComm	1	0.3	25	0.5K
Power Management System	1	0.3	5	0.5K
PC-Motherboard (incl. RAM, SSD etc.)	1	1	125	1K
Nvidia GPUs (w/o fan and heatsink)	2	0.8	350	2K
Liquid Cooling System	1	1	10	0.5K
FLIR Firefly DL Cameras	8	0.32	18	2.4K
FLIR BlackFly S (High Res.) Cameras	4	0.292	17	10K
FLIR Thermal Vision ADK Cameras	12	1.2	48	24K
Velodyne Alpha Prime LiDAR	1	3.5	22	27K
Benewake Horn X2 LiDARs	2	5.6	120	50K
Transceivers' comm antennas	3	0.6	3	1.8K
GPS Antennas	3	0.3	3	1.8K
Garmin Pitot Airspeed sensor	1	1	102	0.5K
HUMS Sensors	20	0.4	20	2K
Capacitive Touchscreen	1	0.5	10	0.1K
Total		18.871	957	131.1K

10.9 Electrical Power Components

Based on the 1.4 kW peak power consumption of the avionics, flight control system actuators, and other electrical loads, appropriately sized FAA-certified 24 V electrical components were selected. The AL24-70 24 V/ 70 A Alternator produced by Plane Power, Ltd, a standard belt-driven alternator used in the general aviation community, meets the requirements for this aircraft's power consumption [55, 56]. With a normal operating range of 2,500 to 10,000 RPM, when the engine is at a fast idle speed with the belt drive system engaged, both alternators provide sufficient power for all aircraft systems. Cooling is provided by air flowing over the alternators, augmented by self-powered fans. The alternators are geared to run at 5,000 RPM when the rotor is spinning at 100%. The forward alternator turns in the standard clockwise direction (viewed from the rear). Due to space restrictions, the aft alternator runs counterclockwise, which requires minor diode and fan orientation modifications. Only one alternator is required to handle all electrical loads above idle speed, providing a 17% margin at peak power consumption. Thus, the two alternators provide safety and redundancy for the autonomous systems controlling the aircraft. With a 46% mechanical to electrical conversion efficiency, 3 kW (4 HP) is required from the engine to provide the peak electrical

power. The alternator’s dimensions are shown in Figure 10.13.

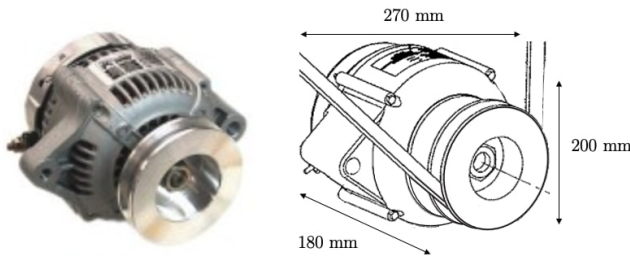


Figure 10.13: Plane Power AL24-70 Alternator

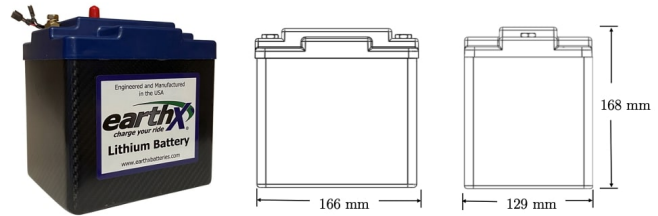


Figure 10.14: EarthX ETX680-24-TSO 24 V battery

The earthX ETX680-24-TSO 24 V battery is a lightweight power source suitable for 70 A alternator installations. Constructed with eight Lithium Iron Phosphate cells, it is approximately half the mass of an equivalent lead-acid battery. This technology generally provides stronger cranking power and more consistent discharge voltage when compared to conventional batteries, and should not be confused with consumer electronics-grade Lithium Ion batteries that have potential safety issues in aircraft. The battery life is advertised as 6 years or 4,000 cycles at 20% depth of discharge. The operating temperature is certified to between -30 °C and 60 °C (-22 °F to 140 °F), with 30 minutes up to 65 °C (149 °F). The allowable storage temperature is between -40 °C and 60 °C (-40 to 158 °F). The battery can operate up to 15,240 m (50,000 ft). The full charge resting voltage is approximately 26.6 V. The integrated Battery Management System is designed to redundantly protect from over discharge, over charge, short circuit, excessive cranking, and cell asymmetry conditions [57, 58, 59]. The battery’s dimensions are shown in Figure 10.14.

The installed Rotax 915 iS engine also contains an internal alternator that is used to power its fuel injection and control system, which is further described in Chapter 8. Its 500 W output is also used to re-charge the battery and support the initialization of some avionics before the belt drive is clutched and the main alternators are engaged. Additional information on the alternator installations and their belt drive systems are provided in Chapter 9. A breakdown of the weight, power and cost estimates for electrical power components are presented in Table 10.5 [55, 58].

Table 10.5: Electrical Power Components

Name	Quantity	Unit Weight / kg	Rated Power	Cost / USD
Plane Power AL24-70 24 V/ 70 A Alternator	2	5.3	1,680 W	821
earthX ETX680-24-TSO 24 V/ 11.7 A-hr Battery	1	3.3	500 A I_{pr}	999

11 Weight and Balance

The Alicorn has an empty weight of 221 kg (487 lb), which is defined with zero usable fuel, no payload, and no payload handling cart. The aircraft will have a total weight at engine start of 298 kg (657 lb) for maximum productivity during the 200 km (108 nmi) Logistics Mission; lower weights are expected for the Local Delivery Mission and if lower speeds are flown. Component weights are shown in Table 11.1.

Each configuration’s fuel and gross weights, center of gravity positions, and moments of inertia are shown



in Table 11.2. The datum for the center of gravity is situated longitudinally (x) near the midpoint between the rotor hubs, aligned laterally with the axis of symmetry (y), and positioned vertically near the bottom of the extended landing gear (z). The standard positive forward, right, and down body axis sign conventions are used. Because of the high excess power required to achieve the 90 m/s (175 kt) cruise speed, the Alicorn is capable of significantly exceeding the RFP requirements in terms of payload and range. This also provides significant room for future mission growth, represented by the “Jumbo” and “Super Jumbo” configurations. Note the CG travel is only about 4 cm (1.6 in) between configurations. The data presented here were applied in Section 13 to accurately model the aircraft’s flight dynamics and to ensure sufficient rotor control authority in each of the weight and balance configurations.

Table 11.1: Weight statement for Logistics Mission

System	Component	Mass		System	Component	Mass	
		kg	lb			kg	lb
Rotor System and Flight Controls	Forward hub and blades	8.75	19.29	Engine	Base engine and speed reduction gearbox	71.23	157.04
	Aft hub and blades	8.75	19.29		Cooling air baffle	0.38	0.84
	Forward rotor shaft	0.30	0.66		Positive Crankcase Ventilation Valve	0.35	0.77
	Aft rotor shaft	0.47	1.04		Oil tank	1.50	3.31
	Forward flight controls	1.30	2.87		Intercooler	1.65	3.64
	Aft flight controls	1.30	2.87		Engine Control Unit	1.13	2.49
	Forward flight control actuators	3.00	6.61		Fusebox	2.02	4.45
	Aft flight control actuators	3.00	6.61		Ambient sensors	0.06	0.13
Transmission	Forward gearbox	3.90	8.60	Fuel System	Wiring harness	2.50	5.51
	Aft gearbox	3.90	8.60		Intermediate flange, overboost valve, air hose	1.72	3.79
	Upper sheave and belts	6.59	14.53		Engine oil and coolant	3.00	6.61
	Lower sheave	2.82	6.22		Fuel system	3.74	8.25
	Aft sheave and belts	1.62	3.56		Fuel (logistics mission, including reserves)	23.60	52.03
	Sync shaft, bearings, couplings, sprag clutch	6.18	13.62		Unusable fuel	0.58	1.28
	Rotor brake	0.50	1.10		Payload Handling System	Ramp and door actuation system	3.17
Clutch system	2.00	4.41	Clamshell doors	4.19		9.23	
Structure	Fuselage structure	21.95	48.39	Ramp		3.00	6.61
	Nose landing gear	2.50	5.51	Payload loading winch		2.00	4.41
	Aft landing gear	5.40	11.90	Cart	3.70	8.16	
Avionics and Electrical System	Forward alternator	5.31	11.71	Payload	50.00	110.23	
	Aft alternator	5.31	11.71				
	Battery	3.30	7.28				
	Main avionics rack	5.96	13.14				
	Sensors	14.71	32.43				
						kg	lb
Gross Weight at Engine Startup						298.34	657.73

12 Vehicle Performance

12.1 Performance Model Validation

The performance model used in this report was validated using UH-60A flight test data [60]. The inputs included data from Howlett’s mathematical model for the Blackhawk that was presented to NASA [61]. As shown in Figure 12.1, the predicted performance follows the actual data very closely.



Table 11.2: Center of gravity and moments of inertia for various configurations

Configuration	Fuel (kg)	Payload (kg)	Container Type	Total Mass (kg)	Center of Gravity (m)			Moments and Products of Inertia About CG (kg-m ²)					
					x	y	z	I _{xx}	I _{yy}	I _{zz}	I _{xy}	I _{xz}	I _{yz}
Logistics	23.6	50	Cube	298.3	-0.086	0.003	-0.998	43.74	199.55	179.72	0.73	10.75	0.08
Launch Site Takeoff	23.6	50	Long	298.3	-0.086	0.003	-0.982	43.34	206.27	184.85	0.73	7.76	0.07
Local Delivery	13.4	50	Cube	288.1	-0.088	0.003	-1.033	43.33	199.65	179.00	0.72	10.74	0.08
Launch Site Takeoff	13.4	50	Long	288.1	-0.088	0.003	-1.016	42.89	206.33	184.13	0.72	7.74	0.06
Local Delivery	7.3	50	Cube	282.0	-0.090	0.004	-1.051	43.45	200.03	178.65	0.72	10.78	0.08
Destination Takeoff	7.3	50	Long	228.3	-0.090	0.004	-1.033	42.99	206.70	183.77	0.72	7.77	0.06
	7.3	0	None	234.7	-0.109	0.004	-1.275	53.25	193.44	158.17	0.59	24.18	0.10
Landing	0	50	Cube	274.7	-0.093	0.004	-1.089	44.41	201.52	177.95	0.72	10.95	0.07
No Fuel Reserve	0	50	Long	274.7	-0.093	0.004	-1.071	43.91	208.15	183.07	0.72	7.92	0.06
	0	0	None	224.7	-0.114	0.004	-1.332	59.62	200.71	157.83	0.59	26.68	0.10
Jumbo	25	75	Cube	324.7	-0.079	0.003	-0.922	47.60	212.60	190.96	0.77	10.28	0.07
	0	75	Cube	299.7	-0.086	0.003	-0.998	44.06	210.12	188.93	0.77	8.82	0.06
Super Jumbo	25	100	Cube	349.7	-0.073	0.003	-0.856	53.96	228.52	202.56	0.81	12.02	0.07
	0	100	Cube	324.7	-0.079	0.003	-0.922	47.06	222.49	200.35	0.81	9.34	0.06

Performance Model Validation, UH-60A Blackhawk

2,000 ft, 20 °C, 16,000 lb

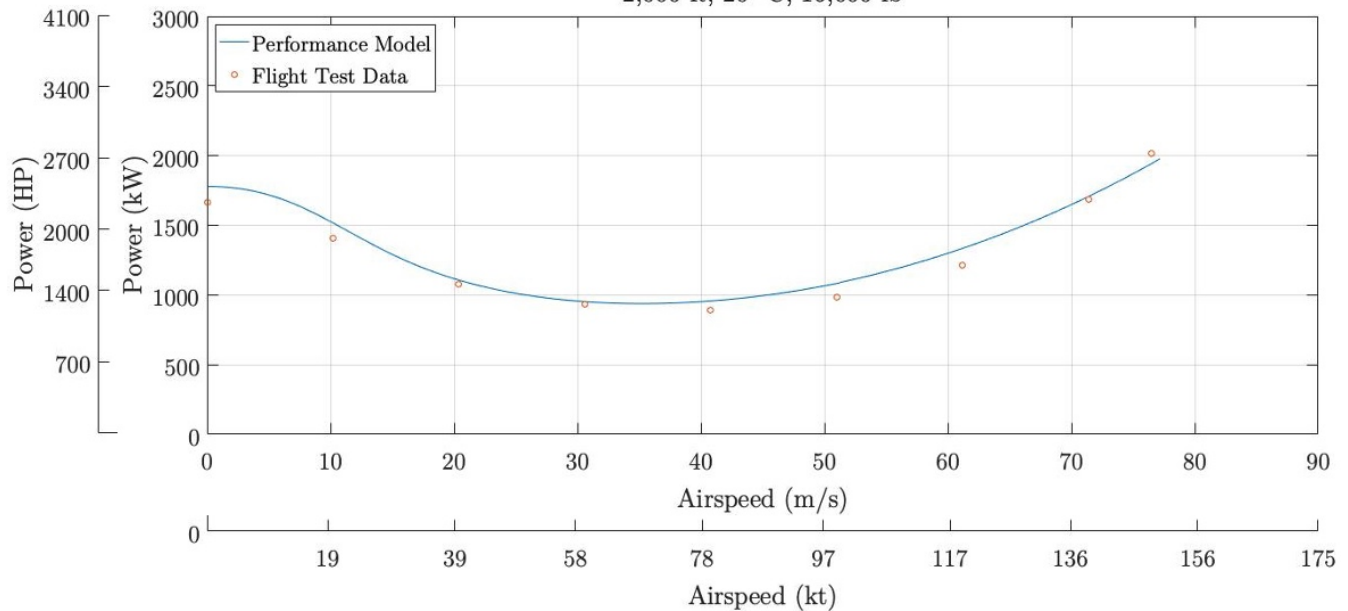


Figure 12.1: Performance model Validation

12.2 Hover

As a tandem rotor system with 1.565 m (5.13 ft) blade radii leveraging the maximum objective vehicle dimensions per the RFP, the Alicorn has a low blade loading of 192 N/m (4 lb/ft²) at its maximum mission weight of 298 kg (657 lb). In addition to its efficient hovering, this results in a low induced velocity of 12 m/s (39 ft/s), which enhances safety when landing in confined areas near people or in the vicinity of debris. Although the low tip speed of 202 m/s (662 ft/s) at 1,231 RPM is optimized for forward flight, the rotor speed can be increased by 5.5% when needed for takeoff or other situations. The Rotax 915's



5-minute Maximum Rated Power (MRP) is raised from the Maximum Continuous Power (MCP) rating of 99 kW (135 HP) to 104 kW (141 HP) while also increasing rotor RPM. The performance of the engine is such that MCP is 95% of the MRP.

As discussed in Section 9 and based on manufacturer data, the efficiency of the belt and pulley system was 97% and the gearbox and driveshaft portions of the transmission were assumed to be 99% [52], resulting in 96% overall drivetrain efficiency. Accessory power was conservatively approximated as a constant 3 kW (4 HP) as discussed in 10.

A modified momentum theory method was utilized to model aircraft performance because it was the most compatible with applying tandem rotor interference data. Blade lift and drag coefficients were based on the properties for the airfoils as discussed in Section 7. Applying empirical corrections based on the rotor overlap and vertical stagger ratios resulted in 10% additional induced power 75% in forward flight [12]. Download was calculated using empirical vertical drag formulas based on the the area distribution and vertical distance of the fuselage under the rotor disks [62]. 6.4% additional thrust was required in hover, with the download vanishing in forward flight. The excess power of the engine results in extraordinary hover performance. Even with a 100 kg payload and 25 kg of fuel, the hover ceiling out of ground effect is nearly unlimited as shown in Figure 12.2.

Ground effect was modeled using the empirical equation determined by Schmaus et al [63]. For hover in ground effect with a 0.3 m (1 ft) landing gear height, the power required was reduced by 2.5%. The benefit of ground effect vanishes when hovering above a 2 m (6.7 ft) landing gear height.

Power Required to Hover for Final Design, Out of Ground Effect

>2 m (6.6 ft) landing gear height

ISA + 20 °C, $\Omega = 1,231$ RPM (100% rotor speed)

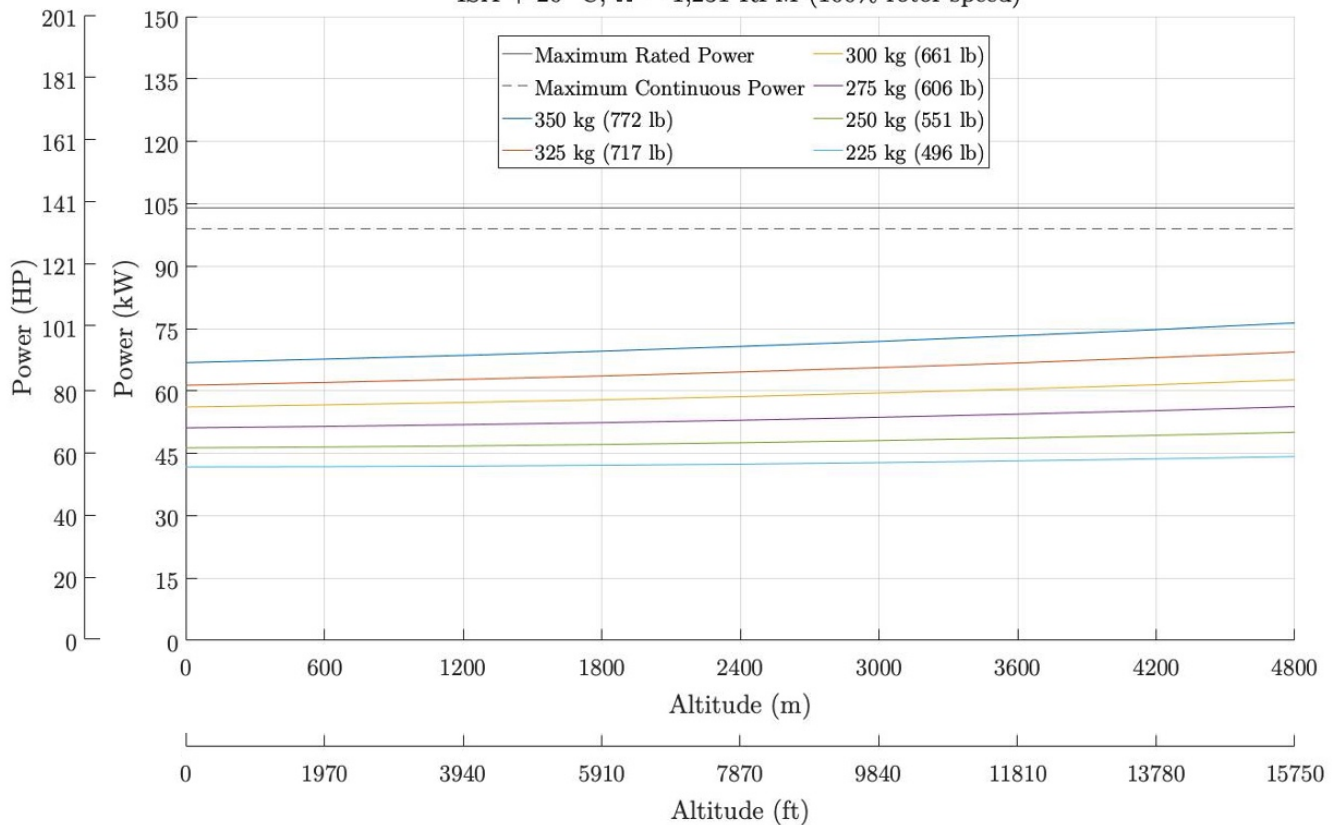


Figure 12.2: Hover performance (out of ground effect)



12.3 Level Flight, Climb, and Autorotation Performance

Forward flight performance was calculated using standard energy methods [63]. Drag was modeled using the CFD results discussed in Section 6, and the hub drag was modeled using a parametric model for two modern, fairing-encased hubs scaled for a 383 kg (844 lb) maximum gross weight aircraft, with a total equivalent flat plate area of 0.182 m² (1.96 ft²). The aerodynamic down-force produced by the fuselage—found to be 160 N (35 lb) at 55 m/s (107 kt) using CFD—was included as a function of airspeed. Compressibility corrections accounting for the 22° swept blade tips and drag divergence Mach number as a function of blade loading were included in the model [64]. An advancing blade tip Mach number that was up to 5% greater than the drag divergence Mach number for the section was allowed to prevent the onset of vibrations and blade oscillations, a conservative estimate considering the thin high-speed-optimized airfoils used in the rotor blade design [63]. As noted in in Section 13, avoiding unsafe rotor blade dynamics (excessive flapping) ultimately limited normal cruise speed to 90 m/s (175 kt), which nevertheless only required 97% of MCP at the maximum expected Logistics Mission weight. The climb performance was also exceptional throughout the envelope and with payloads that greatly exceed the minimums in the RFP. At the maximum Logistics Mission gross weight of 298 kg (657 lb), the aircraft has a maximum vertical climb speed of 14 m/s (2,800 fpm) and a maximum rate of climb of 23 m/s (4,500 ft/min) in forward flight. These facts are presented in Figures 12.3, 12.4, 12.5, and 12.6.

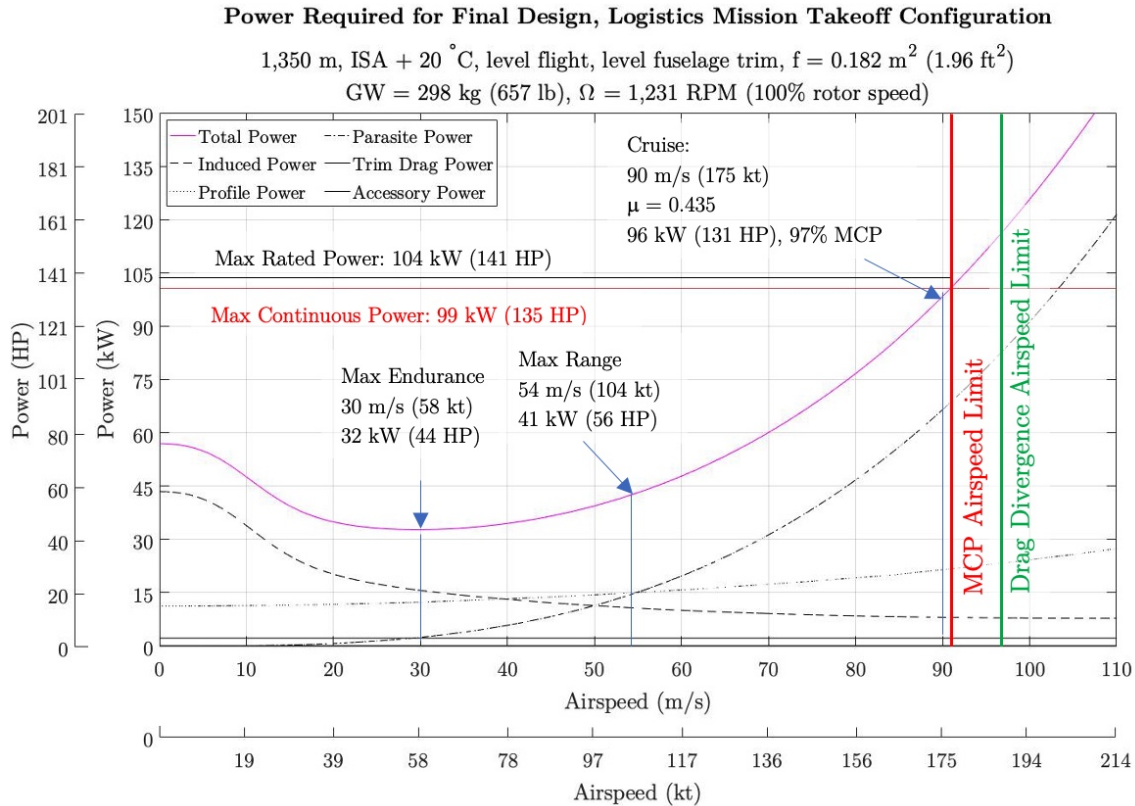


Figure 12.3: Level flight performance, Logistics Mission start weight



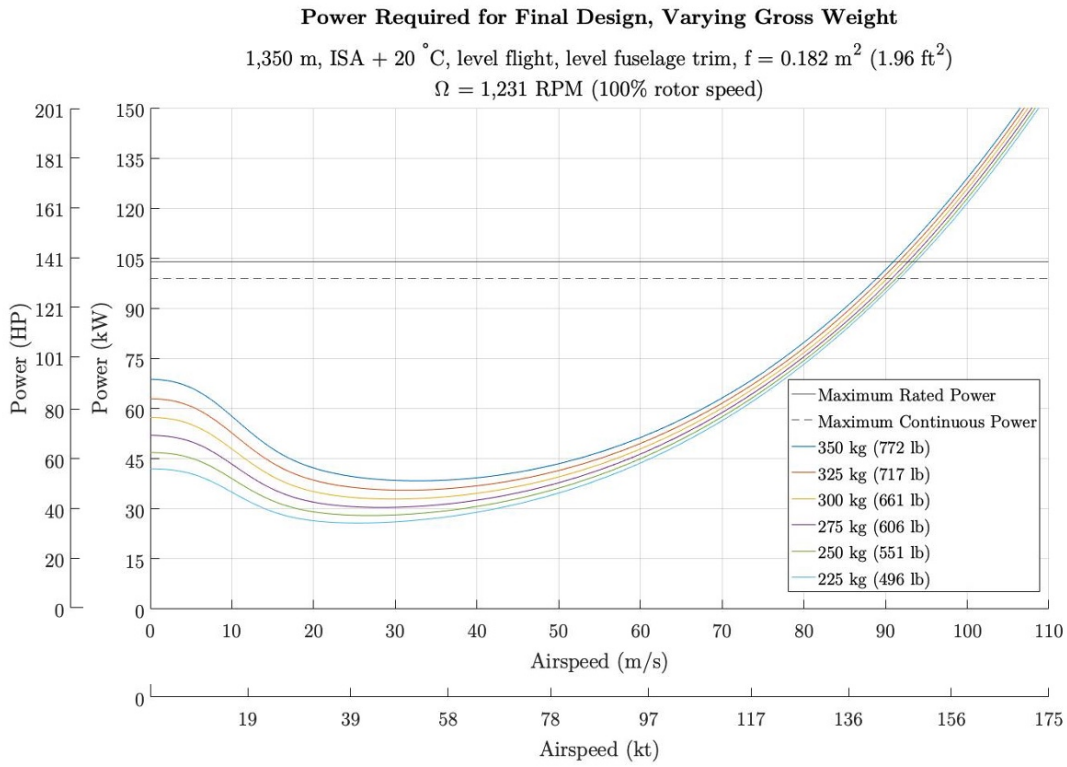


Figure 12.4: Level flight performance, varying gross weight

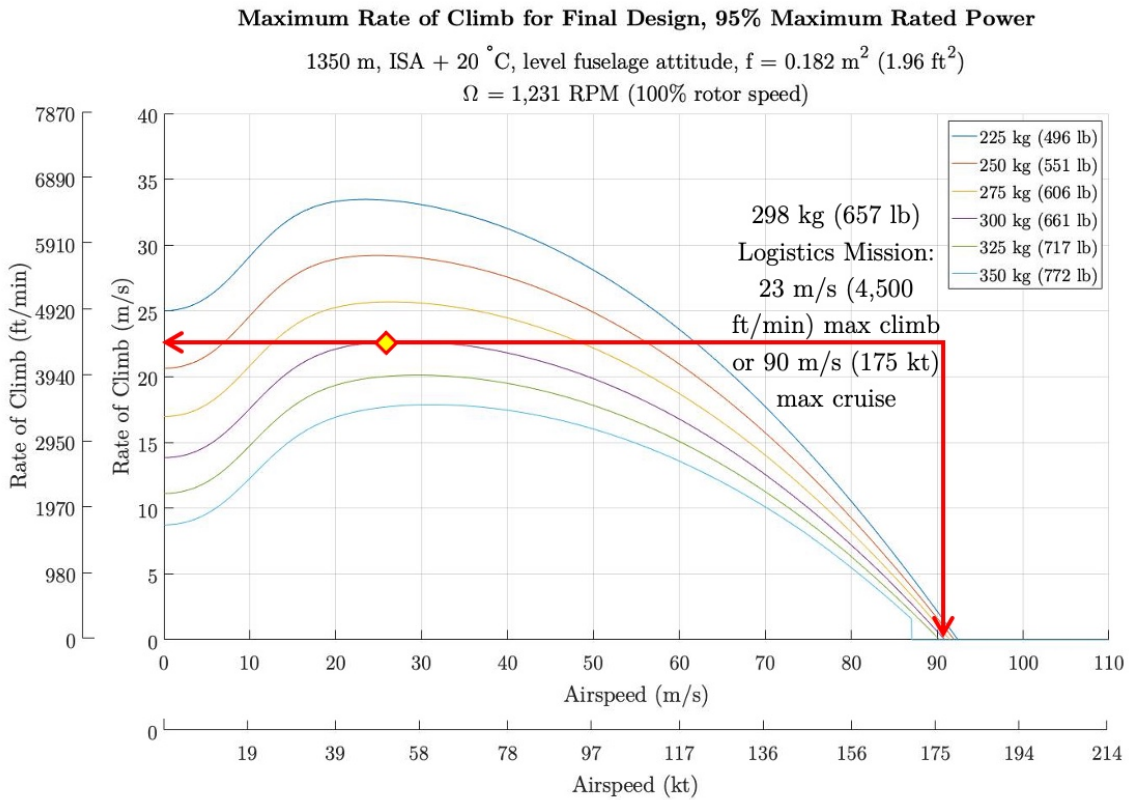


Figure 12.5: Climb performance



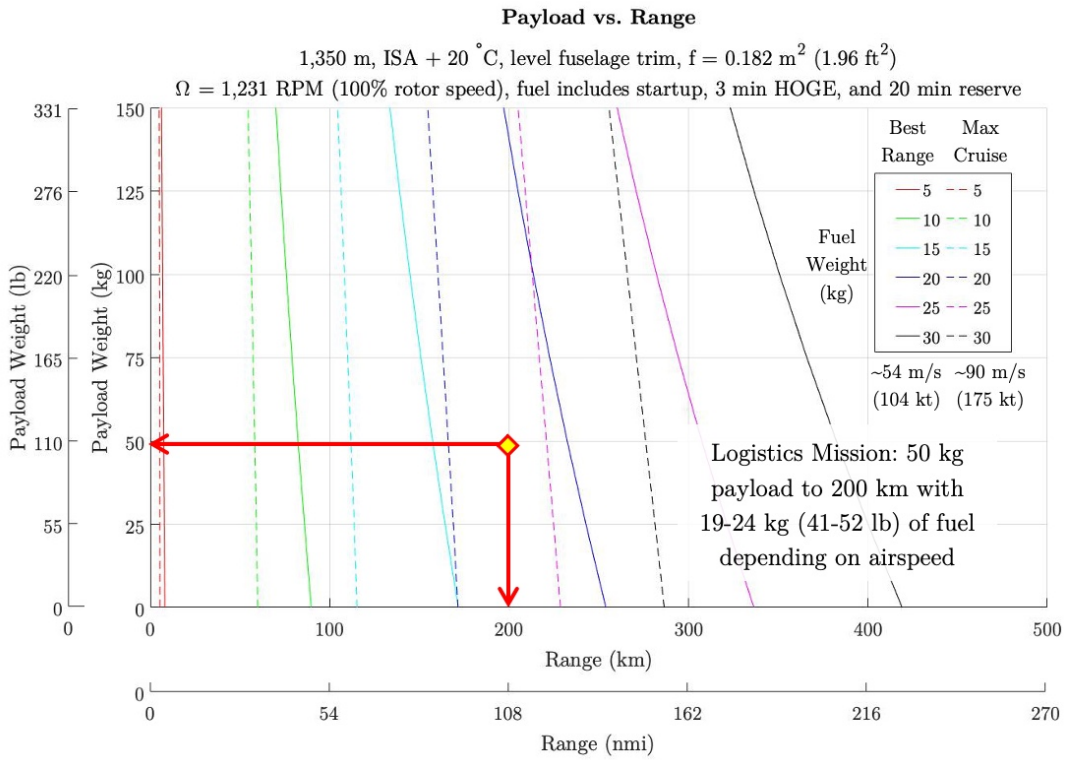


Figure 12.6: Variation of allowable payload with range

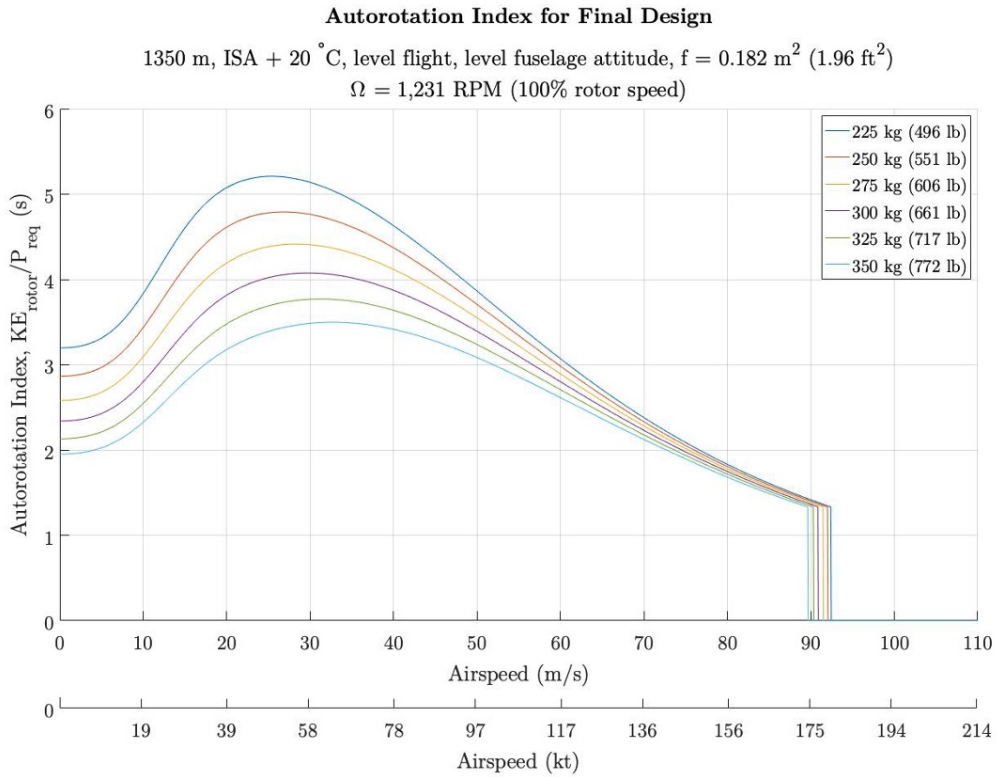


Figure 12.7: Autorotation Index



The Alicorn has a good Autorotation Index (AI) in hover and moderate forward speeds as shown in Figure 12.7. The kinetic energy was based on the rotating speed and moments of inertia of the rotor system as designed in Section 7. Typical manned helicopters have AI values of 2 to 3 seconds [63], and the Alicorn meets or exceeds this range at its mission gross weights for all airspeeds below 76 m/s (148 kt). At high speeds, an engine failure would result in a rapid rotor speed decay in less than a second if the collectives were not reduced. However, this is typical for most helicopters and the autonomous nature of this aircraft allows it to respond much faster than a human to keep the rotor speed in a safe range. Additionally, at high speed the significant kinetic energy of the aircraft can be used to maintain the kinetic energy of the rotor.

12.4 Productivity

Combining the engine’s efficient Specific Fuel Consumption of 0.32 kg/kW-hr (0.52 lb/HP-hr) with the aircraft performance determined above allowed for the computation of block time and Productivity metrics using the engine start gross weight as a baseline. The takeoff fuel is sufficient to accomplish all legs with a 20 min reserve, as well as to meet the return to launch site abort objective (with cargo) as applicable for the Local Delivery Mission. As shown in Section 4, the entire payload deployment and door retraction sequence only takes 22 sec. The required 10 minutes for loading and warmup, as well as the mandatory hover durations, were unchanged as per the RFP. The aircraft is designed to deliver packages in 23.3 min for the Local Delivery Mission and 51.1 min for the Logistics Mission, well below the respective 28 min and 75 min objectives. Productivity is 6.2 m/s (12 kt) for the Local Delivery Mission and 10.9 m/s (15 kt) for the Logistics Mission when flying at the maximum cruise speed on the delivery segments. Flying at the maximum speed of 90 m/s (175 kt) instead of the minimum cruise needed to satisfy the block time objectives only uses 1.3 kg and 5.1 kg more fuel, and increases Productivity by 19 and 43% for the Local Delivery and Logistics Missions, respectively. A breakdown of each mission segment and the Productivity metrics are clearly presented in Tables 12.2, 12.4, 12.1, and 12.3.

Table 12.1: Productivity for Logistics Mission, minimum speed and fuel required

Logistics Mission - Minimum Speed Required to Achieve Required Block Time of 75 min

Segment	Time		Speed		Power		Distance		Fuel Remaining		Gross Weight	
	min	Elapsed min	m/s	kt	kW	HP	km	nmi	kg	lb	kg	lb
Start	0	0.0	0	0.0	0	0	0	0	18.5	40.8	293.2	646.4
Load Package	5	5.0	0	0.0	0	0	0	0	18.5	40.8	293.2	646.4
Warmup	5	10.0	0	0.0	11	14.8	0	0	18.2	40.1	292.9	645.7
Takeoff HIGE	2	12.0	0	0.0	56	75.1	0	0	17.6	38.8	292.3	644.5
Climb/ Acceleration	0.5	12.5	30	58.3	96	128.7	0.9	0.5	17.4	38.3	292.1	643.9
Cruise	60.6	73.1	54.5	105.9	42	56.3	198.2	107.0	3.7	8.2	278.4	613.8
Descent/ Deceleration	0.5	73.6	30	58.3	20	26.8	0.9	0.5	3.7	8.1	278.4	613.7
Land HOGE	1	74.6	0	0.0	57	76.4	0	0	3.4	7.4	278.1	613.0
Unload Package (Block Time End)	0.4	75.0	0	0.0	11	14.8	0	0	3.3	7.3	224.3	494.5
Reserve	20	95.0	30	58.3	32	42.9	0	0	0.0	0.0	274.8	605.8

Block Speed = 200 km / Block Time (m/s): 44.5 (86.5 kt)

Productivity = Payload × Block Speed / Gross Weight (m/s): 7.6 (14.8 kt)



Table 12.2: Productivity for Local Delivery Mission, minimum speed and fuel required

Local Delivery Mission - Minimum Speed Required to Achieve Required Block Time of 28 min

Segment	Time min	Elapsed min	Speed		Power		Distance		Fuel Remaining		Gross Weight	
			m/s	kt	kW	HP	km	nmi	kg	lb	kg	lb
Start	0	0.0	0	0	0	0	0	0	12.1	26.7	286.8	632.3
Load Package	5	5.0	0	0	0	0	0	0	12.1	26.7	286.8	632.3
Warmup	5	10.0	0	0	11	14.8	0	0	11.8	26.0	286.5	631.6
Takeoff HOGE	2	12.0	0	0	57	76.4	0	0	11.2	24.8	285.9	630.4
Climb/ Acceleration	0.5	12.5	30	58.3	96	128.7	0.9	0.5	11.0	24.2	285.7	629.8
Cruise	13.6	26.1	59	114.7	46	61.7	48.2	26.0	7.7	16.9	282.4	622.5
Descent/ Deceleration	0.5	26.6	30	58.3	20	26.8	0.9	0.5	7.6	16.8	282.3	622.4
Land HOGE	1	27.6	0	0	57	76.4	0	0	7.3	16.1	282.0	621.7
Unload Package* (Block Time End)	0.4	28.0	0	0	11	14.8	0	0	7.3	16.0	282.0	621.6
Takeoff HOGE	1	29.0	0	0	57	76.4	0	0	7.0	15.4	281.7	621.0
Climb/ Acceleration	0.5	29.5	30	58.3	96	128.7	0.9	0.5	6.9	15.1	281.6	620.7
Cruise	15.3	44.8	52.5	102.1	39	52.3	48.2	26.0	3.6	8.0	278.3	613.6
Descent/ Deceleration	0.5	45.3	30	58.3	20	26.8	0.9	0.5	3.6	7.9	278.3	613.5
Land HOGE	1	46.3	0	0	57	76.4	0	0	3.3	7.3	278.0	612.9
Reserve	20	66.3	30	58.3	32	42.9	0	0	0.0	0.0	274.7	605.6

Block Speed = 50 km / Block Time (m/s): 29.8 (57.9 kt)

Productivity = Payload × Block Speed / Gross Weight (m/s): 5.2 (10.1 kt)

* Remaining fuel based on contingency of not unloading package; meets return to launch site with full payload objective

Table 12.3: Maximum productivity for Logistics Mission

Logistics Mission - Maximum Productivity

Segment	Time min	Elapsed min	Speed		Power		Distance		Fuel Remaining		Gross Weight	
			m/s	kt	kW	HP	km	nmi	kg	lb	kg	lb
Start	0	0.0	0	0.0	0	0	0	0	23.6	52.1	298.3	657.7
Load Package	5	5.0	0	0.0	0	0	0	0	23.6	52.1	298.3	657.7
Warmup	5	10.0	0	0.0	11	14.8	0	0	23.3	51.5	298.0	657.0
Takeoff HIGE	2	12.0	0	0.0	56	75.1	0	0	22.8	50.2	297.4	655.7
Climb/ Acceleration	0.5	12.5	30	58.3	96	128.7	0.9	0.5	22.5	49.6	297.2	655.2
Cruise	36.7	49.2	90	174.9	96	128.7	198.2	107.0	3.7	8.2	278.4	613.7
Descent/ Deceleration	0.5	49.7	30	58.3	20	26.8	0.9	0.5	3.6	8.0	278.3	613.6
Land HOGE	1	50.7	0	0.0	57	76.4	0	0	3.4	7.4	278.0	613.0
Unload Package (Block Time End)	0.4	51.1	0	0.0	11	14.8	0	0	3.3	7.3	224.3	494.5
Reserve	20	71.1	30	58.3	32	42.9	0	0	0.0	0.0	274.7	605.7

Block Speed = 200 km / Block Time (m/s): 65.3 (127 kt) → 43% Higher Productivity

Productivity = Payload × Block Speed / Gross Weight (m/s): 10.9 (21.2 kt) than minimum speed

Table 12.4: Maximum productivity for Local Delivery Mission

Local Delivery Mission - Maximum Productivity

Segment	Time	Elapsed	Speed		Power		Distance		Fuel Remaining		Gross Weight	
	min	min	m/s	kt	kW	HP	km	nmi	kg	lb	kg	lb
Start	0	0.0	0	0	0	0	0	0	13.4	29.4	288.1	635.2
Load Package	5	5.0	0	0	0	0	0	0	13.4	29.4	288.1	635.2
Warmup	5	10.0	0	0	11	14.8	0	0	13.1	28.8	287.9	634.6
Takeoff HOGE	2	12.0	0	0	57	76.4	0	0	12.5	27.5	287.3	633.3
Climb/ Acceleration	0.5	12.5	30	58.3	96	128.7	0.9	0.5	12.2	26.9	287.0	632.8
Cruise	8.9	21.4	90	174.9	96	128.7	48.2	26.0	7.7	16.9	282.4	622.7
Descent/ Deceleration	0.5	21.9	30	58.3	20	26.8	0.9	0.5	7.6	16.8	282.4	622.6
Land HOGE	1	22.9	0	0	57	76.4	0	0	7.3	16.1	282.1	621.9
Unload Package* (Block Time End)	0.4	23.3	0	0	11	14.8	0	0	7.3	16.0	282.0	621.8
Takeoff HOGE	1	24.3	0	0	57	76.4	0	0	7.0	15.3	281.8	621.2
Climb/ Acceleration	0.5	24.8	30	58.3	96	128.7	0.9	0.5	6.9	15.1	281.6	620.9
Cruise	15.3	40.1	52.5	102.1	96	128.7	48.2	26.0	3.6	8.0	278.4	613.8
Descent/ Deceleration	0.5	40.6	30	58.3	20	26.8	0.9	0.5	3.6	7.9	278.4	613.7
Land HOGE	1	41.6	0	0	57	76.4	0	0	3.3	7.3	278.1	613.1
Reserve	20	61.6	30	58.3	32	42.9	0	0	0.0	0.0	274.8	605.8

Block Speed = 50 km / Block Time (m/s): 35.8 (69.6 kt) → 19% Higher Productivity
Productivity = Payload × Block Speed / Gross Weight (m/s): 6.2 (12 kt) than minimum speed

* Remaining fuel based on contingency of not unloading package; meets return to launch site with full payload objective

13 Trim and Flight Dynamics

13.1 Control Scheme

With two main rotors come 6 sources of control: Collective, lateral cyclic and longitudinal cyclic pitch controls are available from each rotor. However, the traditional axes of control (pitch, roll, yaw and heave) are achieved in a tandem helicopter only when the rotors are controlled in combination. As such, a “ganged/differential” control scheme was adopted. With this scheme, “ganged” controls manipulate the rotor together and in the same direction, while “differential” controls in opposition. For instance, aircraft heave control is achieved using “ganged” collective pitch, where the collective pitch of both rotors is increased together. In contrast, pitch attitude is achieved using “differential” collective pitch, in which the collective pitch of the forward rotor is raised and the rear is lowered.

Translating between the two control spaces is relatively simple utilizing the following mixing matrix.

$$\begin{Bmatrix} \theta_{0,\text{fwd}} \\ \theta_{1c,\text{fwd}} \\ \theta_{1s,\text{fwd}} \\ \theta_{0,\text{aft}} \\ \theta_{1c,\text{aft}} \\ \theta_{1s,\text{aft}} \end{Bmatrix} = \begin{bmatrix} 1 & 0 & 0 & 0.5 & 0 & 0 \\ 0 & 1 & 0 & 0 & 0.5 & 0 \\ 0 & 0 & 1 & 0 & 0 & 0.5 \\ 1 & 0 & 0 & -0.5 & 0 & 0 \\ 0 & -1 & 0 & 0 & 0.5 & 0 \\ 0 & 0 & 1 & 0 & 0 & -0.5 \end{bmatrix} \begin{Bmatrix} \theta_0 \\ \theta_{1c} \\ \theta_{1s} \\ \Delta\theta_0 \\ \Delta\theta_{1c} \\ \Delta\theta_{1s} \end{Bmatrix}$$

Note that the differential pitch angles $\Delta\theta_0$, $\Delta\theta_{1c}$, and $\Delta\theta_{1s}$ are defined such that they describe the difference in pitch angles between the two rotors, rather than the distance from the mean “ganged” control angle.



Table 13.1: Trim control strategy

DOF Name	DOF Symbol	Control Name	Control Symbol
Longitudinal acceleration	\dot{v}_x	Ganged longitudinal cyclic	θ_{1s}
Lateral acceleration	\dot{v}_y	Roll attitude	ϕ_b
Vertical acceleration	\dot{v}_z	Ganged collective pitch	θ_0
Roll acceleration	\dot{p}	Ganged lateral cyclic pitch	θ_{1c}
Pitch acceleration	\dot{q}	Differential collective pitch	$\Delta\theta_0$
Yaw acceleration	\dot{r}	Differential lateral cyclic pitch	$\Delta\theta_{1c}$

Also note that the row corresponding to the lateral cyclic pitch of the rear rotor $\theta_{1c,\text{aft}}$ is negated to account for the opposite direction of rotation. This maintains a convention in which “ganged” cyclic pitch results in rotors’ tip-path-plane tilt in the same physical direction.

13.2 Trim Strategy

Six control positions when combined with two attitude angles (pitch and roll) and a side-slip angle in forward flight over define the trim solution in forward flight. Table 13.1 describes which controls are used to trim which axis. This leaves three sources of control —differential longitudinal cyclic $\Delta\theta_{1c}$, pitch body attitude θ_b , and side-slip angle —undefined. For the preliminary analysis in this report, differential longitudinal cyclic was left centered at zero. Pitch attitude was prescribed and scheduled with airspeed based on drag, hover attitude and flapping angle considerations. Because roll attitude is used to trim lateral acceleration, side-slip was unnecessary and set zero to minimize drag. Figure 13.1 shows the aircraft body attitude as a function of airspeed.

Roll attitude, which fell out of the trim procedure, remains essentially zero at all speeds, highlighting an advantage of the tandem configuration over the single-main-rotor configuration. Pitch attitude is 5 degrees nose up until 30 m/s (58.3 knots, or 98.4 ft/s), at which point the nose is lowered at an increasing rate to keep the longitudinal flapping angle in check. The plots in Figure 13.2 show the flapping angles of both rotors and the control angles in forward flight.

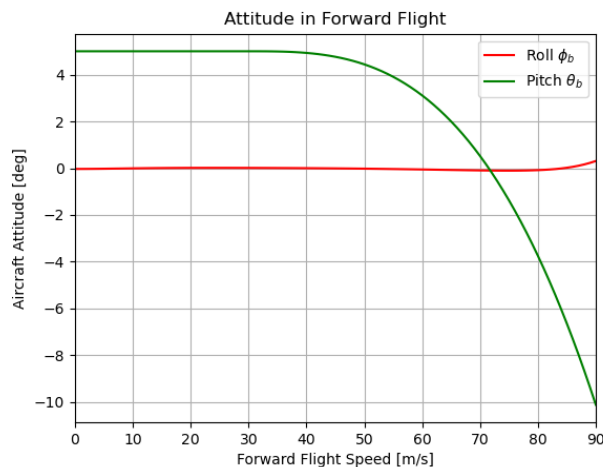


Figure 13.1: Trim attitude in forward flight

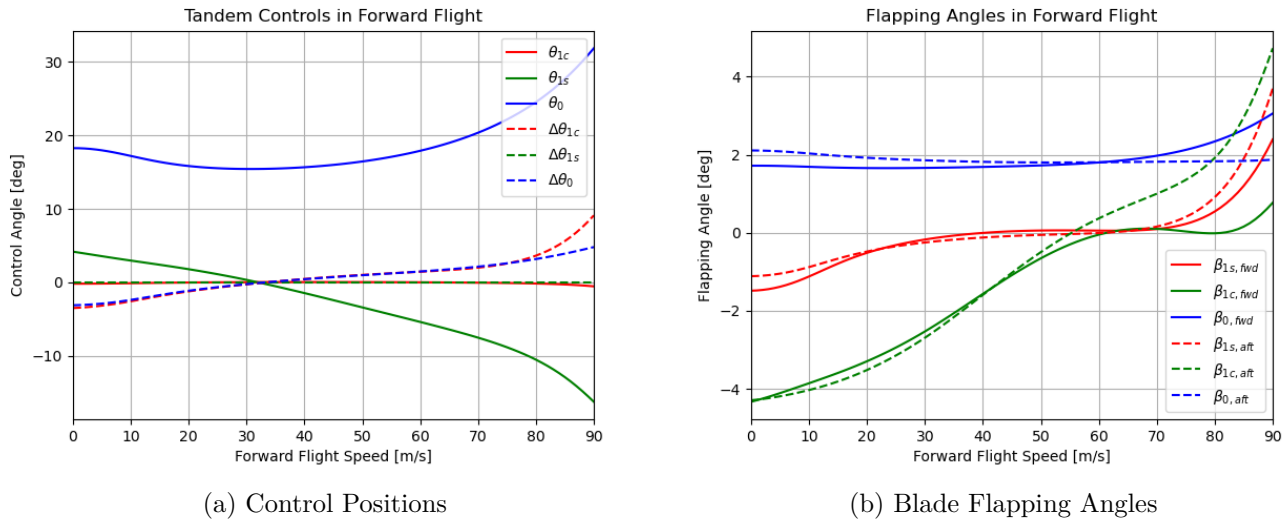


Figure 13.2: Control and flapping angles in forward flight

It can be observed from the plots in Figure 13.2 that the main source of pitch control —differential collective $\Delta\theta_0$ —increases continuously and quite linearly with airspeed from about negative three degrees in hover to about 5 degrees at 90 m/s (175 knots). The convention described previously establishes differential collective as a pitch-up command (i.e. collective, and thus thrust, is increased on the front rotor and decreased on the rear for a positive increment in $\Delta\theta_0$) which indicates that the aircraft requires a continuous pitch up response in forward flight. In a traditionally piloted aircraft, this unstable “stick gradient” would be undesirable. When speaking to engineers at Boeing, this phenomenon was briefly discussed as a characteristic of the tandem-rotor CH-47 Chinook helicopter. An artificial bias is introduced into the longitudinal axis scheduled by airspeed which provides the pilot the perception of a stable stick gradient and airspeed stability. With no pilot flying Alicorn, providing this desirable feel is not important, but maintaining longitudinal stability is. A low-frequency airspeed and high-frequency pitch-rate feedback system would need to be implemented to handle this axis. This would be one aspect of the larger control law development for the aircraft.

Differential lateral cyclic, the main source of yaw authority for the vehicle, tracks almost one-to-one with differential collective for all airspeeds up to 80 m/s (155 knots). This stands to reason as differential collective will inherently introduce a yaw moment due to torque differential, and lateral differential cyclic will be needed to counter it.

Further analysis beyond the preliminary design stage (particularly during control law development) would involve incorporating the unused differential longitudinal cyclic control to optimize cruise performance and better balance the flapping angles of the two rotors at high speed. One significant concern with all tandem helicopters is the threat of a “tunnel strike”, in which the blade slaps down over the fuselage and impacts the cover above the transmission synchronizing shaft. Alicorn is designed such that 15 degrees of flapping would be permitted assuming straight blades. Flap stops are placed on the main rotor protection pate to permit only 10 degrees of negative flapping, permitting additional margin for blade flex. Figure 13.3 shows the blade flapping clearance above the sync shaft tunnel for the front and rear rotors for a flapping angle of negative 10 degrees.

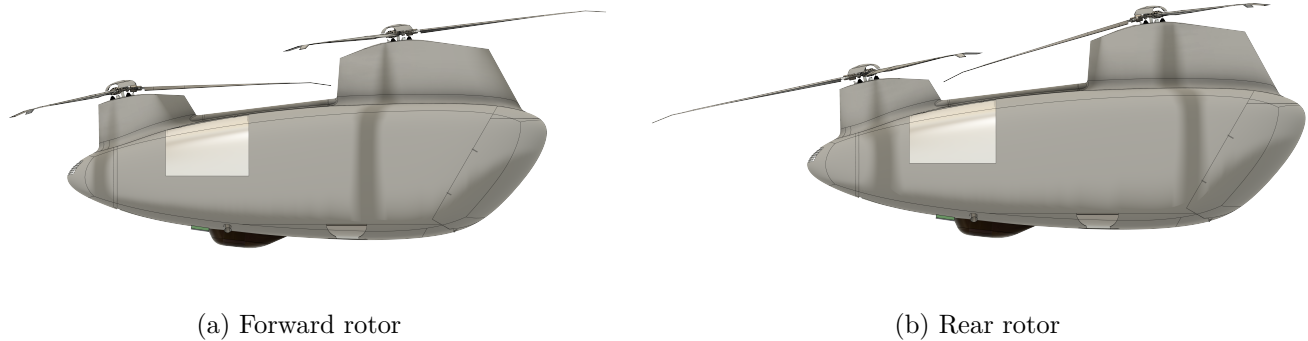


Figure 13.3: Flapping clearance

14 Safety

14.1 Preliminary System Safety Analysis

The design team has recognized the importance of aircraft system safety throughout the design process. To accomplish this a preliminary Functional Hazard Assessment (FHA) was designed using the ConOps to determine Alicorn's functions. Table 14.1 provide part of the initial FHA.

Table 14.1: Functional Hazard Assessment (FHA)

Function Failure Ref.	Function	Failure Condition	Phase of Operation
1.1	Aircraft assembly (fueling, extending rotor blades, etc.)	Aircraft runaway during staging	Maintenance/ transportation
1.2	Aircraft assembly (fueling, Extending Rotor Blades, etc.)	Damaged fuel cap/bad fuel	Maintenance/ transportation
1.3	Aircraft assembly (fueling, extending rotor blades, etc.)	Rotor blade/hub damage during blade extension.	Maintenance/ transportation
1.4	Aircraft assembly (fueling, extending rotor blades, etc.)	Airframe damage during removal and assembly.	Maintenance/ transportation
2.1	Pre-flight aircraft	Exposed internal components	Maintenance/ transportation
2.2	Pre-flight aircraft	Tire/landing gear damage during pre-flight inspection	Maintenance/ transportation
2.3	Pre-flight aircraft	Missed blocked intakes/exhaust	Maintenance/ transportation
2.4	Pre-flight aircraft	Failed to remove protective covers	Maintenance/ transportation
2.5	Pre-flight aircraft	Missed blocked Pitot-static probe	Maintenance/ transportation
2.6	Pre-flight aircraft	Damaged airframe/rotor hub/rotor blades during pre-flight inspection	Maintenance/ transportation

2.7	Pre-flight aircraft	Inspection failed to find damage/leaks	Maintenance/ transportation
2.8	Pre-flight aircraft	Bad fuel/water in fuel tanks	Maintenance/ transportation
3.1	Loading package	Damaged airframe or package while loading	Loading/ unloading
3.2	Loading package	Loading door fail to open/remain close	Loading/ unloading
3.3	Loading package	Cargo loaded improperly to shift CG	Loading/ unloading
3.4	Loading package	Loading UAV beyond weight tolerance	Loading/ unloading
4.1	Turn on UAV/ run diagnostic	UAV fails to turn on/ smoke becomes visible from vehicle	Engine startup/ shutdown
4.2	Turn on UAV/ run diagnostic	UAV fails to recognize issue/ avionics fail to boot	Engine startup/ shutdown
4.3	Turn on UAV/ run diagnostic	Connection to external power source damaged	Engine startup/ shutdown
4.4	Turn on UAV/ run diagnostic	External power source provides damaging voltage/ current	Engine startup/ shutdown
4.5	Turn on UAV/run diagnostic	External power source fails to provide power	Engine startup/ shutdown
5.1	Engine start w/o engaging rotors	Engine fails to turn over	Engine startup/ shutdown
5.2	Engine start w/o engaging rotors	UAV avionics/ flight computer fails/ provides incorrect inputs.	Engine startup/ shutdown
5.3	Engine Start w/o Engaging Rotors	UAV experiences electrical issue	Engine Startup/ Shutdown
5.4	Engine start w/o engaging rotors	Engine has abnormal start/ fire	Engine startup/ shutdown
5.5	Engine start w/o engaging rotors	Fuel leak	Engine startup/ shutdown

Table 14.2: Severity definitions modified from SAE ARP4761

Classification	UAV	External
Catastrophic	UAV is in an emergency configuration looking for ideal spot to land the aircraft in an open field or an open space. Extremely limited power, capabilities, functionality, etc.	UAV imposes severe safety risk to animals, people, and/or property. Propability of loss of life or limb is severe.
Severe Major	UAV has little to no safety margin. Aircraft is aborting mission to the start position for a local delivery or start/end point for long delivery. UAV components are severely stressed.	UAV imposes huge safety risk to animals, people, and/or property. High propability of major injuries but not life threatning.
Major	UAV can still function but with limited safety margin. System will not impose new safety issues to the enviroment (animals, people, property, etc.) but will need to be serviced when mission is concluded. UAV components are being more stressed due to loss of redundancy or a particular component.	UAV imposes marginal safety risks to animals, people, and/or property. Moderate probability for moderate injuries.
Minor	UAV functions with minor issues. Safety margin is slightly reduce. UAV components are midly stressed service may be required but not necessary. Daily/hourly inspections required by the technician.	UAV imposes little to no safety risk to animals, people, and/property. Low probability of minor injuries.

Then the Preliminary System Safety Analysis (PSSA) was derived using the FHA to determine what systems caused the function to fail. The system PSSA would then identify the subsystems or components that caused the hazard stated in the FHA. When applicable, the PSSA further decomposed hazards to identify the components that cause the subsystem, system, and functional hazards. To determine severity, the SAE ARP4761 definitions were modified to fit the purpose of this RFP. Table 14.2 presents those definitions.

The design team chose to keep the FAA defined probability of failure and determined the value using equation 5:

$$\lambda = \frac{1}{MTBF} \quad (5)$$

A unique Hazard Identifier (ID) were given to keep track of the hazards. The FHA Hazard ID number was based on the placement of the function within the ConOps. Referring to figure 2.3, “Unload/Assemble/Fuel Aircraft” is the first activity conducted so in the FHA “Aircraft Assembly (Fueling, Extending Rotor Blades, etc.)” was given a 1. Then each subsequent activity would be 2, 3, and so on. When a hazard was discovered the Hazard I.D would follow 1.1, 1.2, 1.3, etc. until all hazards were identified per that function. In certain cases, activities were combined to expedite the analysis where similar hazards would be identified.

At the PSSA the FHA Hazard ID provided initial identification to the system level hazard. As with each new FHA Hazard, each system level hazard was identified as 1.1.1, 1.1.2, 1.1.3, etc. until all system level hazards were analyzed. For subsystem level analysis, the same approach for identification was used but the Hazard ID followed 1.1.1.1, 1.1.1.2, and so forth. This identification allows the design to monitor the progress of each hazard and verify that the appropriate measures were taken to close out that particular hazard. Table 14.3 depicts the hazard identification for the PSSA.

Table 14.3: Preliminary System Safety Assessment of Avionics, Electrical, and Engine

FHA Reference	Refer-	Hazard I.D.	System	Failure Condition	Hardware Failure
6.1, 7.1, 8.1, 9.1, 10.1		7.1.2	Avionics	Sensor(s) fail to notify flight computer of issues.	Sensors
6.1, 7.1, 8.1, 9.1, 10.1		7.1.3	Avionics	Sensor(s) provide false positive of an issue	Sensors
6.1, 7.1, 8.1, 9.1, 10.1		7.1.8	Avionics	Flight computer experiences a blue screen due to hardware issue.	Flight Computer
6.5, 8.5, 9.5, 10.5		6.5.1	Engine	Engine fire	Engine
6.5, 8.5, 9.5, 10.5		6.5.2	Engine	Loss of oil pressure	Engine
6.5, 8.5, 9.5, 10.5		6.5.3	Engine	Abnormal noises/ engine vibrations.	Engine
6.5, 8.5, 9.5, 10.5		6.5.4	Engine	Abnormal engine temperatures	Engine
6.5, 8.5, 9.5, 10.5		6.5.5	Engine	Abnormal RPM/ torque values	Engine
6.6, 8.6, 9.6, 10.6		6.6.1	Electrical	Alternator fails	Alternator
6.6, 8.6, 9.6, 10.6		6.6.2	Electrical	Battery Fails	Battery
6.6, 8.6, 9.6, 10.6		6.6.3	Electrical	Volt regulators fail to control power levels to flight computer and other components.	Voltage Regulators
6.6, 8.6, 9.6, 10.6		6.6.4	Electrical	Alternator delivers a power spike	Alternator
6.6, 8.6, 9.6, 10.6		6.6.5	Electrical	Wiring fails to provide power to components	Wiring
6.6, 8.6, 9.6, 10.6		6.6.6	Electrical	Wiring fails and heats up causing an electrical fire.	Wiring
6.6, 8.6, 9.6, 10.6		6.6.7	Electrical	Battery fails and starts an electrical fire	Battery
6.6, 8.6, 9.6, 10.6		6.6.8	Avionics	Sensor(s)/ flight computer draws to much power indicating failure.	Sensor(s)/ Flight Computer

Once the hazards were identified, analysis for the severity and probability were conducted. The design team first determined the failure effect from historical data and individual experience. After the failure effect was determined, appropriate severity and probability of failure were assigned. If the subsystem and/or component did not have an MTBF, the value was left blank. Table 14.4 provides the severity and probability for the identified hazards.

Table 14.4: Severity and Probability based on Failure Effect

Hazard I.D.	System	Failure Effect	Classification	Probability
7.1.3	Avionics	Sensor(s) can cause an inadvertant abort of the mission if sensor is misreading.	Minor	Improbable (1E-5 - 1E-7)
7.1.8	Avionics	Engine continues to run without any inputs from the flight computer. UAV cannot conduct mission	Severe Major	
6.5.1	Engine	Total loss of vehicle and package.	Catastrophic	Improbable (1E-5 - 1E-7)
6.5.2	Engine	Engine can seize and lose power.	Severe Major	Improbable (1E-5 - 1E-7)
6.5.3	Engine	Engine will eventually fail due to piston failure or another component getting damaged.	Severe Major	Improbable (1E-5 - 1E-7)
6.5.4	Engine	Engine fails due to overheating cuasing piston to seize.	Severe Major	Improbable (1E-5 - 1E-7)
6.5.5	Engine	Engine gear box starts to lose teeth and slips causing RPM fluctuations.	Severe Major	Improbable (1E-5 - 1E-7)
6.6.1	Electrical	Flight computer loses power and shuts down meaning UAV cannot conduct mission.	Catastrophic	Improbable (1E-5 - 1E-7)
6.6.2	Electrical	Since alternator remains still intact aircraft will have diminished safety margin but can still fly.	Major	Improbable (1E-7 - 1E-9)
6.6.3	Electrical	Failure of voltage regulators will cause damage to sensors and flight computer	Severe Major	Improbable (1E-7 - 1E-9)
6.6.4	Electrical	Damage to voltage regulators if sized incorrectly. And subsequent damage to flight computer or sensors.	Severe Major	Improbable (1E-7 - 1E-9)
6.6.5	Electrical	Flight computer fails to receive power from the alternator or battery. Aircraft loses some control authority has to initiate divert back home.	Severe Major	Improbable (1E-5 - 1E-7)
6.6.6	Electrical	Electrical fire is caused degrading components, damaging package, and critical electrical components	Catastrophic	Improbable (1E-5 - 1E-7)
6.6.7	Electrical	Electrical fire is caused degrading components, damaging package, and critical electrical components	Catastrophic	Improbable (1E-5 - 1E-7)
6.6.8	Avionics	Flight computer experiences failure degrading safety of aircraft causing it divert to base.	Severe Major	Improbable (1E-7 - 1E-9)

To determine whether a mitigation was required depended on the severity and probability as well as the complexity/weight the mitigation imposed on Alicorn. Referring to FAA AC25.1309-1A, all catastrophic or severe major hazards were closely scrutinized to verify that the probability was “Improbable $10e^{-7} - 10e^{-9}$ ” or “Extremely Improbable $< 10e^{-9}$ ” and that single point of failure did not result in a catastrophic failure. If this was not the case, mitigations would be implemented as redundancies to prevent the severity or reduce the probability. Table 14.5 supplies the applicable mitigations to all hazards.

Table 14.5: Mitigations to the hazards mentioned in Table 14.4

Hazard I.D.	Hardware Failure	Mitigation	Residual Classification	Residual Probability
7.1.3	Sensors	Operator notified of issue as well as multiple sensors that provide information to the flight computer	Minor	Improbable (1E-7 - 1E-9)
7.1.8	Flight Computer	Recommend an abort procedure written into the software once the flight computer fails.	Severe Major	Improbable (1E-7 - 1E-9)
6.5.1	Engine	Conduct overhaul at manufacturer specified 1200 hrs.	Catastrophic	Extremely Improbable (< 1E-9)
6.5.2	Engine	Conduct overhaul at manufacturer specified 1200 hrs.	Severe Major	Extremely Improbable (< 1E-9)
6.5.3	Engine	Conduct overhaul at manufacturer specified 1200 hrs.	Severe Major	Extremely Improbable (< 1E-9)
6.5.4	Engine	Conduct overhaul at manufacturer specified 1200 hrs.	Severe Major	Extremely Improbable (< 1E-9)
6.5.5	Engine	Conduct overhaul at manufacturer specified 1200 hrs.	Severe Major	Extremely Improbable (< 1E-9)
6.6.1	Alternator	Require another battery or alternator to meet power consumption of aviation components. Further analysis deemed alternator best option.	Major	Improbable (1E-7 - 1E-9)
6.6.3	Voltage Regulators	Recommend adding fuses or other features to prevent hardware from getting damaged.	Severe Major	Improbable (1E-7 - 1E-9)
6.6.4	Alternator	Recommend making sure that the voltage regulators are rated to handle the highest power loads.	Severe Major	Improbable (1E-7 - 1E-9)
6.6.5	Wiring	Incorporate redundant electrical feeds to critical components.	Severe Major	Improbable (1E-7 - 1E-9)
6.6.6	Wiring	Incorporate heat sensors to monitor wiring as well as circuit breakers to cut power to failing wires.	Major	Improbable (1E-7 - 1E-9)
6.6.7	Battery	Incorporate heat sensors to monitor wiring as well as circuit breakers to cut power to battery	Severe Major	Improbable (1E-7 - 1E-9)

A great example of the system safety approach is the alternator Hazard I.D. 6.6.1 in both Table 14.4 and Table 14.5. Early in the design stages the team determined that a generator or alternator would be required to provide the sufficient power to all the electrical components. To save on weight and space the team determined that one alternator would be sufficient to power the aircraft. When the PSSA was conducted for an alternator failure it was shown that the battery did not have enough power to continuously operate the UAV with the minimum required electrical components. Thus turned a severity from a Severe Major in which the aircraft could abort into a Catastrophic failure in which the aircraft is executing an emergency landing. This is completely unacceptable to the design team standards, so an analysis was conducted to determine if extra batteries or another alternator would be required. Due to weight and space consideration



the team determined an additional alternator would be required to reduce the severity from Catastrophic to Major and reducing the probability from Improbable $10e^{-5} - 10e^{-7}$ to Improbable $10e^{-7} - 10e^{-9}$.

Another system modified by the system safety approach was the unloading and loading phase of flight. To meet the block time specified in the RFP, the design team focused on a simple, quick, and lightweight design to load and unload the package. This design involved placing the package on a cart and transporting both the package and the cart to the destination. Then Alicorn would unload the cart and package by gravity and fly away. While this design is simplistic and quick, it has some safety issues that need to be addressed. When conducting the PSSA analysis on this concept some concerning hazards were identified. The major of these was an out of control state when the package was unloaded. The severity of this occurrence was given a Severe Major due to the possibility of someone sustaining a serious injury getting hit by the package as well as the high probability of severely damaging the package. The probability of this hazard was given an Improbable ($1e^{-5}$ - $1e^{-7}$). To address these concerns, the design team conducted some trade studies to determine a viable solution. Some of these concepts were winch assisted gravity release, automated cart, breaks attached to the cart, or accepting the current risk. After extensive study, that focused on weight, release time, safety to people, and safety of the package, the design team decided to incorporate both breaks on the package as well as an assisted gravity winch. These decisions were heavily influenced by safely releasing the package from the UAV and maintaining control of the package until the package came to a stop. While this solved the initial risk, a new PSSA had to be conducted on the winch and braking system to determine the severity and probability of those systems failing. Once completed, it was determined that the overall severity and probability were reduced to a Major and Improbable ($1e^{-7}$ - $1e^{-9}$).

When design redundancies were impractical due to space constraints or meeting the RFP, the design team decided to add other features to monitor the component health and require a strict overhaul schedule defined by the components manufacturers specification. An example of this is the ROTAX 915 engine. Due to size and weight constraints, Alicorn could only support one engine within the fuselage. If Alicorn lost the engine for any reason, the event would be considered a Catastrophic event. To mitigate this risk, the design team implemented an overhaul schedule based on ROTAX manufacturer's specifications. In addition to the overhaul schedule dictated by ROTAX, Alicorn will be designed with HUMS monitoring all engine functions to detect possible issues within the engine preventing a Catastrophic event from occurring.

14.2 Critical Parts

Once the PSSA was fully populated, the design team could determine what parts were critical and provide a replacement/overhaul schedule for those parts. The determination of whether a part was critical or not came from the severity of that particular component failing. Take for example a camera on the outer skin, if one camera fails the UAV loses some safety margin and ability to detect objects near or in the path of the aircraft. This does not entirely prevent the UAV from completing it's mission. On the other hand if the flight computer were to fail, then the UAV loses a significant amount of navigational, control, and other computing functionalities. Limiting the safety of Alicorn and forcing the system to abort the mission and return to base for immediate maintenance. Using these examples, the design team identified the critical parts of the UAV. With the critical components identified, the design team used the MTBF for the material to determine the overhaul schedule. When no information was provided, best judgment as well as the frequency of use were the determining factors to when a part should be replaced/overhaul. Table 14.6 provides all the critical parts as well as their replacement/overhaul schedule.

The replacement/overhaul will be conducted at every engine overhaul unless specified otherwise. Procedure for each critical part is described below:

- **HUMS Data Processing Unit:** During the nose removal HUMS processing unit will be removed from the avionics box. The unit will undergo a verification test to determine if the unit is still

Table 14.6: Critical Parts and the replacement/overhaul schedule

Critical Part	MTBF (hrs)	Schedule (hrs)
HUMS Data Processing Unit	3.53E+04	1200
HUMS Sensors	3.00E+05	1200
Lithium-Ion Polymer Battery	5.00E+03	1200
PC-Motherboard	3.00E+05	1200
Rotor blade		1200
Swash Plate		1200
Hub		1200
Pitch Casing		1200
Lag Damper		1200
ROTAX 915	1.20E+03	1200
Alternators	2.00E+03	1200
Pulley Transmission	1.25E+04	1200
Gear Boxes	8.00E+03	1200
Drive Shaft		1200
Structure		1200

operating efficiently. When the unit approaches the end of servicing it will then be replaced.

- **HUMS Sensors:** All sensors will be visually inspected for any wear. Once the visual inspection is complete, tests will be conducted on each sensor to verify functionality is within design specification for that particular sensor.
- **Lithium-Ion Polymer Battery:** Battery will be visually inspected for any wear. Then cables will be removed from the battery connectors. A voltmeter will be used to check that the battery is still within specifications.
- **PC-Motherboard:** The avionics box and motherboard will be visually inspected for wear. Then the technician will hook up a laptop to verify the motherboard is working optimally and within design specification. Any new software updates will be provided through the technician's computer.
- **Rotor blade:** The rotor blades will be removed and visually inspected for wear. Non Destructive Inspections (NDI) will be performed to verify the integrity of the blades. The blades will also be balanced and tuned to maintain correct frequencies.
- **Swashplate:** Swashplate will be visually inspected for wear to determine if the plate needs to be replaced.
- **Hub:** Hub should be visually inspected for wear and corrosion.
- **Pitch Casing:** Pitch casing shall be visually inspected for wear and corrosion. Pitch casing shall be disassembled to check the bearings inside for damage and to check the oil level. Once re-assembled bearings should be re-greased.
- **Lag Damper:** Lag damper should be visually inspected for wear and corrosion. Check the fluid to make sure that damper can still function.
- **Engine:** Engine should be checked in accordance with ROTAX specifications. Mounts shall be visually checked for wear. Clutch attachments visually inspected to verify that engine is not going to engage rotors until required.
- **Alternators:** Alternators shall be visually inspected for wear. Then disassembled and inspected in accordance with manufacturer's specifications.



- **Pulley Transmission:** Pulley system should be visually inspected for wear. Tensioners shall be inspected to verify the correct position. Belts shall be moved one pulley counter clockwise. After every 4 engine overhauls belts shall be replaced.
- **Gear Boxes:** Gear boxes shall be visually inspected for wear. Oil levels shall be checked and oil changes need to be conducted per engine overhaul. Gear boxes need to be disassembled and inspected every 4 engine overhauls and replaced accordingly.
- **Drive Shaft:** Drive shaft shall be visually inspected for wear. Grease bearings and flex bearings need to be inspected for wear. NDI should be used to make sure the drive shaft is within tolerances as well as flex bearing and grease bearings.
- **Structure:** Air frame shall be visually inspected for any wear. NDI shall be used on critical structures to make sure that they are within tolerances. Skin shall be checked for any tears or holes. Titanium inserts and aluminum parts shall be inspected for corrosion.

Based on critical schedule and conditional maintenance as well as looking at historical data Alicorn is expected to achieve a 99.6% dispatch reliability with a 95% probability of abort.

14.3 Autorotation

As shown in Section 12, the Alicorn has an above average Autorotation Index. While the likelihood of an engine failure is very low, the aircraft will be able to land with a low rate of descent in a controlled manner. Its redundant electrical system ensures that the avionics and flight controls are powered even in the event of an engine failure. In order to ensure a rapid response to a drivetrain malfunction, the Alicorn constantly analyzes available landing sites in order to attempt the safest and most rapid landing possible.

14.4 Safety Features

The Alicorn will be installed with a clutching mechanism to engage and disengage the rotors. The clutching mechanism will allow Alicorn to stop the rotors in the event that an animal/person approaches the UAV while rotors are spinning. To provide warning that Alicorn is taking off or landing alarms will be installed. Beside providing warning, the alarms will deter wildlife from entering the flight path or landing zone.

To comply with FAA regulations for Night and day Visual Flight Rules (VFR) Alicorn will have anti collision lights installed to provide location and direction the aircraft is flying. On the bottom Alicorn will have a landing light as well as the strobe light installed. Towards the aft part of the UAV a rotary beacon will be installed. Per FAA flight rules a green light will be installed on the right side of the UAV, a red light will be installed on the left side of the UAV, and a white light will be installed on the aft part of the aircraft.

To help provide visual cues to the rotor area reflective tape will be installed on the tips to provide indication of where the rotor ends. This will be especially important at night where visibility is minimum. The design chose a yellow reflective tape for the rotor tips due to its contrast at night allowing for quick visibility.

15 Acoustics

The potential delivery sites of the aircraft, which include hospitals, community centers, and health camps, cannot afford to have high noise levels emitting from delivery air vehicles. Moreover, as per the RFP, the aircraft flies only 150 m above ground level and over rural and medium density suburban populations. Therefore, it is important to ensure Alicorn has a low noise signature during both hover and cruise.



The main sources of noise for an aircraft of this scale are tonal noise, broadband noise, blade vortex interaction noise (BVI), and engine noise. Tonal noise consists of loading noise, which arises from the acceleration of blade loads and thickness noise, which comes from the displacement of the airflow due to the thickness of the blade. Broadband noise arises mostly due to turbulent flow over the aerodynamic surfaces. BVI arises from the interaction between the blades and trailing blade vortices. The rotor blades of Alicorn were designed with a 10° anhedral with the sole purpose of minimizing BVI noise.

The main drivers of aircraft noise are the rotational speed of the rotor and the thrust produced. Urban air mobility (UAM) vehicles use the distributed propulsion/lift concept to reduce propeller/rotor noise by distributing the thrust over multiple propellers/rotors. In that sense, the tandem configuration provides a benefit by distributing the lift over two rotors. The noise generated by two rotors doesn't double the noise of a single rotor.

The tonal noise of Alicorn was analyzed using ACUM (Acoustic Code of the University of Maryland) [65], a code that is based on Farassat's formulation 1A [66] of the Ffowcs Williams - Hawkings equation [67]. The blade geometry, blade loading, and other rotor and flight data were inputted to the code to calculate the tonal noise and broadband noise at pre-selected observer locations. Broadband noise was calculated using the BPM semi-empirical model [68]. Both rotors were considered in the noise computations. Observers were located in a hemisphere below the aircraft. The radii were set to 30 m for hover and 150 m for forward flight corresponding to the mission altitude. The observer locations for the two cases are shown in Figure 15.1.

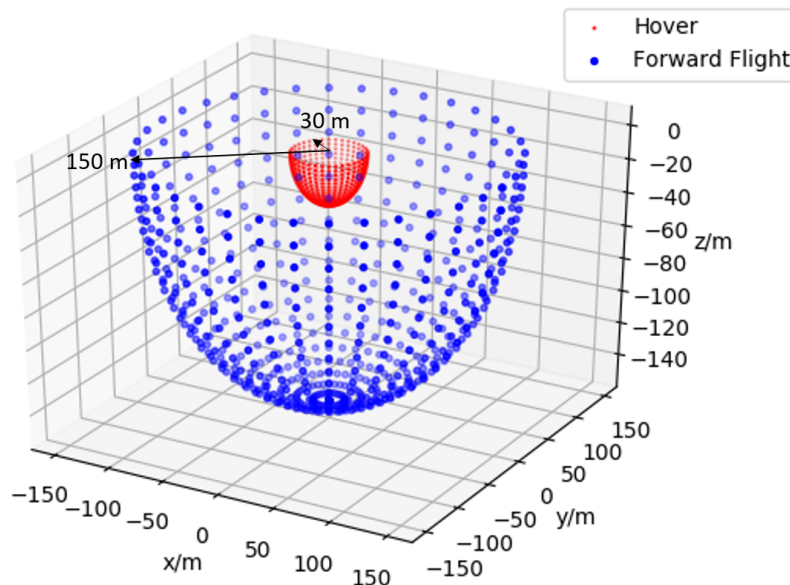


Figure 15.1: Observer locations for hover and forward flight

The A-weighted overall sound pressure level (OASPL) during hover is given in Figure 15.2. The A-weighting considers the difference in sensitivity of the human ear to different frequencies [69]. The broadband noise clearly outweighs the tonal noise in hover and therefore, the total noise signature is similar to the broadband component. The tonal noise is significantly low directly below the aircraft, while maintaining a 61.3 dB(A) maximum at the horizontal plane of the aircraft. On the contrary, the broadband noise reaches its highest value directly below the aircraft reaching a maximum value of 75.6 dB(A). The total OASPL is also the same as the broadband noise because the tonal noise is negligible below the aircraft.

Figure 15.3 shows the A-weighted OASPL in forward flight, where the aircraft is moving from right to left. It shows a much lower noise than hover because of the 150 m distance to the observer. The tonal

noise produces a maximum OASPL of 66.4 dB(A) towards the front of the aircraft. The broadband noise produces a maximum noise of 65.2 dB(A) below the aircraft, slightly towards the rear. The maximum total noise is only 66.5 dB(A).

Phase of Flight	Distance to Observer / m	Maximum noise / dB(A)
Hover	30	75.6
Forward flight	150	63.1

Table 15.1: Maximum OASPL in different phases of the mission

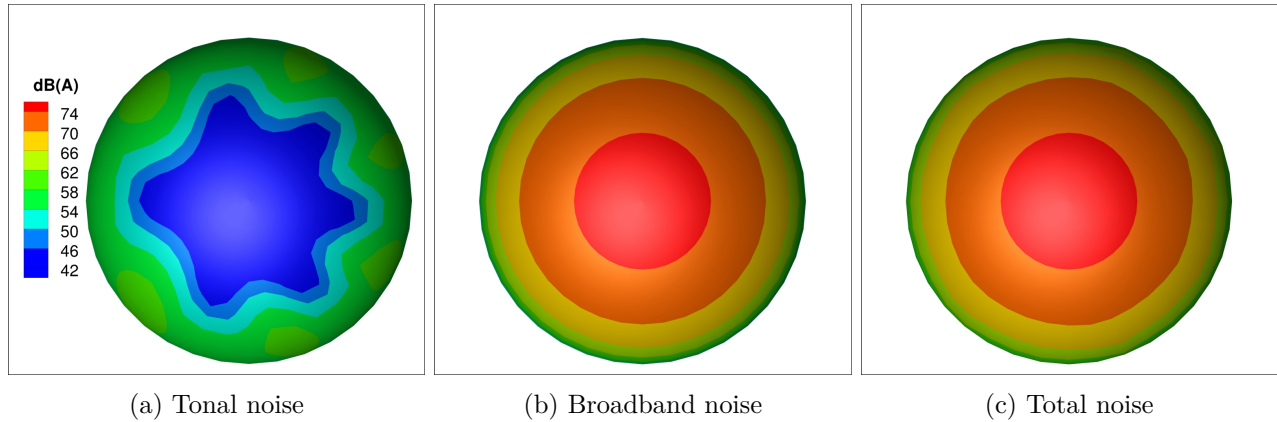


Figure 15.2: OASPL in dB(A) for hover

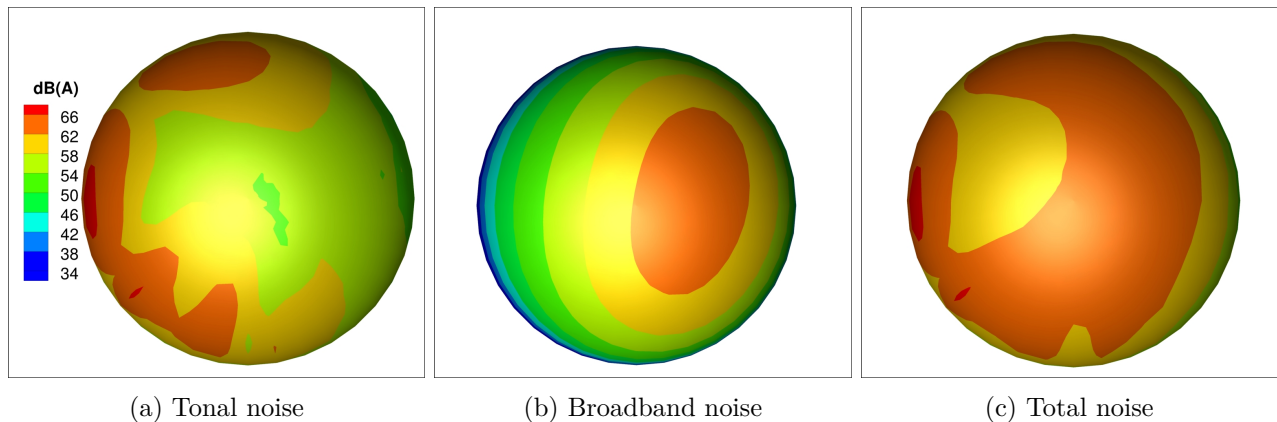


Figure 15.3: OASPL in dB(A) for forward flight

Both hover and forward flight noise levels are well below the acceptable limit of 78.5 dB(A) [70]. The hover noise level is similar to that of a vacuum cleaner, whereas the noise level in forward flight is of the level of a conversation [71]. The engine noise was found to be around 72 dB(A) during take-off and landing [70], which is also well below the acceptable limit. Therefore, Alicorn can be identified as an eco-friendly aircraft with a very low noise signature.

16 Ground Operations

16.1 Ground Control Station

The ground control station shown in Figure 16.1 comprises a rugged laptop to which the radio telemetry, the LTE and the Satcom modules are connected. A tablet or a cell phone will also be able to connect to the laptop via wifi or bluetooth. Radio communication instruments, power supplies, and display screens will be housed in a 4 ft × 2 ft × 1 ft storage container for ease of transportation and setup. The antennas for all the communication modules will be placed on a stable and an elevated platform, such as a tripod. Power for ground system components will be supplied by a commercially available 1kW portable power station. Total ground system weight is estimated to not exceed 30 kg with these components allowing for complete setup from a single technician/supervisor.

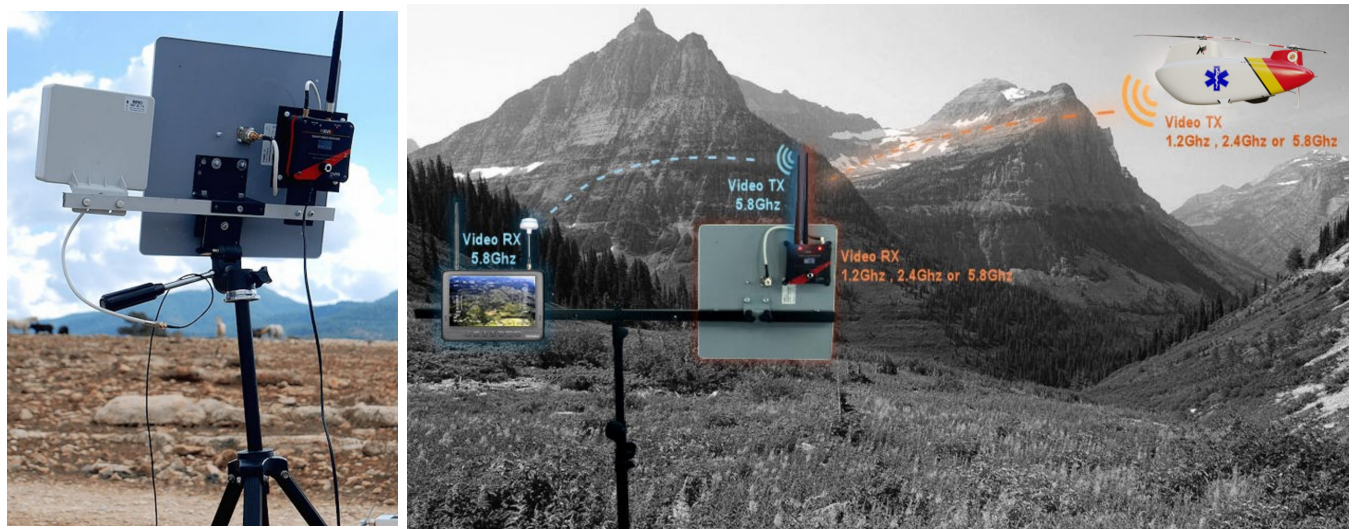


Figure 16.1: Ground Control Station (GCS)

16.2 Servicing

The servicing of Alicorn will rely on HUMS data. As depicted in the Concept of Operations, prior to the initial flight and at the end of the day technicians will review all the data stored in HUMS. Quick Response (QR) codes will be implemented to preflight the aircraft to determine if Alicorn is airworthy for that day's mission. After every successful mission, Alicorn will transmit its HUMS data to a technician to review and monitor the system. This will ensure that the aircraft remains airworthy throughout the day. At the end of the day, Alicorn will transmit the final report along with data analysis for all component wear. By providing this information, Alicorn allows the user to provide the correct sparing for parts while also keeping the aircraft available for the mission.

The servicing schedule will be a conditional based maintenance. The timing and part changes will depend on HUMS information. A mandatory overhaul will be scheduled at every 1200 hrs when the engine requires its manufacturer overhaul. This preventive maintenance is an added safety measure to capture and prevent issues early before they impose a major safety risk. As the data matures, technicians and Alicorn will be able to predict and procure the correct spare parts to quickly and efficiently replace components.

Servicing of oil and other fluids will be done in accordance with manufacturers specification for the engine, gear boxes, etc. Fueling the aircraft will be done through fuel caps positioned towards the top on either side of the UAV. Fuel caps and placement are depicted in Figure ???. The fuel required is 100LL aviation fuel per the ROTAX specifications.



Figure 16.2: Alicorn transport vehicle

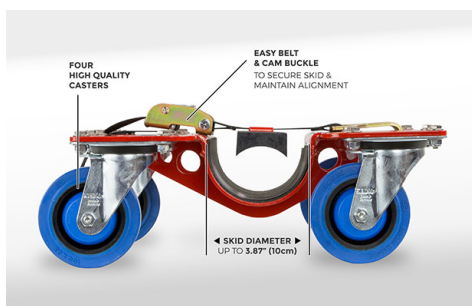


Figure 16.3: Skid dollies



Figure 16.4: Possible blade storage

16.3 Staging and Tear Down

Alicorn has been designed with the mindset of being able to be transported in a box truck presented in figure 16.2. To manage this, blades will be removed at the last day of flight and placed in a storage container presented in figure 16.4. Then the aircraft's skids will be placed on a dolly represented in figure 16.3 so that it can be easily wheeled around. This concept allows for a minimal logistical footprint in moving

Alicorn to the staging areas without having to fly it to the location. Another benefit is when overhaul maintenance needs to be conducted Alicorn can be broken down and easily shipped to the maintenance facility to conduct the required maintenance. When ready to stage the Alicorn will be removed from the transport vehicle, wheeled on the dollies to staging area, and finally assembled to conduct that days missions.

17 Certification

Alicorn will be flown under a Part 135 Air Carrier Certification as a Standard Operator under Title 14 of the Code of Federal Regulations (also known as the Federal Aviation Regulations). Per the FAA, “A Standard operator holds a certificate with no limits on the size or scope of operations. However, the operator must be granted authorization for each type of operation they want to conduct.” This decision was heavily influenced by FAA’s approval of United Parcel Service’s (UPS) Flight Forward Inc. UAV in this category. The Standard Operator designation perfectly fits the nature of the RFP. This allows for a fleet of autonomous Alicorns to deliver essential supplies to disaster or emergency areas. To obtain this type of certification, the aircraft will need to complete all five phases of certification specified in the Part 135.

Phase 1: Pre-Application

A request for Part 135 Air Carrier Standard Operator will submitted in order to meet the timeline for a final certification by 2025 to the Safety Assurance System (SAS). During this process, a Director of Operations, Chief Operator, and Director of Maintenance will be identified. The company will provide the Pre-Application Statement of Intent that will highlight the simplistic design concept specified in Section 3 along with previously certified components stated in Section 8, 9, and 10 that meet the mission outlined in Section 2. Development and operational testing will comply with and support the Certification Service Oversight Process.

Phase 2: Formal Application

Alicorn and the FAA certification team will develop a schedule of events (SOE) that will define the timeline and order of design documents to be provided. Due to the simplicity and robustness of the design, a condensed SOE would be suitable and would meet the deadline for 2025 certification. A Formal Application Letter will be submitted that will detail operator’s intent to receive the Part 135 certification. This letter will highlight the simplistic design concept as well as all the pre-certified components within the aircraft. Other material delivered to FAA will include Compliance Statement, applicable Company Manuals, Management Qualification Attachments, SAS specific information, and proposed operations specifications (CONOPS). This will culminate with the Formal Application Meeting and the subsequent Design Assessment.

Phase 3: Design Assessment

No issues with this phase are anticipated. Alicorn is designed to be easily certified through the use of FAA and EASA approved components such as the engine (see Section 8) and proven designs like the pulley drive system which is implemented in many aircraft, including Robinson’s R22 and R44 (see Section 9). Besides components and designs featured in other certified aircraft, the design team was meticulous in the seamless integration of all the systems. This is evident in the Avionics (see Section 10), where the design team created a software architecture that integrates the information from all the avionic components into one continuous data stream to the flight computer. The design team conducted a thorough safety analysis (see Section 14.1) of all the systems and components to determine the critical parts, the failures could potentially lead to a catastrophic event, and the mitigation that are necessary which exceed the safe operating practices that FAA emphasizes.



The design team meticulously reviewed all applicable regulations for flight through rural and suburban regions. This added additional design features such as external lighting to meet night Visual Flight Rules (VFR) (see Section 14.4). Along with installing appropriate equipment, the team determined the proper maintenance schedule (see Section 16.2) that complies with Part 43 of the Federal Aviation Regulations (FAR). Thus guaranteeing that the FAA certification team will certify the design presented.

Phase 4: Performance Assessment

The design team's approach to simplistic designs and use of commercial off the shelf (COTS) components allow for minimum training to maintain and operate the aircraft. An integrated autonomous package requires little interface from the operators in verifying safe operations [10]. Using the HUMS as well as providing easy access to critical components and a user friendly maintenance procedure [16.2] requires less routine servicing and training to fix components. Allowing the FAA certification team to quickly and efficiently grant certification to Alicorn.

Phase 5: Administrative Functions

The design team has no reservations that FAA will certify the operations specifications for Alicorn defined in Section 2. Alicorn's simplistic design and COTS allows for a quick and effortless evaluation from FAA. If the end user decides to incorporate a different mission set outlined in Section 19, the design team is confident that FAA will certify Alicorn for those mission sets as well.

18 Cost Analysis

18.1 Method

As noted in Section 8, the Rotax 915 iS retails engine for 40,350 USD. In Section 10, avionics and electrical system component expenses were estimated at 131,100 USD.

The Harris-Scully CTM Rotorcraft Cost Model discussed in the NDARC manual [14] were used to provide the cost estimates below.

18.2 Purchase Price

Based on a statistical relationship for past rotorcraft prices, the Alicorn is estimated to have a bare aircraft purchase price of 218,000 USD. Including the specialty avionics mentioned above, the total price is estimated as 349,100 USD.

18.3 Maintenance Cost

The maintenance cost per flight hour is expected to be 88 USD. The Harris-Scully model predicts 0.21 maintenance man hours per flight hour.

18.4 Operational Cost

The operational cost per year is estimated as 12.5 million USD if five sorties are flown per day with 10% of the aircraft available as spares. This also assumes 15-year loan and depreciation periods.

19 Multi-Mission Capability

Alicorn was specifically designed to perform the delivery and logistics missions outlined in the RFP, with the utmost focus on safety and productivity. Besides that, it was also designed to be generic enough to perform a number of other missions without having to be drastically reconfigured. This was deliberately done at the design stage to ensure that Alicorn doesn't idle between pandemics or natural disasters, improving its economic benefit to the customer.

19.1 Commercial Delivery

Most commercial delivery drones such as Prime air, Parcelcopter, and Flerty are designed to deliver one small package to the end customer. Alicorn on the other hand, has a much larger payload carrying capacity, range, and speed. Therefore, it is well suited to deliver multiple packages to multiple customers in one mission without going back and forth to the warehouse, drastically reducing the cost of autonomous aerial delivery. It can carry up to 70 FBA (Fulfillment by Amazon) Small and Light type amazon packages (16" × 9" × 4") [72] or 20 standard size packages in one flight. The operational size of Alicorn is small enough for it to land on an area as small as two parking lots, and therefore, having easy access to most delivery sites. The autonomous cart (see Ch.6) can be upgraded to unload the packages individually at each delivery site. This way, Alicorn can be used for commercial package delivery with economies of scale benefits.

Alicorn can also be used in supply chain management, carrying raw material or finished products between different sites or to distribution centers. Alicorn's speed and autonomy can drastically reduce the delivery time, especially benefiting the transportation of perishable goods such as agriculture, meat, and dairy products. Reduction in delivery time would reduce the cost of refrigeration and other related expenses providing economic benefits to the user.

19.2 Agriculture

Alicorn can also be used as an agricultural aircraft for crop dusting or aerial application. It can be used to spray crops with pesticides and fertilizers or plant certain types of seeds in large areas. Alicorn has more than twice the payload capacity and more than 4 times the hovering time of the DJI Agras T16 drone, which is widely used in agriculture. An auxiliary spraying system can be mounted below the fuselage that can be integrated to the operating system of Alicorn to autonomously spray the product with a higher precision. The state-of-the-art software architecture and object sensing platform of Alicorn will be useful in precision agriculture as well.

19.3 Emergency Personnel Hoisting

The 95th percentile male weight is 97.98 kg [73], which is slightly below the 100 kg maximum payload capacity of Alicorn. Therefore, Alicorn is capable of lifting people under normal conditions, if needed, with a reduced fuel weight and range. However, the cargo bay is not large enough to hold a person in the lie-down position. Therefore, the person needs to be hoisted using a stretcher such as the one shown in Figure 19.1, which weighs 8 kg [74]. Since the in-board winch system is built to pull the 50 kg payload along the ramp, it needs to be modified to lift the new payload. A small opening can be built into the bottom of the fuselage near the winch to get the cable out. Therefore, after these minor modifications, Alicorn can be used to hoist people in emergency situations.

19.4 Search and Rescue

The advanced object detection and terrain analyzing capability of Alicorn becomes extremely useful in a search and rescue mission. Alicorn is able to identify a person in a difficult terrain and provide him with the necessary assistance. The modified aircraft provides Alicorn with rescuing capability. Once the hoist is lowered enough, the person can be placed on the stretcher by another person or by the person himself, and once Alicorn identifies the person is fully restrained using its cameras, it can transport the person to a safe zone or a hospital in an optimal speed, allowing a ground crew to monitor the person at all times. Alicorn's range, payload capacity and speed become helpful for a mission of this type.



Figure 19.1: Ferno Traverse Rescue Stretcher

19.5 Shipboard Supplies

Another application of Alicorn would be to deliver essential supplies including medical and other emergency equipment to ships sailing or anchored close to land. Alicorn's top speed is more than three times that of a small boat, and therefore, would be extremely useful in an emergency. In an epidemic situation on a ship, it would be more beneficial to use Alicorn instead of a boat to deliver vital supplies, to avoid the spread of the disease. Alicorn's software architecture is capable of safely landing on a ship deck and unloading the package. It can also bring back goods from the ship to the land such as test samples or even a person using a hoist. It can also be used by cargo or cruise ships to get supplies from land.

19.6 Airborne Data and Communications relay

Alicorn being modular and easily re-configurable can also be used to act as an Aerial base station: a flying antenna system that works as a hub between the backhaul network and the access network. Establishing a fly ad-hoc network (FANET) is also possible with Alicorn. The aircraft is designed to have 3.4kW of electric power and it only needs 1.4kW maximum power. More than 2 kW is reserved for any applications that require high power. Alicorn can deploy on-demand networks at specific locations and provide "connectivity from the sky". Ground users will get access to premium services with high quality wireless links, poor degradation, high capacity and low interference. Furthermore, it'll provide connectivity during temporary events and emergency situations, and in zones or rural areas without pre-existing solid network infrastructure.

19.7 Geographical survey

Alicorn is equipped with high resolution bottom facing cameras and multiple long-range LiDARs which can be used for aerial photogrammetry. Alicorn can be used for the full geodetic survey of a study site by creating a point cloud of measurements of nearly homogenous quality and accuracy as shown in Figure 19.2. Intricate maps of terrain or a city could be built autonomously by the aircraft providing a low-cost and flexible alternative. Additionally, Alicorn can conduct geomagnetic surveys to predict the location of mineral deposits. Furthermore, Alicorn's ceiling is greater than 15,000 ft and if equipped with air quality monitors it can provide real time air analysis at various elevations.

19.8 Surveillance, Inspections and Monitoring

Alicorn can perform a wide range of surveillance tasks such as livestock monitoring, wildfire mapping, pipeline security, home security, road patrol and antipiracy. It can also check for integrity of oil and gas pipelines, dams and related installations. Additionally, thermal cameras onboard Alicorn can be used for solar panel or power-plant inspections as shown in Figure 19.3. Furthermore, Alicorn's autonomous object detection capability can be used to locate and track objects of interest like people and vehicles in real-time.

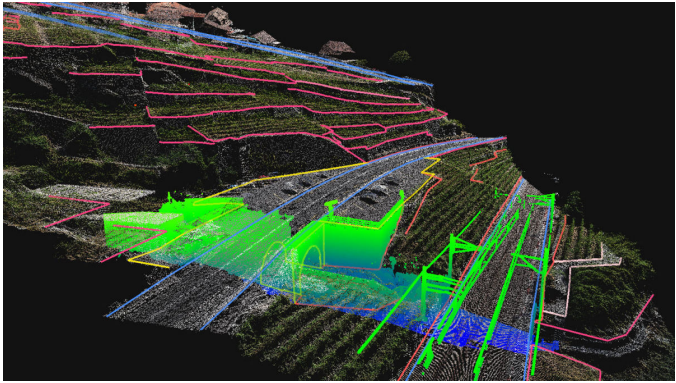


Figure 19.2: Combined LiDAR and photogrammetry point clouds.

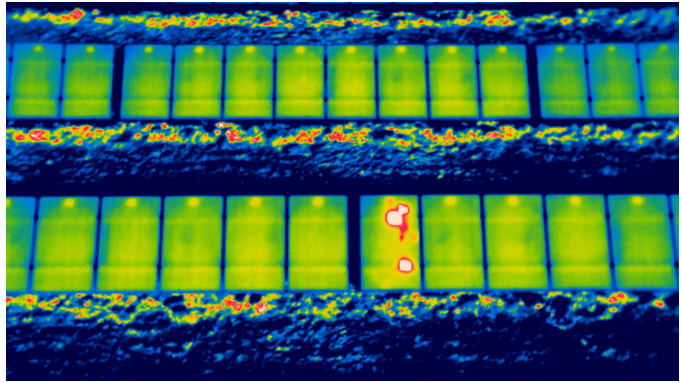


Figure 19.3: Thermographic inspection of solar panels.

20 Summary

The University of Maryland Graduate Design Team designed Alicorn to meet the vehicle and operational requirements specified in the Request for Proposal for medical equipment distribution in a pandemic or a disaster. Alicorn is a tandem rotor helicopter designed predominantly to carry a bulky payload more efficiently at a high speed. Higher system safety and mission productivity were the principal design objectives based on the customer's requirements. System safety took precedence over everything else in every step of the design.

Being a tandem helicopter, one of the biggest advantages of Alicorn is its ability to tolerate variations in the CG of the payload. This is a useful feature to have in a pandemic or any other disaster or emergency situation. The aircraft was designed to have a slightly forward CG location to allow for a much larger backward CG movement with the payload at the back. This also improves payload handling and makes packaging more convenient. The winch-assisted gravity cart that is custom-made for Alicorn also enhances the customer experience by providing a convenient way to maneuver the payload at the loading and unloading sites. Alicorn also comes with an optional automated cart if the customer prefers not to have the cart at the delivery site. The cart also provides modular payload capability, accommodating payloads that consist of multiple packages instead of a single large box. Due to the fragile nature of medical equipment, the payload is additionally secured using inflatable clamp tubes and a level package attitude is always maintained during flight allowing only up to 5° of inclination either way. The tandem configuration also offers sufficient clearance between the rotors and package when loading and unloading, improving safety of the ground personnel, especially compared to a single main rotor helicopter. The automated loading and unloading mechanism enables the customer to easily handle the package, while ensuring its safety. This becomes extremely useful at delivery sites such as hospitals and medical camps.

In order to increase the efficiency in forward flight, a rigorous analysis was carried out with the help of CFD to come up with the optimum fuselage shape that incurs the lowest amount of drag. This was an important

step of the design process in making Alicorn highly productive. Thrust compounding was considered but left out due to its complexity and the increase in fuselage drag. The propeller did not lead to an increase in overall aircraft performance.

Safety and reliability were key factors in designing the individual aircraft components such as the powerplant, transmission system, rotors, and avionics. The autorotation capability of the tandem configuration makes Alicorn inherently safer than most other rotor configurations. The redundancy in sensing, processing, and actuation with early failure detection and mitigation enhances Alicorn's safety. The state-of-the-art software package allows day and night operations, obstacle avoidance, and autonomous decision making in emergency situations aborting the mission and flying back to the launch site when safety tolerances are not met. In the event of an emergency, the software package guides Alicorn to land on a predetermined safe landing site ensuring the safety of the vehicle, the payload and the surrounding environment. The avionics is designed with a high level of autonomy to enhance the safety of the aircraft.

All things considered, Alicorn offers a practical solution for medical equipment distribution using existing technologies that are well proven. System safety, mission productivity, and customer satisfaction are at the very heart of the design. It also can be used in many other applications including commercial delivery, agriculture, search and rescue, and surveillance. Therefore, Alicorn becomes the ideal unmanned air vehicle to serve communities in a future pandemic or disaster.



Figure 20.1: Alicorn in action

References

- [1] Sunghun Jung and Hyunsu Kim. Analysis of amazon prime air uav delivery service. *Journal of Knowledge Information Technology and Systems*, 12:253–266, 04 2017.
- [2] Dhl’s parcelcopter: Changing shipping forever. <https://www.dhl.com/discover/business/business-ethics/parcelcopter-drone-technology>. Accessed: 2021-05-06.
- [3] Agras t16. <https://www.dji.com/t16>. Accessed: 2021-05-06.
- [4] Schibel camcopter s-100. <https://schiebel.net/products/camcopter-s-100/>. Accessed: 2021-05-06.
- [5] Dpi uav systems. <https://www.dragonflypictures.com/products/dp-14-multi-mission-uas/>. Accessed: 2021-05-06.
- [6] Zipline. <https://flyzipline.com/>. Accessed: 2021-05-07.
- [7] Flirty. <https://www.flirtey.com/>. Accessed: 2021-05-07.
- [8] Pfizer-BioNTech. Shipping and handling guidelines.
- [9] Eurocopter x3. https://www.wikiwand.com/en/Eurocopter_X%C2%B3. Accessed: 2021-05-07.
- [10] S-66 aafss, advanced aerial fire support system. <https://www.sikorskyarchives.com/S-66%20AAFSS.php>. Accessed: 2021-05-07.
- [11] Ansys fluent - fluid simulation software. <https://www.ansys.com/products/fluids/ansys-fluent>. Accessed: 2021-05-07.
- [12] CN Keys and WZ Stephniewski. Rotary-wing aerodynamics. volume 2: Performance prediction of helicopters. 1979.
- [13] LogiMover: The Independent Fork System from EISENMANN. Press Release, Datasheet Davinci Magazine .
- [14] Wayne Johnson. NDARC-NASA design and analysis of rotorcraft theoretical basis and architecture. 2010.
- [15] Solidworks. <https://www.solidworks.com/>. Accessed: 2021-05-07.
- [16] Blender. <https://www.blender.org/>. Accessed: 2021-05-07.
- [17] Autodesk fusion 360. <https://www.autodesk.com/products/fusion-360/overview?term=1-YEAR>. Accessed: 2021-05-07.
- [18] Dylon Jude, Bumseok Lee, Yong Su Jung, Jannik Petermann, Bharath Govindarajan, and James Baeder. Application of a heterogeneous cfd framework towards simulating complete rotorcraft configurations. In *American Helicopter Society, 74th Annual Forum Proceedings, Phoenix, Arizona, May 14-17, 2018*.
- [19] Roberto Jimenez, Fabrizio De Gregorio, Mathieu Legrand, and José Nogueira. Characterization of the flow around a helicopter fuselage equipped with vortex generators for drag reduction. In *18th International Symposium on the Application of Laser and Imaging Techniques to Fluid Mechanics*, pages 4–7, 2016.
- [20] Franky F1 Aerodynamics. <https://tianyizf1.wordpress.com/tag/y250-vortex/>. Accessed: 2021-05-07.
- [21] Robert E Sheldahl and Paul C Klimas. Aerodynamic characteristics of seven symmetrical airfoil sections through 180-degree angle of attack for use in aerodynamic analysis of vertical axis wind turbines. Technical report, Sandia National Labs., Albuquerque, NM (USA), 1981.



- [22] GK Yamauchi and Wayne Johnson. Trends of reynolds number effects on two-dimensional airfoil characteristics for helicopter rotor analyses. *NASA TM*, 84363, 1983.
- [23] Wen Zhong Shen, Robert Flemming Mikkelsen, Jens Nørkær Sørensen, and C Bak. Evaluation of the prandtl tip correction for wind turbine computations. In *2002 Global Windpower Conference and Exhibition*, 2002.
- [24] Joanne L Walsh. Performance optimization of helicopter rotor blades. 1991.
- [25] Travis Wiens and Brendan Deibert. A low-cost miniature electrohydrostatic actuator system. *Actuators*, 9(4), 2020.
- [26] LiquidPiston engine specifications. <https://www.liquidpiston.com>. Accessed: 2021-04-7.
- [27] AE50R Technical Data Sheet. https://austroengine.at/uploads/images/2010092010AE50R_Technical_Data_Sheet.pdf. Accessed: 2021-04-12.
- [28] Engine Manual, Operation / Maintenance / Installation: IAE50R-AA, Doc. No. E1.01.05-E, Rev 6, 10 March 2011. Link to Manual. Accessed: 2021-04-12.
- [29] Pipistrel Flies WATTsUP Electric Trainer. <https://www.avweb.com/recent-updates/business-military/pipistrel-flies-wattsup-electric-trainer/>, note = Accessed: 2021-05-24.
- [30] Lithium-Ion Battery. <https://www.cei.washington.edu/education/science-of-solar/battery-technology/>. Accessed: 2021-05-24.
- [31] Rotax 915 iS Limited Edition 141 hp. <https://www.flyrotax.com/produkte/detail/rotax-915-is-limited-edition.html>. Accessed: 2021-04-15.
- [32] UAV Engines AR682R. <https://uavenginesltd.co.uk/wp-content/uploads/2019/03/ar682r.pdf>. Accessed: 2021-04-7.
- [33] Operator’s Manual, Lycoming O-320 Series, 3rd Ed, October 2006. <https://www.lycoming.com/sites/default/files/0-320%20Operator%20Manual%2060297-30.pdf>. Accessed: 2021-04-12.
- [34] Turboshaft Engine PBS TS100. <https://www.pbs.cz/en/Our-business/Aerospace/Aircraftgines/Turboshaftgine-PBS-TS100>. Accessed: 2021-04-15.
- [35] UAV Engines AR682R. <https://www.rolls-royce.com/products-and-services/civil-aerospace/helicopters/rr300.aspx#section-overview>. Accessed: 2021-04-15.
- [36] Rotax aircraft engines brochure. https://www.rotax.com/files/userdata/rotax/downloads/produkte/BroschuereAircraft_210x297mm.pdf. Accessed: 2021-04-16.
- [37] Operators Manual for Rotax Engine Type 915 i A Series, Rev 2, December 2020. <https://www.flyrotax.com/services/technical-documentation.html>. Accessed: 2021-04-15.
- [38] EASA Certification of Rotax 915. <https://www.rotax.com/en/news/latest/detail/easa-certification-of-rotax-915-isc3-a-aircraft-engine-in-time.html>. Accessed: 2021-04-15.
- [39] Installation Manual for Rotax Engine Type 915 i A Series, Rev 3, October 2020. <https://www.flyrotax.com/services/technical-documentation.html>. Accessed: 2021-04-15.
- [40] Rotax 914 UL — F Datasheet. <https://www.flyrotax.com/files/Bilder/ProdukteRotax/Datasheets>. Accessed: 2021-04-16.
- [41] Rotax 915iS Engine - 140 HP. <https://www.leadingedgeairfoils.com/rotax-engines-parts/new-rotax-engines/rotax-915is-engine.html>. Accessed: 2021-05-20.
- [42] Lycoming Engines O-320-D2A. <http://www.airpowerinc.com/productcart/pc/TLEngineDetail>.



- asp?catID=33&prodID=8914. Accessed: 2021-05-20.
- [43] Report of USATECOM Project No. 4-4-0240-02, Flight Evaluation of the T63-A-5 Turbo Shaft Engine Installed in a UH-13R Helicopter (ATA-TR-63-7). Technical report, U.S. Army Test & Evaluation Command, 1964.
- [44] The Market for Aviation Turboshaft Engines. https://www.forecastinternational.com/samples/F642_CompleteSample.pdf. Accessed: 2021-05-20.
- [45] Dynali H3 Clutch Engagement. https://www.youtube.com/watch?v=CaIYeF4_nos. Accessed: 2021-04-22.
- [46] Dynali UAV Transmission. <https://www.dynali.com/images/slider/main-transmission.jpg>. Accessed: 2021-04-22.
- [47] Reliability of the Robinson R22 helicopter belt drive system. https://www.atsb.gov.au/media/4120236/ai-2009-038_final.pdf. Accessed: 2021-04-22.
- [48] Stephen P. Radzevich. *Dudley's Handbook of Practical Gear Design and Manufacture, Second Edition*. CRC Press, Taylor & Francis Group, Boca Raton, Florida, 2012.
- [49] *AGMA Standard 908-B89, Information Sheet: Geometry Factors for Determining the Pitting Resistance and Bending Strength of Spur, Helical and Herringbone Gear Teeth*. American Gear Manufacturer's Association, Alexandria, Virginia, 1999.
- [50] *ANSI/AGMA 2005-D03, Design Manual for Bevel Gears*. American Gear Manufacturer's Association, Alexandria, Virginia, 2003.
- [51] MatWeb: Carpenter Pyrowear 53 Tool Steel, Core Tensile Properties. <http://www.matweb.com/search/datasheet.aspx>. Accessed: 2021-04-12.
- [52] Optibelt Technical Manual: V-Belt Drives. <https://www.optibelt.com/fileadmin/pdf/produkte/keilriemen/Optibelt-TM-v-belt-drives.pdf>. Accessed: 2021-04-23.
- [53] Ratnesh Madaan. Wire detection, reconstruction, and avoidance for unmanned aerial vehicles. Master's thesis, Pittsburgh, PA, August 2018.
- [54] Ratnesh Madaan, Daniel Maturana, and Sebastian Scherer. Wire detection using synthetic data and dilated convolutional networks for unmanned aerial vehicles. In *2017 IEEE/RSJ International Conference on Intelligent Robots and Systems (IROS)*, pages 3487–3494, 2017.
- [55] AL24-P70 Plane Power Alternator. <https://www.aviationpartsinc.com/product/al24-p70-plane-power-alternator>. Accessed: 2021-05-19.
- [56] AL24-P70 Installation Instructions. <https://planepower.aero/wp-content/uploads/2019/10/AL24-70-Installation-Instructions.pdf>. Accessed: 2021-05-19.
- [57] FAA approved 24V ETX680-24-TSO designed for certified aircraft. <https://earthxbatteries.com/shop/etx680-24-tso>. Accessed: 2021-05-19.
- [58] ETX680-24-TSO Battery Specifications. <https://earthxbatteries.com/wp-content/uploads/2021/01/ETX680-24-TSO-Product-Spec.pdf>. Accessed: 2021-05-19.
- [59] Installation Maintenance Manual (IMM), ETX680-24-TSO Battery. Accessed: 2021-05-19.
- [60] UH-60A/L Blackhawk Performance Planning Card, DA Form 5703-R, Version 1.0, November 2003. <http://www.gensale.net/wp-blackhawk/PPC/UH-60%20PPC%20Guide.pdf>. Accessed: 2021-05-29.
- [61] John James Howlett. UH-60A Black Hawk engineering simulation program, Volume 1: Mathematical model. 1981.
- [62] Robert A Makofski and George F Menkick. Investigation of vertical drag and periodic airloads acting



- on flat panels in a rotor slipstream. 1956.
- [63] Wayne Johnson. *Rotorcraft Aeromechanics*. Cambridge University Press, 2013.
- [64] Preston B Martin. Rotor blade airfoil design for high-altitude, long-endurance vtol uavs. In *31st European Rotorcraft Forum*, pages 11–1–15, 2005.
- [65] Mathieu Amiraux. *Numerical Simulation and Validation of Helicopter Blade-Vortex Interaction Using Coupled CFD/CSD and Three Levels of Aerodynamic Modeling*. PhD thesis, University of Maryland, College Park, 2014.
- [66] F Farassat and George P Succi. The prediction of helicopter rotor discrete frequency noise. *Vertica*, 7(4):309–320, 1983.
- [67] John E Ffowcs Williams and David L Hawkings. Sound generation by turbulence and surfaces in arbitrary motion. *Philosophical Transactions of the Royal Society of London. Series A, Mathematical and Physical Sciences*, 264(1151):321–342, 1969.
- [68] Thomas F Brooks, D Stuart Pope, and Michael A Marcolini. *Airfoil self-noise and prediction*, volume 1218. National Aeronautics and Space Administration, Office of Management, 1989.
- [69] Juhani Parmanen. A-weighted sound pressure level as a loudness/annoyance indicator for environmental sounds—could it be improved? *Applied Acoustics*, 68(1):58–70, 2007.
- [70] European Union Aviation Safety Agency. *Type-Certificate Data Sheet for Noise*, 7 2019.
- [71] Decibel level comparison chart. <https://ehs.yale.edu/sites/default/files/files/decibel-level-chart.pdf>. Accessed: 2021-05-06.
- [72] FBA Small and Light. https://sellercentral.amazon.com/gp/help/external/G201706140?language=en_US. Accessed: 2021-04-15.
- [73] The Evolution of Anthropometrics and User Control. <https://www.hermanmiller.com/research/categories/white-papers/the-evolution-of-anthropometrics-and-user-control/#:~:text=In%20this%20database%2C%20a%2095th,between%20military%20and%20civilian%20databases>. Accessed: 2021-04-15.
- [74] Ferno Traverse Rescue Stretcher . <https://mfimedical.com/products/ferno-traverse-rescue-stretcher>. Accessed: 2021-04-15.

